

FABRICATION AND ANALYSIS OF AN ARTIFICIAL HUMAN HIP JOINT FOR SQUAT POSTURE

Ph.D. THESIS

by

ANKIT SAXENA



DEPARTMENT OF MECHANICAL AND INDUSTRIAL ENGINEERING
INDIAN INSTITUTE OF TECHNOLOGY ROORKEE
ROORKEE-247667 (INDIA)
JULY, 2019



FABRICATION AND ANALYSIS OF AN ARTIFICIAL HUMAN HIP JOINT FOR SQUAT POSTURE

A THESIS

*Submitted in partial fulfilment of the
requirements for the award of the degree*

of

DOCTOR OF PHILOSOPHY

in

MECHANICAL ENGINEERING

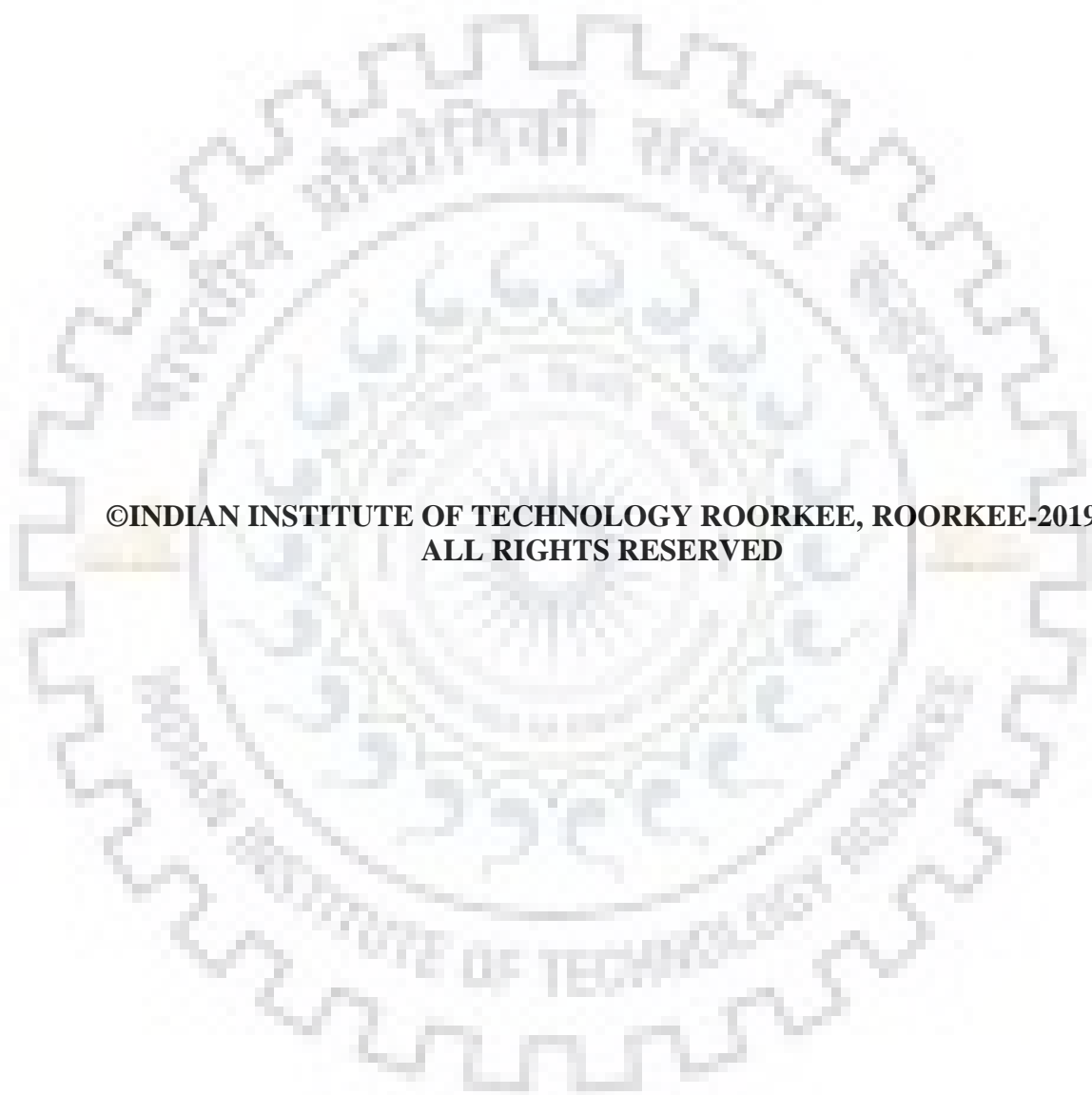
by

ANKIT SAXENA



DEPARTMENT OF MECHANICAL AND INDUSTRIAL ENGINEERING
INDIAN INSTITUTE OF TECHNOLOGY ROORKEE
ROORKEE-247667 (INDIA)
JULY, 2019





**©INDIAN INSTITUTE OF TECHNOLOGY ROORKEE, ROORKEE-2019
ALL RIGHTS RESERVED**





INDIAN INSTITUTE OF TECHNOLOGY ROORKEE ROORKEE

CANDIDATE'S DECLARATION

I hereby certify that the work which is being presented in the thesis entitled “**FABRICATION AND ANALYSIS OF AN ARTIFICIAL HUMAN HIP JOINT FOR SQUAT POSTURE**” in partial fulfilment of the requirements for the award of the Degree of Doctor of Philosophy and submitted in the Department of Mechanical and Industrial Engineering of the Indian Institute of Technology Roorkee, Roorkee is an authentic record of my own work carried out during a period from July, 2013 to July, 2019 under the supervision of Dr. Rahul S. Mulik, Associate Professor, Department of Mechanical and Industrial Engineering, Indian Institute of Technology Roorkee, Roorkee.

The matter presented in the thesis has not been submitted by me for the award of any other degree of this or any other Institute.

(ANKIT SAXENA)

This is to certify that the above statement made by the candidate is correct to the best of my knowledge.

(Rahul S. Mulik)
Supervisor

Date:

The bone is highly adaptive to habitual loading, regulating its structure according to components of its loading regime and mechanical environment, inclusive of strain magnitude - strain rate - strain frequency - strain distribution and deformation. Certainly, the greatest forces usually applied to bone, arise from muscular contractions. Indeed, in the past three decades have seen substantial advances in our understanding of “how these forces shape bone throughout life”. It is essential to estimate the strength of the bone to realize the fact that, the capacity/capability of bone and its joints under different configurations of human body viz., different activities, dissimilar weights, altered postures, etc., is limited. The human bones possess different strengths like mechanical elements and linkages, under different configurations i.e., the shoulder joint, hip joint, femur bone, knee joint, tibia, etc., would have different load carrying capacities. The load carrying capacities are described by the bone strength.

In addition to the bone strength, it is also essential to understand the mechanical failures of human bones. This background helps the implant designer to have better understanding of types of failure and causes of failure, in context to human subjects. The compatibility and feasibility of fixing the implant is always being challenge to the implant designer in context to the human subjects, whether it can retain to its original mobility and strength with specified geometry. The strength of a bone is described the stresses induced under different load. Therefore, the present study is focused to evaluate the stresses induced in the femur bone with different combination of body weight, length of bone, and body postures.

The numerical analysis has been done on the femur bone to investigate the stress distribution along the length of the femur bone. The femur bone is numerically investigated under the five familiar configurations obtained while performing successful deep squat. The bone properties are taken close to the human bone properties in the numerical analysis. The maximum deformation is observed at the superior femur and greater trochanter for all the postures. The maximum deformation is observed for the chair posture followed by knee bend and pre-squat postures. It could be due to the change of nature of axial and translating force components at contact surface of femur head inside the acetabulum cup.

The location of maximum stress in the femur bone vary based on the body posture. This non-uniform distribution of the stress along the femur bone is due to irregular geometry, the change of bone properties and the physical configuration of the femur bone viz., one end fixed and other is loaded. The maximum stress is observed at the “medial epicondyle” under the

standing posture. The knee-bend posture exhibits the maximum stress at the “patellar surface - close to lateral epicondyle”. The maximum stress is observed at the “patellar surface – close to medial epicondyle” under the chair posture. The maximum stress is observed at the “patellar surface - close to lateral epicondyle” under the chair posture. The maximum stress is observed at the “intercondylar fossa - just above the lateral condyle” under the chair posture.

The dry bone has been investigated experimentally to reveal the stress distribution along the femur bone as well as to estimate the stresses in critical locations of pelvis bone. The variation of stress with respect to body mass is noted to be independent. The higher body mass results high stress. The stress behavior with respect to the strain gauge location for critical body postures would be as follows.

$$\sigma_{SG4} < \sigma_{SG2} < \sigma_{SG3} < \sigma_{SG1}; \text{ \#standing posture;}$$

$$\sigma_{SG3} < \sigma_{SG2} < \sigma_{SG4} < \sigma_{SG1}; \text{ \#knee bend posture;}$$

$$\sigma_{SG3} < \sigma_{SG2} < \sigma_{SG4} < \sigma_{SG1}; \text{ \#chair posture;}$$

$$\sigma_{SG3} < \sigma_{SG2} < \sigma_{SG4} < \sigma_{SG1}; \text{ \#pre – squat posture;}$$

$$\sigma_{SG3} < \sigma_{SG2} < \sigma_{SG4} < \sigma_{SG1}; \text{ \#deep – squat posture;}$$

A mathematical model has been developed to predict the stress variation in the femur bone while performing the successful deep squat.

The magnitude of stress is relatively high in pre-squat posture while performing successful squat as well as standing activity. It is evident that, the stresses in femur head are insignificant as compared to the shank and neck portions of the femur bone. The neck portion experiences high stress as compared to femur shaft and femur head portions. In all three zones of the femur bone the compressive or tensile stress is noticed to be increased with the knee flexion till pre-squat posture. Further, the extension of the knee i.e., the standing-up activity exhibits more compressive or tensile stress than the sitting-down activity. The deep squat posture exhibits less stress as compared to pre-squat posture. On the other hand, the nature of the stress was also evaluated for complete duty cycle. When the knee flexion varies from 0 to 90°, the femur bone experiences compression stress. While the remaining portion from 90° to 155°, the femur bone experiences tensile stress.

ACKNOWLEDGEMENTS

I would like to express my deepest gratitude to my supervisor *Dr. Rahul S. Mulik* for pushing my ability limits to a great extent. I would never have been able to complete my research work without the invaluable guidance of my research supervisor *Dr. Rahul S. Mulik*. I would also like to express my special thanks to him for his excellent guidance and support during my Ph.D. work. He has always been a supportive and encouraging guide to me during the ups and downs of my research journey in past years. His guidance to me in my research work and career has always been precious and invaluable.

I would also like to express my gratitude to Chairman, Departmental Research Committee (DRC) and Chairman, Student Research Committee (SRC), *Dr. Navneet Arora*, SRC members *Dr. P. K. Jha* (Internal Expert) and *Dr. Vimal Kumar* (External Expert) for being supportive and providing their valuable suggestions to improve the quality of my research work.

I would like to express my gratitude to *Dr. S. P. Harsh*, *Dr. S. S. Arora*, *Dr. Tarun Goyal*, *Dr. Pavan Kankar* and *Dr. T. V. K. Gupta* for their valuable time during discussions regarding my work, for motivating and supporting me during my time of PhD.

I express my gratitude towards all the human subjects who invested their valuable time in data collection required in the PhD work and became the key factor towards completion of my research work. I am thankful to *Mr. Rohit Powel Joseph*, *Mr. Pranay Saxena*, *Mrs. Taru Saxena* and other physiotherapists, radiologists who were available to collect research related data in correct format. My deepest gratitude towards the human subject whose body parts were utilized in making this work successful. May his sole rest in peace.

I would also like to mention the support received from Ministry of Human Resources Development (MHRD), Government of India for providing research assistantship to carry on my research work smoothly.

I would like to recognize the support provided by *Mr. Jasbir Singh*, *Mr. Mohd. Idrish*, *Mr. Butaram*, *Mr. Pradeep Kumar*, *Mr. Madan Verma* and Lab technicians for their physical and mental contribution in developing the experimental set-up.

I express my deepest gratitude to my friend *Dr. Dubba Santhosh Kumar* for always being with me as a mentor during research discussions, for continuously motivating me in all successes and learnings during the PhD related work and for sharing my joy and pain throughout my journey in IIT Roorkee. I pay my regards to him for being supportive in all my tough times and being the universal solution of each and every problem related to research work.

I express my deepest gratitude toward my fellow researchers *Dr. Nav Rattan Kaushik, Mr. Jasbir Singh, Mr. Sharad V. Gaikwad, Mr. Umashankar Tripathi,* and *Mr. Ankit Rajkumar Singh* for their constructive suggestions/ideas in personnel as well as research and being with me during ups and downs.

I express my deepest gratitude toward *Mr. Daljit Singh* (Volleyball Coach, IIT Roorkee), *Mr. Arun Jakhmola* (Volleyball Coach, BEG Roorkee, Indian Army) for valuable time spent and for being supportive.

I am grateful to *Prof. Navneet Arora* for their love towards me and never let me go down under difficult times by enlightening me through his motivational lectures from the teachings of Late *Shri S. N. Agnihotri* (Devatma).

I am always pleased and grateful to be included in the joy of *Miss Rashmi Sharma, Mrs. Uma Thakur, Mr. Prayag Dixit, Mr. Somil Goswami, Mr. Luvkush Verma, Mr. Divyansh Patel, Mr. Om Namah Sharma, Dr. Aditya Sharma, Mr. Sandeep Chaudhary, Mr. Mahavir Sagwal, Dr. Rakesh Meena, Mr. Wajid Hussain, Mr. Sandeep Dhankad, Mr. Rohit Patel, Mr. Neeraj Upadhyay, Mr. Madhav Yadav, Mr. Chetan Dhiman, Mr. Sunil* and I would like to thank them for being part in my Ph.D. work.

My sincere thanks to batch mates and fellow researchers *Mr. Bhogadi Bhaskar Rao, Dr. Vinay Panwar, Dr. Avinash Chaudhary, Dr. Santosh Rathore, Dr. Rahul Goel, Mr. S. V. Sujith, Mr. Jayant Thakre, Dr. Nitin Simha Vihari, Mr. Naveen Kothapalli,* for their support, inspiration and love without which this work would not have been accomplished.

My sincere thanks to my family *Mr. Santosh Chandra Saxena, Mrs. Anita Saxena, Mr. Deepesh Saxena, Mrs. Anubha Saxena, Ms. Alpana Saxena Ms. Deepmala Chauhan* and all family members for the encouragement and support offered during my research work. Their trust in me strengthen me in this journey.

Finally, I would like to extend my heartfelt thanks to all the people who helped me in many ways to accomplish my work.

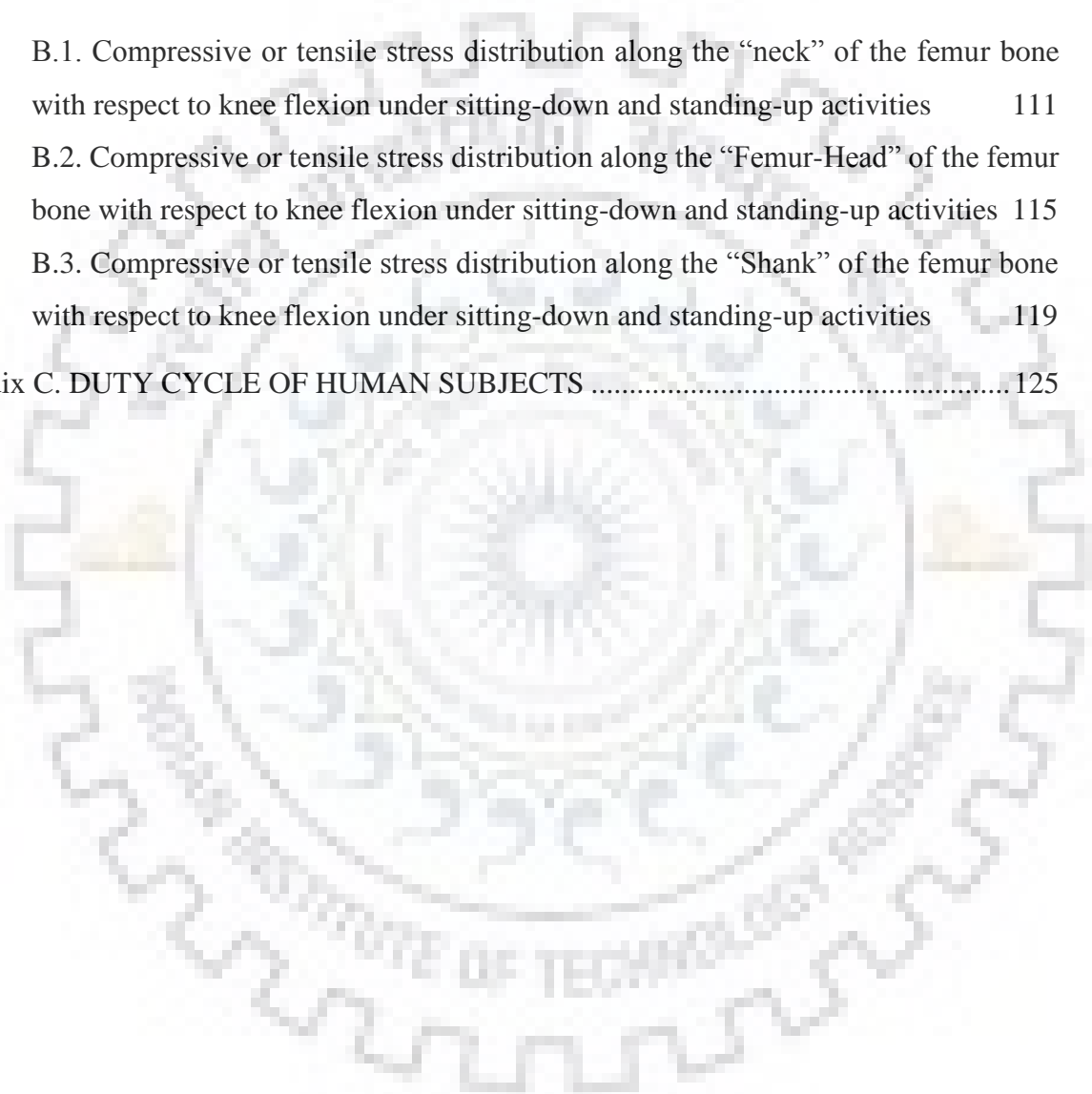
ANKIT SAXENA

ABSTRACT.....	i
ACKNOWLEDGEMENTS.....	iii
CONTENTS.....	v
LIST OF FIGURES	ix
LIST OF TABLES.....	xiii
NOMENCLATURE	xv
LIST OF PUBLICATIONS	xvii
1. INTRODUCTION	1
1.1. Anatomy.....	2
1.2. Geometry-terminology.....	4
1.3. Biomechanics	5
1.4. Kinetics	5
1.5. Hip joint	5
1.5.1 Bones and joints.....	6
1.5.2 Ligaments and Tendons	6
1.5.3 Muscles	7
1.5.4 Nerves	7
1.5.5 Blood Vessels.....	8
1.5.6 Bursa	8
1.6. Motivation.....	8
1.7. Thesis Overview.....	9
2. LITERATURE REVIEW	11
2.1. Research Gaps.....	35
2.2. Proposed research work	36
2.3. The Objectives	36
3. NUMERICAL METHODOLOGY.....	37
3.1. Numerical methodology.....	37
3.1.1 Boundary conditions	37
3.1.2 Free body diagram	38

3.1.3 Material definition	40
4. EXPERIMENTAL SET-UP	43
4.1. Experimental Test-Rig	43
4.1.1 Pelvis holder.....	44
4.1.2 Proximal femur holder	44
4.1.3 Distal femur holder	45
4.1.4 Horizontal guideway	45
4.2. Design Specifications and Considerations	47
4.2.1 Width of space	47
4.2.2 Length of the base	47
4.2.3 Maximum weight could be tested	47
4.3. Dry bone.....	48
4.4. Instrumentation	50
4.4.1 Strain gauge	50
4.4.2 Data logger.....	51
4.4.3 Weight measurement	52
4.5. Experimental Procedure.....	52
5. MATHEMATICAL MODEL.....	55
5.1. Mathematical model.....	55
5.1.1 Physical analogy	55
5.1.2 Kinematic constraints of individual links/joints:	55
5.1.2.1 Tarsus.....	55
5.1.2.2 Tibia.....	56
5.1.2.3 Femur.....	56
5.1.2.4 Pelvis.....	57
5.1.3 Development of Mathematical model.....	57
5.1.4 Operating Parameters.....	61
5.1.4.1 Tibia flexion/extension, θ_{1t}	61
5.1.4.2 Angular displacement of femur bone on xy-plane, θ_{2t}	61
5.1.4.3 Knee flexion/extension, φ	61

5.1.4.4 Time period, T	61
5.1.4.5 Length of the femur/tibia	62
5.1.4.6 Radius of the femur head, R	62
6. RESULTS AND DISCUSSION	63
6.1. Numerical model	63
6.1.1 Deviatoric stress	64
6.1.2 Total deformation	65
6.1.3 Location of max. stress and deformation	67
6.1.3.1 Standing posture	67
6.1.3.2 Knee bend posture	68
6.1.3.3 Chair posture	69
6.1.3.4 Pre-squat posture	70
6.1.3.5 Deep-squat posture	71
6.2. Experimental investigation	74
6.2.1 Strain distribution	74
6.2.2 Estimation of bone strength	78
6.2.2.1 Effect of location of strain gauge on stress	79
6.2.2.2 Effect of body mass on stress	83
6.3. Mathematical model	84
6.3.1 The geometry of femur bone	84
6.3.2 Time period of one duty cycle	85
6.3.3 Effective weight on the pelvis	86
6.3.4 Tibial flexion	87
6.3.5 Knee flexion	87
6.4. Summary	91
6.4.1 Implant design	92
7. SUMMARY, CONCLUSIONS AND FUTURE SCOPE	95
7.1. Summary	95
7.2. Conclusions	96
7.2.1 Numerical simulation	96

7.2.2 Experimental highlights	97
7.2.3 Mathematical prediction	97
7.3. Future Scope	97
REFERENCES	99
Appendix A. 3D CAD MODELS	107
Appendix B. DATA PLOTS.....	111
B.1. Compressive or tensile stress distribution along the “neck” of the femur bone with respect to knee flexion under sitting-down and standing-up activities	111
B.2. Compressive or tensile stress distribution along the “Femur-Head” of the femur bone with respect to knee flexion under sitting-down and standing-up activities	115
B.3. Compressive or tensile stress distribution along the “Shank” of the femur bone with respect to knee flexion under sitting-down and standing-up activities	119
Appendix C. DUTY CYCLE OF HUMAN SUBJECTS	125



LIST OF FIGURES

Figure 1.1 3D Photo graphic view of Pelvis and femur © Google.....	2
Figure 1.2 Hip implant being used in hip arthroplasty ©Google	3
Figure 1.3 Different anatomical planes (Kirkwood et al., 2007).....	4
Figure 1.4 The kinematic linkage (ball-socket joint) between the femur bone and pelvis bone to form a hip-joint ©Google	6
Figure 1.5 Ligaments of hip-joint ©Google.....	7
Figure 2.1 The deep flexion activities: (A) deep kneeling position in double leg motions, (B) rising/descending phase in double leg motions, (C) kneeling position in single leg motions, and (D) rising/descending phase in single leg motions.....	24
Figure 2.2 (a) Movement of foot in about three axes (lateral view, left foot) (b) Motion of orthosis about three axes (c) fabricated club foot orthosis (Khas et al., 2018)	27
Figure 3.1 A discretized 3D CAD model of a femur.....	37
Figure 3.2 An isometric view of a femur showing the orientation towards squat with respect to global coordinate system	38
Figure 3.3 Free body diagram of the femur for different posture styles (a) Standing (b) Knee bend (c) Chair (d) Pre-squat (e) Deep squat	40
Figure 3.4 Defining the properties of femur based on the inner structure of a human bone	42
Figure 4.1 Photographic view of an experimental set-up	43
Figure 4.2 Photographic view of ‘pelvis holder’	44
Figure 4.3 Photographic view of ‘proximal femur’ holder.....	45
Figure 4.4 Schematic view of an experimental set-up.....	46
Figure 4.5 Dry bone set.....	48
Figure 4.6 Strain gauge used for measuring strain (BKNIC-20).....	50
Figure 4.7 Strain gauge connection	51
Figure 5.1 Path traced by hip-joint while performing a successful deep squat	56
Figure 5.2 Kinematic movement of a Human hip-joint under deep squat posture	58
Figure 5.3 Kinematic constraints of a Human hip-joint with different knee flexion.....	59
Figure 6.1 Stress boundary conditions.....	63

Figure 6.2 Effect of loading on Distortion stress for different postures of the body.....	65
Figure 6.3 Effect of loading on Deformation	66
Figure 6.4 Total deformation in a femur bone with knee flexion under different body postures (M = 60 kgs)	67
Figure 6.5 Location of maximum stress for different posture	68
Figure 6.6 Total deformation in a femur bone with knee flexion under different body postures (M = 60 kgs)	68
Figure 6.7 Location of maximum stress for different posture	69
Figure 6.8 Total deformation in a femur bone with knee flexion under different body postures (M = 60 kgs)	69
Figure 6.9 Location of maximum stress for different posture	70
Figure 6.10 Total deformation in a femur bone with knee flexion under different body postures (M = 60 kgs)	71
Figure 6.11 Location of maximum stress for different posture	71
Figure 6.12 Total deformation in a femur bone with knee flexion under different body postures (M = 60 kgs)	72
Figure 6.13 Location of maximum stress for different posture	72
Figure 6.14 Variation of magnitude of strain with respect to knee flexion and location of strain gauge for different body weights	77
Figure 6.15 Stress distribution above the convexity of ‘Pelvis bone’ – Opposite wall of Acetabulum cup, under different body configurations	79
Figure 6.16 Stress distribution at Metaphysis femur shaft – Near Trochanters, under different body configurations.....	80
Figure 6.17 Stress distribution at Diaphysis femur shaft – Minimum cross section area, under different body configurations.....	81
Figure 6.18 Stress distribution at distal femur – Just above the Condyles, under different body configurations.....	82
Figure 6.19 Change of angular velocity of ‘tibia’ with time step for one complete duty cycle of successful deep squat	87
Figure 6.20 Change of angular velocity of ‘femur’ with time step for one complete duty cycle of successful deep squat	88
Figure 6.21 Stress distribution along the “Femur head” with respect to knee flexion during one working cycle of successful deep-squat	89

Figure 6.22 Stress distribution along the “Neck” with respect to knee flexion during one working cycle of successful deep-squat	90
Figure 6.23 Stress distribution along the “Diaphysis femur shaft – Minimum cross section area” with respect to knee flexion during one working cycle of successful deep-squat	91
Figure A.1 Meshing and Discretization.....	107
Figure A.2 Load configuration in standing posture	107
Figure A.3 Load configuration in knee bend posture	108
Figure A.4 Load configuration in chair posture	108
Figure A.5 Load configuration in pre-squat posture.....	108
Figure A.6 Load configuration in deep-squat posture	109





LIST OF TABLES

Table 1.1 Terminology used in the present study, Hamilton, (2011); Nigg et al., (2000)	3
Table 2.1 Kinetics and kinematics of lower extremity of the human body	28
Table 3.1 The component forces of a resultant force with respect to knee flexion angle	39
Table 3.2 Physical properties of femur Yousif & Aziz, (2012).....	41
Table 4.1 Specifications of the Femur bone	49
Table 5.1 Range of operating parameters	62
Table 6.1 Details of location of strain gauges	75
Table 6.2 Increase of magnitude of stress according to the location of the strain gauge	83
Table 6.3 The factorial design of simulation of mathematical model	85
Table C.1 Details of human subjects and time period (1-DC) to perform deep squat	125



NOMENCLATURE

Symbol	Description	Greek letter	Description
r	Length of the tibia bone, mm	μ	Dynamic viscosity, Pa-S
l	Length of femur bone, mm	ρ	Density, kg m ⁻³
m	Mass, kg	ϑ	Kinematic viscosity,
a	Acceleration, m.S ⁻¹	θ	Angular displacement, rad
F	Force, N	ϕ	Knee flexion, rad
f	Frequency, cycles.S ⁻¹	ω	Angular velocity, rad.S ⁻¹
R	Resultant force, N	σ	Normal stress, kPa
t	Time, Sec	τ	Shear stress, kPa
K	Knee	Subscripts	Description
E	Young's modulus, GPa	1	Tibia angular displacement
G	Rigidity modulus, GPa	2	Femur angular displacement
k	Constant	Max	Maximum
T	Time period, Sec	Up	Standing up
x	X-coordinate	Down	Sitting down
y	Y- coordinate		



LIST OF PUBLICATIONS

1. Ankit Saxena & Rahul S. Mulik, Evaluation of Failure Stresses in a Femur under Progression of a Successful Squat with Different Body Weights: A Position Analysis Study, 7th International Conference on “Experiments / Process / System / Modeling / Simulation / Optimization” (7th IC-EpsMsO), July 5-8, 2017, Learning foundation in Mechatronics, Athens, Greece.
2. Ankit Saxena & Rahul S. Mulik, Analytical evaluation of mechanical strengths associated with material properties of a femur bone in response to daily activities, International workshop on nano/micro 2d-3d fabrication, manufacturing of electronic – biomedical devices & applications (IWNEBD-2018), 31st October-2nd November, 2018, IIT Mandi.
3. Ankit Saxena & Rahul S. Mulik, “Kinematic Analysis of a femur and pelvis bone to evaluate the stresses with different knee flexion”, Part H: Journal of Engineering in Medicine. (Communicated)







1. INTRODUCTION

The traditional engineering approaches are being used to analyze the biological systems as a part of biomechanics. This assists to give correct approximations to the mechanics of many biological systems through the concepts of Newtonian mechanics and/or material sciences. On the other hand, structural analysis, kinematics and dynamics play prominent roles in the study of biological systems using traditional engineering science Holzapfel Gerhard & Ogden ray, (2009). Certainly, man-built systems evolved based on the standard theories and therefore easy to analyze such systems. While the biological systems are structured through many irregularities, which are complex to analyze with the existing standard theories. Therefore, numerical methods and mathematical concepts are applied in biomechanical study. These methods are used to simulate the actual biological systems through some appropriate assumptions.

The researchers have been working in the field of biomechanics to reveal the mechanical failures of the biological systems. The mobility and strength restore of a hip joint is always being a challenge to the biomechanical engineering community. The mobility of a biological system depends on the kinematic constraints, even before and after surgery. The kinematic constraints would be directly related to the type of joints and links. On the other hand, it is also essential to understand the joint reaction forces occurred from daily activities and the body weight as well. Thereby the stress and deformations in the bones would also be evaluated. These stresses and deformations would give better understanding of mechanical behavior of a biological system. Therefore, the researchers are being consistently working in the field of biomechanics to reveal the mechanical stresses and deformations under different configuration of the biological system. As a part of that, the present study focused to understand the mechanical behavior of human hip-joint. The first performed hip replacement surgery is one of the most successful operations in all of medicine in 1960. Since 1960, improvements in joint replacement surgical techniques and technology have significantly improved the effectiveness of total hip replacement. However, the mechanical stresses in femur bone and acetabulum is still to be examined.

The mobility of a typical hip joint is analogues to a simple lower pair with degrees of freedom of three (rotational) Arnold et al., (2010). Human hip has highest degrees of freedom after the shoulder joint. It is also the joint with maximum stability with mobility. Common causes of failure of natural hip joint are arthritis, fracture and avascular necrosis Margo et al., (2003). Focus of research on hip joint is to explore the reasons of failure of joint Hefzy et al.,

Introduction

(1998), develop a suitable prosthesis Judet & Judet, (1950); Papagiannis et al., (2016) and analyzing the problems after hip arthroplasty Heckman, (2008); Lamontagne et al., (2012).

1.1. Anatomy

The hip is one of the body's largest joints as shown Figure 1.1. The kinematic structure of hip-joint is a ball-socket joint Anderson et al., (2010); Arnold et al., (2010). Certainly, the socket is formed by the acetabulum and the ball is simple femoral head. The acetabulum and femur head are the portions of the large pelvis bone and upper end of the femur respectively. The bone surfaces of the femur head and acetabulum are covered with articular cartilage. The cartilage is smooth tissue that cushions the ends of the bones and allows them to move easily.

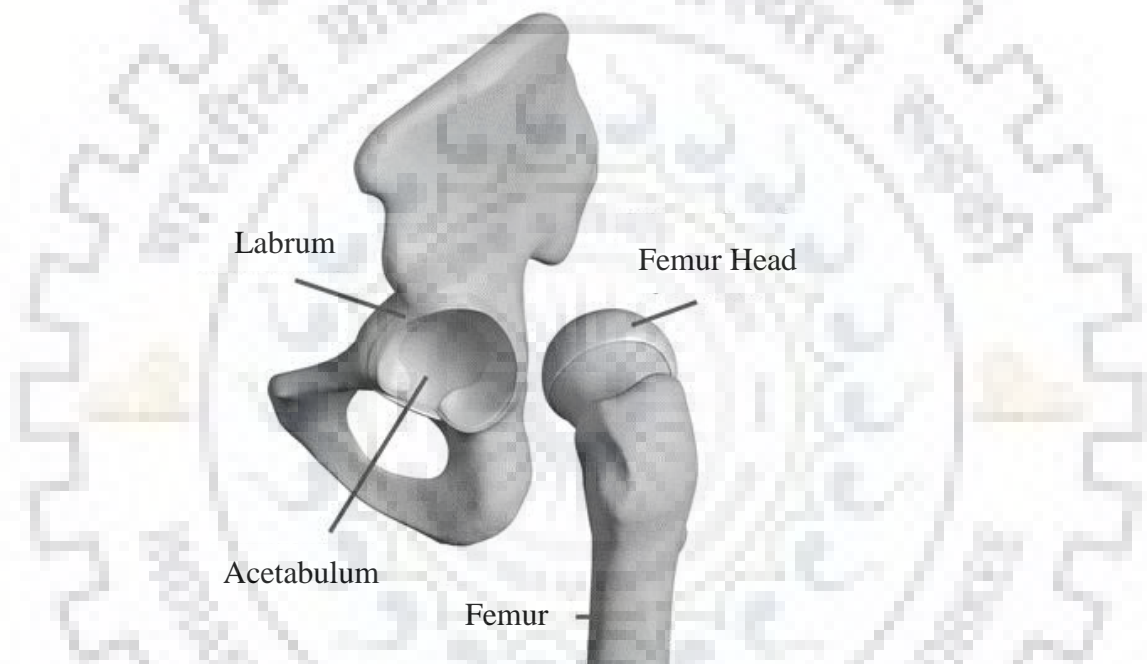


Figure 1.1 3D Photo graphic view of Pelvis and femur © Google

A thin tissue called synovial membrane surrounds the hip joint. The function of synovial membrane, in a healthy hip, is to produce small amount of fluid that lubricates the cartilage and allows free movement of the hip joint without any friction. Ligaments are the tissues that connects the femur head inside the acetabulum and provide stability to the joint. However, the hip replacement surgery would not ensure synovial membrane and ligaments to exist to retain the exact mobility of a biological system. Therefore, a hip implant as shown in Figure 1.2, was introduced and being used over the decades in hip replacement surgeries.

Introduction

Table 1.1 Terminology used in the present study, Hamilton, (2011); Nigg et al., (2000)

Geometrical appellation	Description
Anterior	toward the front
posterior	toward the rear
superior means	toward or closer to the head
inferior	closer to the feet
medial	refers to a location closer to the midline of the body
lateral	refers to a location away from the midline
proximal	nearer to point of observation
distal	away to point of observation

Biomechanical knowledge of magnitude and type of stresses developing at hip is important for designing a successful hip prosthesis. A finite elemental analysis was carried out to reveal the stress and strains of the femur, thigh muscle forces and contact forces at joints by Duda et al., (1998); Nareliya, (2011) investigated stress distribution, total deformation and fatigue failure of femur for a healthy male of 75 kg weight. The biomechanical behavior of the human femur bone has been revealed using FEM Chowdhury & Kumar, (2013); Yousif & Aziz, (2012).



Figure 1.2 Hip implant being used in hip arthroplasty ©Google

The model helps in evaluating the segmental masses, acceleration, joint centers and moment of inertia acting at various joints. Arnold et al., (2010) inspected the force and moment generation capacities of muscles about the ankle, knee, and hip with specified ranges of -30-20° ankle dorsiflexion, 0-100° knee flexion, -20- 90° hip flexion, and -40-10° hip adduction

Introduction

Hamilton, (2011); Nigg et al., (2000). A FEM analysis of proximal human femur was carried out to understand the characteristics of typical femur under physiological load conditions by Shireesha et al., (2013). A comparative study revealed that, Ti-6Al-4V (Titanium alloy) undergoes less deformation on static loading. The total deformation, equivalent Von Mises stress, maximum principle stress, fatigue tool and percentage variation in femur were determined by Francis et al., (2012). There are no standard formulations universally, which can explain the nature and magnitude of femoral stresses during squat described by Nagura et al., (2002a); Nareliya, (2011). This has led authors to work on finite elemental analysis of a femur while performing a squat. The numerical simulation has been performed on a 3D CAD model of a femur to obtain the resultant stresses. The dimensions of computed model are ≈ 470 mm in length, femur head diameter ≈ 46.5 mm. This simulation has been carried out for different positions of femur from standing to squatting.

1.2. Geometry-terminology

Human body and its movements can be described by three dimensional coordinate system formed by three anatomical planes Holzzapfel Gerhard & Ogden ray, (2009) as shown in Figure 1.3.

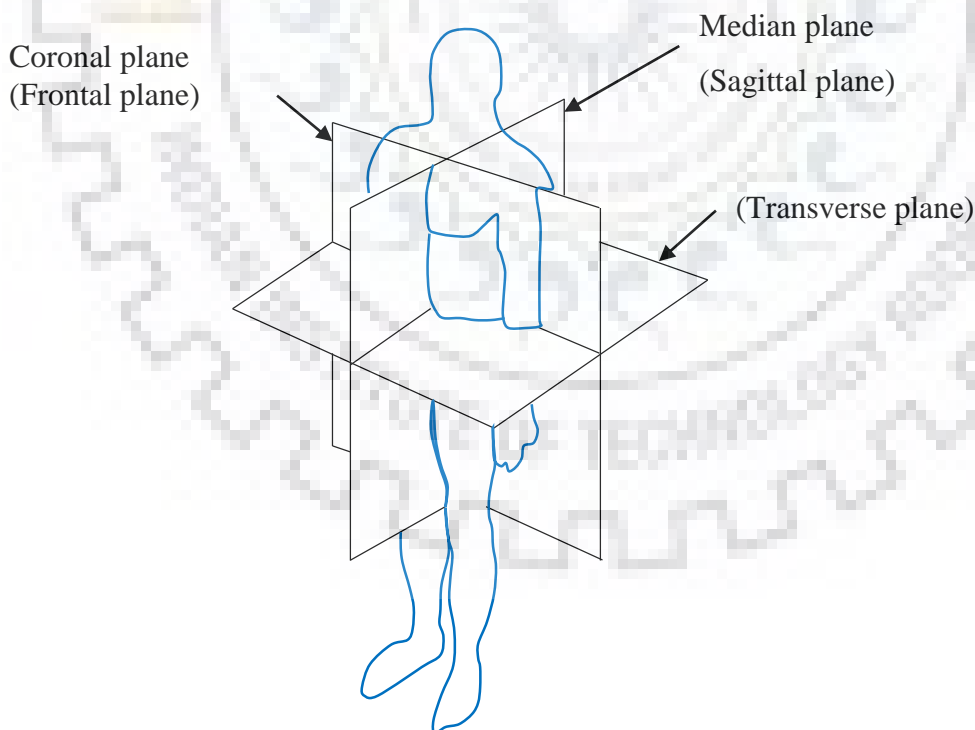


Figure 1.3 Different anatomical planes (Kirkwood et al., 2007)

Sagittal plane: Passes through center of body to divide the body in left and right halves

Coronal plane: Passes through center of body to divide the body in front and back portion

Introduction

Transverse plane: Passes through center of body to divide the body in upper and lower parts

Standard geometrical appellations are used in the present study. Table 1.1 describes the terminologies used throughout the work.

1.3. Biomechanics

Biomechanics of the human movement is an interdisciplinary area which describes, analyzes and assesses the movement of an individual animal. The history of analyzing human joint mechanism takes us to Aristotle who studied the motion and gait (rate of moving) of humans and animals. The combined effect of contraction and relaxation of ≈ 600 muscles present in human body generates adequate amount of force to perform any physical activity. Each activity is defined by the central nervous system (instructor) and musculoskeletal system (follower). The human central nervous system decides the most optimal combination of muscles to perform task, thereby, the musculoskeletal system would be a highly flexible and efficient system. When a trauma provokes some dysfunction of certain part of a system, the functioning of whole neuromuscular system is hindered. This limits the routine movement of the body. The effect and cause of movement are studied under separate branch called as kinematics and kinetics.

1.4. Kinetics

Kinetics is the branch of mechanics concerned with the forces that cause motions of bodies. Force momentum, ground reaction forces, power and mechanical work performed by joints are kinetic variables needed to be studied for strength, fixation, wear and friction of prosthesis for optimizing their design and materials. Force momentum portrays collective strengths by muscles, tendons, ligaments and bones to counter the external forces acting on our body. Muscles always contract either concentrically or eccentrically. Concentric contraction indicates positive work since muscles generating energy into the system while eccentric contraction indicates negative work since muscle absorbs energy from the system.

1.5. Hip joint

The hip joint is diarthrosis joint analogous to ball (femur head) and socket (acetabular cup) joint. The hip joint allows large range of motion to perform routine activities like walking, stair climbing, stair down, running, jumping etc. and complex activities like kneeling, squatting, sitting cross leg etc. Hefzy et al., (1998). Femur is the longest bone and second in bearing the load. The physical structure and the kinematic motion is described by the other important parts viz., ligaments, bones, muscles, etc. The details of vital parts of hip-joint are explained below.

Introduction

1.5.1 Bones and joints

The hip-joint is combination of the femur bone and pelvis bone as shown in the Figure 1.4. The proximal femur has a shape similar to ball and called as femoral head. The femoral head fits into a circular shaped socket on the side of the pelvis known as acetabulum. This femoral head is connected to the long femur shaft by a short section of bone called the femoral neck. Greater trochanter is a large bump located at the side of hip next to the femoral neck. Greater trochanter connects with important muscles that enables the femur to move for performing daily activities. One such muscle is the gluteus medius. It is a key muscle for keeping the pelvis level as you walk.

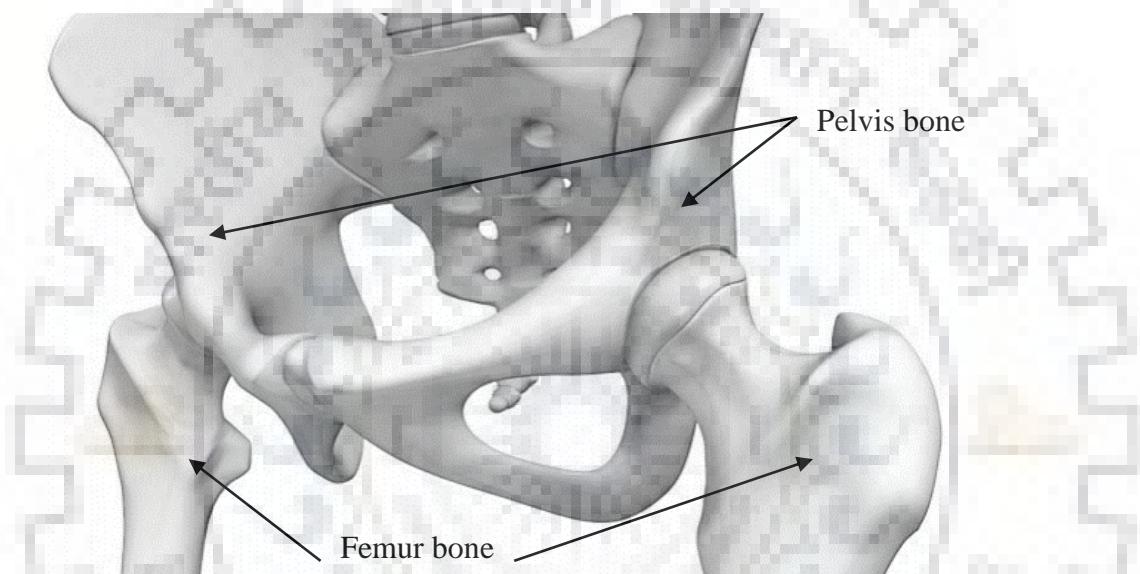


Figure 1.4 The kinematic linkage (ball-socket joint) between the femur bone and pelvis bone to form a hip-joint ©Google

1.5.2 Ligaments and Tendons

There are several vital ligaments in the hip to make a balanced posture of the human body as shown in Figure 1.5. Ligaments are soft tissue structures. They connect one bone to other. Ligaments surrounds the joint with a watertight sac. Three ligaments connects the femoral head to acetabulum cup to cover the hip joint. These ligaments would lead to a stable body posture. They help to hold the hip in place. Ligamentum teres is a trivial ligament that connects the tip of the femoral head to the acetabulum. However, it does not control hip movement like the main hip ligaments. Certainly, it has a small artery within the ligament that brings a very small blood supply to the femoral head. A long tendon iliotibial band runs side by side the femur from the hip to knee which connects the several hip muscles. A rigid iliotibial band might may cause the hip and knee problems. Labrum is another ligament inside the hip with a unique structure. The

Introduction

labrum is attached almost completely around the edge of the acetabulum. The structure of the labrum assists to provide a deep socket to hold the femur head. This small rim of cartilage might be damaged and causes pain.

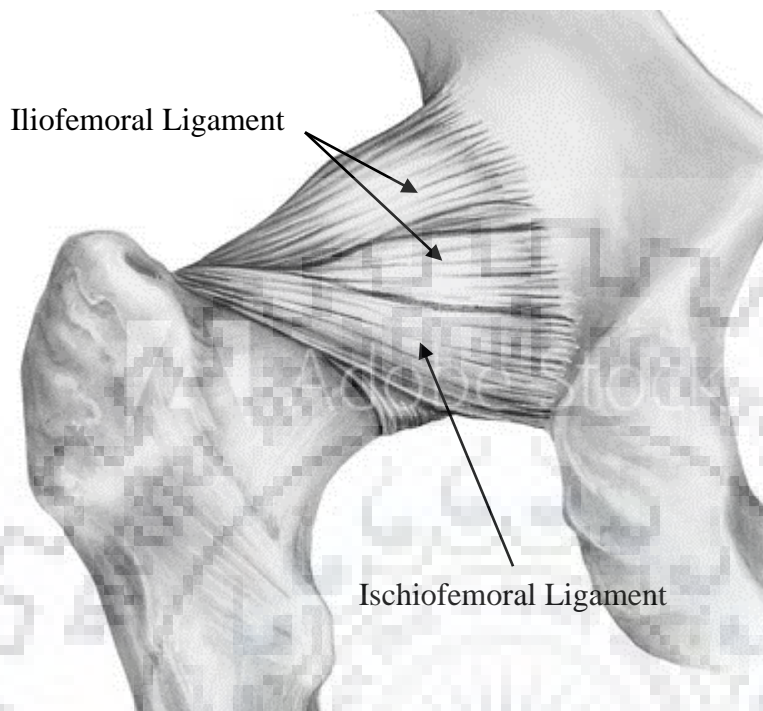


Figure 1.5 Ligaments of hip-joint ©Google

1.5.3 Muscles

The hip is surrounded by powerful thick muscles. Subsequently, the gluteal form up the muscles of the buttocks on the back of the hip. The inner thigh is formed by the adductor muscles. The key role of the adductors is to pull the leg in medial direction i.e. towards the other leg. The muscles that flex the hip are located at the anterior portion of the hip joint. Iliopsoas muscle is one such flexor muscle. This muscle initiates in the distal back and pelvis and connects the inside edge of the upper femur. Rectus femoris is another hip flexor muscle. The rectus femoris is one of the quadriceps muscle, which is the largest group of muscles at the anterior portion of the thigh. Lastly, the hamstring muscles initiates from the bottom of the pelvis and run down the back of the thigh. Hamstring muscles runs from the posterior hip to knee helps in extending the hip by pulling it backwards.

1.5.4 Nerves

Entire human body nerves travel down the thigh pass by the hip. The vital nerves are the femoral nerve in front and the sciatic nerve in back of the hip. Obturator nerve are small nerves that passes the hip. The function of the nerves is to carry the signal from brain to the muscles

Introduction

of hip for required movement. Another function of the nerves is to carry the signals back to the brain about sensations such as touch, pain, and temperature.

1.5.5 Blood Vessels

The large vessels travel with nerves, supply the lower limb with blood. The large femoral artery begins within the pelvis. It passes by the anterior hip and pull down toward the inner edge of the knee. Blood vessels could be felt by touching the anterior thigh. Pulsing of large artery is easily recognizable. The femoral artery has a deep branch named, “profunda femoris”. The profunda femoris sends two vessels that passes through the hip-joint capsule. These vessels provides the blood supply to the femoral head. The ligamentum teres contains a small blood vessel that provides supply of blood to the superior femoral head. Other small vessels originates within the pelvis and supply the blood to the back portion of the buttocks and hip.

1.5.6 Bursa

A bursa is a tiny sac of tissue that contains fluid to lubricate the portion in order to reduce friction. The body produces bursa wherever friction between surfaces occurs. A bursa is sandwiched between the greater trochanter and the muscles and tendons that cross over the greater trochanter. All these parts collectively respond or get affected for any type of motion and body posture. Amongst them squat or sitting on heel position is a complex body posture which is very commonly found in the Indian subcontinent or south Asian population.

1.6. Motivation

The squat is one of the most commonly used exercises in the arena of weightlifting and power lifting Schoenfeld, (2010). It is also a routine sitting posture for south Asian subcontinent people in their daily life activities Acker et al., (2011). Farmer sowing/harvesting fields, person washing clothes, utensils, cleaning floor, sitting cross legged on the ground for eating, Asian sitting position in toilets are few examples of the postures very common for the residents of Indian subcontinent. On the basis of degree of flexion of knee, squat can be categorized in three groups. Partial squats at more than 40° knee angle, half squats at about 70° to 100° and deep squats greater than 100° Judet & Judet, (1950); Papagiannis et al., (2016). During the squat, hip flexion rises which is followed by hip torques. The highest torque occurs near the bottom segment of movement. Gluteus Maximus (GM) and the hamstrings (one of the tendons at the back of the knee) are the primary parts which involved in squat. The GM is a powerful extensor which when acts eccentrically and controls downward movement during squat while acts

Introduction

concentrically to resist the upward movement during squat. Load varies at different positions as per the behavior of the muscles.

The common position of loads are low bar back squats with the bar somewhat below the level of acromion (the outermost point of the spine of the shoulder blade), high bar back squats with the bar slightly above the level of the outermost point of the spine of the shoulder blade, and front squats with the bar held in front of the chest at the clavicle (one linking the scapula and sternum) Heckman, (2008); Lamontagne et al., (2012). Since, trunk has a superior forward inclination, the low bar position has been shown to produce larger hip extensor torque while high bar squat produce lesser knee extensor torque Judet & Judet, (1950); Papagiannis et al., (2016). This translates into reduced patellofemoral compression and anterior cruciate ligament (ACL) strain in the low bar squat. Front squats generates lesser maximal joint compressive forces at the tibiofemoral joint. Front squats has reduced lumbar stress as compared with back squats, with small variation in shear forces (Heckman, (2008); Lamontagne et al., (2012)). This was accomplished without compromising muscle activity in the quadriceps and hamstrings. Front squats may be a better alternative than back squats in the case of ligament or meniscal injuries. Also, the front squat may isolate the quadriceps to a greater degree than the back squat, making it a possible choice to optimize development of the frontal thighs in comparison with the gluteal muscles.

1.7. Thesis Overview

The Thesis work has been presented in seven chapters which are discussed as follows in brief

Chapter 1: This chapter presents an introduction, the anatomy of hip joint, general terminologies used throughout the thesis, biomechanics and kinetics involved, brief information about various parts that characterize the hip joint. At the last, motivation of the research with thesis overview has been discussed in brief.

Chapter 2: This Chapter provides detailed study of the literature review on the biomechanics of hip joint, knee joint, force and momentum involved in hip movement during routine activities. The research gaps have been highlighted at the end of the review and the possible opportunities have also been identified. Based on the literature review and research gaps, a suitable problem has been formulated.

Chapter 3: The chapter describes the numerical methodology employed in the present work. The procedure of load applications and distribution as per the orientation of the CAD model has been described using free body diagram of the femur bone performing a successful squat.

Introduction

The boundary conditions incorporated and material properties of the CAD model has been discussed here.

Chapter 4: This chapter explains the fabrication of experimental test rig. In this chapter, various parts of the test rig are discussed separately. Design specification and test section are discussed and the detailed procedure of conduction experiments has been discussed. Specifications of the dry bone used in the study and various instruments utilized are also explained in the chapter.

Chapter 5: This chapter explains the development of mathematical model for the validation of numerical and experimental work. Chapter explains human bones as kinematic links through which load is transferred. Range of motion of kinematic links, resultant force against the body weight for a successful squat has been discussed. Chapter explains the stress generation in the hip joint while completing a squat gait cycle.

Chapter 6: This chapter explains the results obtained from numerical analysis, experiments and mathematical model. The chapter includes discussion regarding the common trend obtained in three methods which explains the pre squat posture is the critical posture for evaluation of design criterion for artificial implant. The chapter suggests the design criterion and materials to fabricate an artificial hip implant for south Asian population who frequently makes squats in routine activities.

Chapter 7: This chapter includes summary of individual chapters with overall conclusions from the present work. Also, it discuss about the future scope of the work.

2. LITERATURE REVIEW

The field of biomechanics is being an attractive to the researchers because of the complex problems related to human operational challenges. It ranges across the several biological system categories viz., physiology (with a special focus on the musculoskeletal, cardiovascular, respiratory, and digestive apparatuses), pathology (orthopaedics and traumatology, maxillofacial surgery, dentistry Kumar et al., (2018); Sharma et al., (2019) and orthodontistry Nayak, Jain, Kankar, et al., (2019); Nayak, Kankar, et al., (2019), cardiovascular and respiratory surgery), forensics (accident reconstructions, crime scene investigation), vehicle safety (car safety, helmets), ergonomics and workplace safety, defense and social security (combat and law enforcement protection, effectiveness of projectile weapons), and sport (performance optimization, protection devices) Duda et al., (1998); Nareliya, (2011).

Pinilla et al., Hospital, (1996) determined experimentally the influence of impact direction on failure load and fracture patterns of the elderly proximal femur. They claimed that impact direction is independent to bone mineral density for failure of femur. Authors also found that for a longer neck axis length, failure load rises. They showed that even a trivial variation in the line of action of impact force due to fall significantly modifies the failure load of the proximal femur.

The Wallis device is an interspinous prosthesis that is used to stabilize dynamic lumbar. The implant is proposed to enhance the stability of the treated intervertebral lumbar segment without affecting its mobility and local lordosis. Zaoutsos & Iakovakis, (2010) studied the Wallis device with mechanical point of view in order to provide rigidity and support loading from human body and action. Authors examined three types of materials experimentally in order to achieve a material optimum selection and improvement of the mechanical response of the implant. A numerical analysis of the Wallis system was also performed in terms of a given simulated mechanical loading and its response under this loading is investigated. The study proposed an alternative configuration of the Wallis device for further investigation. The results concerning the mechanical response of Wallis occurring from experimental testing and numerical analysis were encouraging in its use in the proposed biomedical application.

Politis et al., (2013) analyzed the strain patterns for variety of neck by using a modular neck prosthesis implanted in composite femur. The experiments result higher stress at anterior surface in the case of anteverted neck combinations and at posterior surface in retroverted neck case. Thus anteverted neck combinations are more prone to anterior thigh pain. Authors also verified the universal agreement that compressive stress was higher at calcar portion of the

Literature Review

femur and aggravated by the use of varus neck. In this article different types of modular neck combinations were experimented on the same composite femur. A custom-built fixture designed to reproduce loading conditions during the single-leg stance phase of walking. The femur was tilted in to 12° of valgus and was positioned neutral on the sagittal plane. Three 350Ω triaxial rosette strain gauges were mounted on transtrochanteric portion. Three 350Ω uniaxial strain gauges at the femur shaft below the lesser trochanter. The position of strain gauges was checked constant with the use of a phantom femoral model.

Birnbaum & Pandorf, (2011) calculated the hip centralizing forces of the iliotibial tract along the femoral neck which further transfers to femoral head and consequently to acetabulum. The study predicts the effects of changing forces on femoral head inside the acetabulum after hip dysplasia with a varus or valgus centrum collum diaphysis (CCD) angles of the femoral neck. The authors assessed that the forces on the femoral head decreases with reducing CCD angles i.e. from valgus ($155^\circ = 2422\text{N}$) to physiological ($128^\circ = 2360 \text{ N}$) to varus ($115^\circ = 1601 \text{ N}$) while the hip centralizing forces of the iliotibial tract on the surface of greater trochanter varies contrary i.e. increases from valgus (438 N) to physiological (655.5 N) to varus (997 N). CCD angle is the projection of the angle between diaphysis (femoral shaft) and the femoral neck onto an X ray image. CCD angle decreases with age. The total hip force resulting from all applied forces was 2360 N. Its line of action was parallel to the femoral neck axis.

Lutz et al., (2016) introduced a new approach for computing lower extremity muscle forces that minimize femoral bending. The new approach incorporates constraints in form of mathematical equations that consider “bone structure” and “prevention of bending by load reduction” in to conventional method that considers “minimal total muscular force”. The new approach introduced here being supported by equations for evaluating muscular force resulted in more accurate femoral stress-strain patterns. Muscle forces counteract gravitational forces (body weight) without exerting moments around the x and y axis of the femoral diaphysis (femoral shaft portion).

Pandey, Mahapatra and Kumar, et al., (2018b) determined the effects of diffusible hydrogen content on the flexural strength, lower critical stress, and tensile strength of P91 steel welds with respect to several electrode conditions. In the study, the axial stress and transverse stress were measured using the blind hole drilling method for dissimilar situations of welding consumable. The maximum value of residual stresses had been stated at the mid of the weld fusion zone. The diffusible hydrogen content was not observed to have any noticeable effect on the residual stresses. The revised residual stress values have also been predicted by considering the plasticity-induced error.

Literature Review

Giri et al., (2015) measured residual stress by using strain gauge rosette by blind hole drilling technique which is related with plastic deformation of material that is removed from hole. The study also measured the stress concentration effect of multipoint cutting tool. The study describes the plasticity and stress concentration effects of blind hole drilling technique on the measurement of residual stresses. The results from strain gauge rosettes in case of uniaxial loading were explored experimentally through tensile testing and in case of biaxial loading through numerical modeling.

Pandey, Mahapatra, & Kumar, (2018) measured the residual stresses in welded pipe using blind hole drilling technique. The residual stress quantification was done by using the strain gauge rosette. The rosette was associated with the plastic deformation of material and stress concentration effect of multi-point cutting tool. Strain gauge output was calculated by tensile testing for the uniaxial loading. For biaxial loading FEM was used. The corrective formulation was established for estimation of the corrected value of residual stresses from the measured strain values.

Pandey, Mahapatra, Kumar, et al., (2018a) examined the effect of different kind of notch geometry, notch depth and angle on mechanical properties with varying “strain rate”. In quasi-static rates, the P91 steel presented a positive strain rate sensitivity for 1 mm notch depth with constant rate of strain. It was observed that notch strength and fracture toughness increases with the increase in notch angle from 45 to 60. The highest value was found in U-type notch. Other two parameters viz notch angle and notch depth has a negligible effect on P91 steel strength and fracture toughness.

Hara et al., (2016) quantified the dynamic hip kinematics for four popular activities (viz. walking, chair rising, squatting and twisting) in the subjects with osteoarthritis hip disorders just before total hip arthroplasty. The authors revealed OA subjects were unable to flex their femur bones deeply because of limited range of movement of the hip joints, and they have to tilt their pelvises more posteriorly to make a successful squat posture. A limited range of hip flexion could persist even after THA, which could affect postoperative functional results during routine work, specifically the postures which require deep flexion. Subjects’ function and ability are directly affected by joint kinematics.

Hara et al., (2014) analyzed dynamic hip kinematics during routine activities (like walking, chair rising, squatting and twisting) over six human subjects. The authors in the present study revealed kinematics of healthy hip joints with corresponding pelvic and femoral dynamic movements for routine human activities. The maximum hip flexion angles observed for walking, chair rising and squatting were 29.6°, 81.3°, and 102.4°, respectively. The pelvis was

Literature Review

tilted anteriorly around 4.4° on an average for full gait cycle of walking. The maximum anterior/posterior pelvic tilt averaged $12.4^\circ/11.7^\circ$ and $10.7^\circ/10.8^\circ$, for chair rising and squatting activities respectively. Hip flexion is highest for the movement due to further anterior pelvic tilt while performing chair-rising and squatting. For twisting, the highest absolute value of hip internal rotation and external rotation are 29.2° and 30.7° respectively. Kinematics' data for daily activities provide significant insight to evaluate kinematics of pathological and reconstructed hips.

Femoral fractures were predicted by Keyak & Rossi, (2000) in their study based on finite element model developed from computer tomography scan images. They examined nine stress and strain based failure theories, out of them six predicts tensile and compressive strengths of the material. All the nine theories were examined in two load configurations viz. load transfer at hip joint while single limb stance and impact load due to fall. Authors claimed that distortion energy and maximum shear stress failure theories were the two most effective theories for evaluating the performance of femur for two very different loading conditions. The observation supports the hypothesis that distortion energy and maximum shear stress theories are the most robust for femoral fracture analysis.

Hamai et al., (2009) analyzed dynamic knee kinematics for medial osteoarthritis during kneeling, squatting and stair climbing. The study demonstrated the variability in knee mechanics for healthy and medial osteoarthritis (OA) case and also evaluated the medial OA for different activities. Bone-fixed coordinate systems and CT-based bone model surfaces were used to obtain 3D joint kinematics and contact locations. Authors observed femoral external rotation gradually increased with flexion for squatting and kneeling, and gradually decreased with extension for stair climbing in medial osteoarthritis knees. Authors displayed a femoral internal rotation bias of about 8° for medial OA knees compared to normal knees and femoral external rotations of 4° (during 20° to 100° flexion) and 15° (during 100° to 120° flexion) while squatting with medial OA knees compared to 12° and 24° observed in normal knees.

Vishvesha et al., (2017) forecasted the welding distortion for a complex welded structure. For huge and complex welded structures, the thermo-mechanical elasto-plastic investigation can be computationally prohibitive. Further, simplistic butt and T-joints, this distortion prediction technique is not suitable to accommodate reliable results when applied to large complex 3-D welded structures. Hence, inherent strain method is proposed here to predict distortion. They have used inherent "strain based technique" for the aforementioned welded structure in elastic finite element analysis for the accurate prediction of 3-D distortion patterns with reduced computational time. The predicted and measured values of 3-D distortions of GBC

Literature Review

were observed to be in good agreement with the ones provided from the shop floor, indicating the adequacy of inherent strain based method for the prediction of welding distortion in large and complex welded structures. As part of this investigation, a suitable welding fixture was also designed and welding sequence was modified, which were verified through inherent strain method to aid in minimizing the distortion of welded GBC.

Schileo et al., (2014) evaluated validity of a linear FE modelling procedure, fully based on independently determined parameters, for predicting the failure characteristics of the proximal femur in stance and sideways fall loading configurations. Authors monitored fourteen fresh frozen cadaveric femurs, seven for stance and seven for fall, with high speed videos. Authors claimed that FE models correctly identified the failure mode i.e. tensile in stance and compressive in fall. Also, the femoral region where fracture started i.e. supero-lateral neck. While the location of failure onset was accurately predicted in eight specimens.

Bergmann et al., (2001) measured contact forces at hip joint with the help of instrumented implant and synchronous analysis of gait patterns and ground reaction forces during some routine human activities. The study revealed that generally load at hip joint of patient is about 238% of the BW while walking at about 4km/h and slightly less when standing on one leg. The joint contact force is 251% and 260% of body weight for climbing upstairs and downstairs respectively. Authors concluded implants should mainly be tested with loading environments that mimic walking and stair climbing.

Kinetic models were formulated by Chowdhury & Kumar, (2013) to realize biomechanics of human gait, which helps in accurate measurement of segmental masses, acceleration, joint centers and moment of inertia acting at different joints. Inverse dynamic technique was used to compute the forces and moments with the help of free body diagrams and link segment model.

A mathematical model formulated by Collins & O'connor, (1991) is used with gait analysis. The model calculated muscle, cruciate ligament and tibio femoral contact forces during walking. Authors assumed femur, tibia and two cruciate ligaments as four bar linkages. The mathematical model takes account of rolling and sliding of femur over tibia during flexion and extension and the direction change in ligaments. The model considered the forces by quadriceps, hamstrings, gastrocnemius, cruciate ligaments (both ACL and PCL) and tibio femoral contact. The study advocated that the ligaments show a major role in load transmission during gait.

Yousif & Aziz, (2012) created a three dimensional model of human femur bone with the help of Computer tomography images to describe mechanical behavior of femur bone. Authors investigated the behavior of human femur for one GAIT cycle of walking and standing up by

Literature Review

providing hip contact forces. The results of finite element analysis reveal the biomechanical behavior of the human femur bone which is helpful for surgeons to understand femur surgeries and bone prosthesis.

Arnold et al., (2010) created a model that predicted the fiber lengths and forces on muscles. The model was used to inspect the interaction between moment arms and architecture in order to measure the changes in muscle forces and joint moments for a wide range of body postures. The model also allowed detailed inspection of the force and moment generation capacities of muscles about the ankle, knee, and hip. The model represented the moment generation properties of the included muscles over the ranges of -30° to 20° ankle dorsiflexion, 0° to 100° knee flexion, -20° to 90° hip flexion, and -40° to 10° hip adduction.

Gullett et al., (2008) studied differences in kinetics between front squats and back squats. Front squats were found to produce considerably lesser maximal joint compressive forces at the tibiofemoral joint as well as reduced lumbar stress in comparison to back squats, with little difference noted in shear forces. They suggest that front squats may be a better substitute than back squats for the subjects with ligament or meniscal injuries. Moreover, the front squat may isolate the quadriceps to a higher degree than the back squat, making it a feasible choice for the subjects seeking to optimize development of the frontal thighs in comparison with the gluteal muscles.

Calcium phosphate cements (CPCs) has the biological and mechanical properties resembling to natural bone tissues. Therefore, CPC are suitable materials to be considered as an alternative for bone repair as bone defect fillers. Mouzakis et al., (2016) focused on the experimental characterization of the mechanical properties of CPCs that are used in clinical applications. Also, hydroxyapatite crystals were reinforced in some samples and tested in compression. They were compared with the tested porous CPCs. The study improves the knowledge about the biomechanical properties by controlling their structure in a micro level, and finds a way to compromise between mechanical and biological response.

Mouzakis et al., (2016) prepared calcium phosphate bone cement paste by mingling α -TCP with sodium phosphate solution and the final hardening occurred post immersion in Ringer's solution. Their internal structure evolution from the hydrolysis of α -TCP to the formation of calcium deficient hydroxyapatite was observed by scanning electron microscopy. Authors applied time temperature superposition principle to investigate their time- and temperature dependent dynamic response. Authors claimed that nanostructure of hydroxyapatitic platelets and needles grows in 10 days, after specimen immersion for maturing in a Ringer's solution.

Literature Review

The subsequent nanostructure was confirmed by means of scanning electron microscopy and x-ray diffraction techniques.

With the help of CT scan data, a finite element model of bones is generated by Shireesha et al., (2013). The behavior of proximal human femur bone is analyzed by simulation in ANSYS under physiological load conditions. A comparative study was done by simulating stainless steel and Ti-6Al-4V implant materials. Authors concluded that Ti-6Al-4V gave less deformation on static loading. Furthermore, titanium alloy has some distinguished properties such as low density and bio compatibility makes it ideal material for using it as prosthetic implant.

In a study by Kirkwood et al., (2007) range of motion, power, force momentum and mechanical work are the process parameters analyzed for studying the performance of hip and knee joints of elder people with age of about 55 to 75 years. They observed a total effort of magnitude 0.40 J/kg by hip joint. It is distributed 22% on the frontal plane, 76% on sagittal plane and 2% on the transverse plane. Similarly, 0.30 J/kg total efforts are generated at knee joint with 7% on frontal plane, 90% on sagittal plane and 3% on transverse plane.

Francis et al., (2012) predicted facts about bone morphology and tissue density. They created 3D finite element models of the right human proximal femur for three subjects of different age groups. The study determined the total deformation, equivalent Von Mises stress, maximum principle stress, and fatigue tool and percentage variation. Authors claimed that total deformation, equivalent Von Mises stress and maximum principal stress increases with increase in the angle of inclination. The Bone mineral density is maximum in 32 yrs male then 17 yrs male and minimum in 40 yrs male. The safety factor is maximum in 32 yrs male then 17 yrs male and minimum in 40 yrs male for same body weight. Safety factor also decreases with increase in angle of inclination of physiologic loading.

Wagner et al., (2010) developed a highly automatic method for finite element model generation for walking. A total body musculoskeletal inverse dynamic analysis was carried out to extract muscle forces and joint reaction forces. The methodology determines the physiological loads more accurately which certainly aids implant designers and orthopedic surgeons. Boundary conditions were obtained with the help of inverse dynamics technique which when applied over whole musculoskeletal body extracts muscle forces and joint reaction forces as well as their moments.

Masood et al., (2013) focused on an exclusive way of modeling and analysis of mechanical stress of human femur bone. A model developed by 3D animated software Blender is transformed as CAD model by Pro Engineers and simulation was performed by ANSYS. It was

Literature Review

detected that the maximum deformation occurs at the point of load application. The deformation reduces with the distance from the pressure application location. Authors detected that peak stresses and least deformations are maximum at the restraint end of femur and reduces towards the free ends which shows its cantilever beam behavior.

Sowmianarayanan, (2003) studied the biomechanical behavior of femur and the implant assembly. A subtrochanteric fracture positioned 30 mm below the lesser trochanter in transverse direction and a non-linear contact analysis is implemented to study the fractured femur with prosthesis assembly. The prosthesis is examined for deflection, stress and strains. They also concluded that Proximal Femur Nail (PFN) implanted femur results in lesser stresses on the femur. When comparing the deflection pattern, the PFN enables the femur to deflect extra in the lateral direction. Due to this proximal femur above the fracture plane slips and healing procedure would take extra time. For the quicker healing of fractures, the contact surface area should be effectively stressed.

Nareliya, (2011) investigated stress distribution, total deformation and fatigue failure of femur for a healthy male with 75 kg weight. A total deformation of 0.023496 m was obtained for eccentric loading. It was observed that amount of deformation is higher at the femur head while lesser at lower end. It was also concluded that mechanical properties vary across the femur bone under physiological conditions and also with individuals.

Duda et al., (1998) calculated stresses and strains of the femur, thigh muscle forces and contact forces at joints with the help of finite element model. They demonstrated that it is the cooperative and collective effort of muscle forces to replicate a physiological strain distribution in the femur. For the systematic simulation of bone modeling, remodeling or bone density distributions fully balanced external load systems is required. The authors determine strain distribution during gait depending on a loading situation and have included all thigh muscles. The researchers aimed to compare the strain distribution found with this loading situation with previously formulated simplified load regimes. Also attempt was made to simulate the loading conditions for the proximal femur by determining the muscle forces that shall be included to provide maximum physiological relevance. The finite element model was developed using endosteal and periosteal contours as suggested by Cristofolini et al., (1996). A standard femur model was used and a subsequent element pattern was added to proximal femur which represents femoral neck and head regions. As far as material properties are concerned the bone are considered as homogenous and isotropic. Investigations have been made to understand the effect of higher ranges of seat heights on peak joint moment for sit to stand movement at the lower limb. The experimentation is carried out on eight young fit subjects, the seat heights were

Literature Review

10, 20, 30, 40, 50 and 60 cm, inverse dynamics method was used to calculate joint moments. The analytical and experimental approaches suggested that mechanical load is at highest value when thigh is at or near horizontal position at low and normal seat heights. Researchers also indicated that highest mechanical load and highest hip and joint moment are constant with change of seat height at low to normal seat height i.e. (10 to 40 cm). However as per the study conducted in range of high to normal seat height i.e. (60 to 40 cm), the mechanical load and maximum hip and knee joint moments increase inversely to seat heights. Researchers found a maximum strain difference of 6% between quadratic and linear displacement functions, hence suggested that linear element model holds good to analyze the distribution of strain in the bone. The peak surface strains found were less than 2000 $\mu\epsilon$ with all thigh muscles at 45% gait cycle, while it is near to 3000 $\mu\epsilon$ with simplified load regimes. However the difference of approximately 26% was found in proximal femur in both cases. Although researcher also indicated during the study that this difference can be reduced to 5% if adductors are included along with abductors, iliotibial band and hip contact. In this study it was suggested that three vastus muscles must be included in modelling approach of diaphysis femur bone part and role of gastrocnemius muscle must be taken in consideration while modeling distal part of the femur bone.

A model of the human lower body part was developed by Scott L Delp et al., (1990). They studied about changes due to surgery in musculoskeletal geometry and effect of musculotendon parameters on muscle force and its moment about the joints. They established a graphical interface of the model which permits the consumer to visualize the musculoskeletal geometry and to manipulate the model parameters to study the biomechanical consequences or orthopedic surgical processes.

Singh et al., (2015) attempted to deposit nano sized hydroxyapatite (nHA) on orthopedic implant of Ti alloy material. The process used for the purpose was electrostatic spray deposition. Nano sized hydroxyapatite has similar structure, biocompatibility and composition as of natural bone, hence it is a widely used material for coating on orthopedic implants. On the contrary Nano hydroxyapatite has high surface area and preferred osseointegration. Investigations were made for roughness, morphology and corrosion resistance. The size of Nano scaled hydroxyapatite was 25-30 nm as measured from atomic force microscopic image. The particle size reduced with sintering temperature. SEM characterization was done to understand the morphology. Researchers observed flake –like structure of n HA from SEM micrograph. The formation of nHA having 1.71 Ca/p ratio is confirmed by FTIR spectrum and elemental analysis. It was also claimed that the corrosion resistance after coating of n HA on Ti

Literature Review

alloy has greatly improved. However, S. Singh et al observed the change of phase of nHA from crystalline to amorphous in XRD pattern and also surface roughness was found to be increased after coating.

JOST & SCHOFIELD, (1982) determined that due to superior forward inclination of the trunk, the low bar position of power lifters has been observed to produce larger hip extensor torque and smaller knee extensor torque compared with weight lifter's high bar squat. Thus, unless contraindicated by an existing injury, both positions are suitable for the majority of lifters.

Bourne et al., (2010) examined 1703 patients after TKA for the satisfaction level of patients after the surgery. The study suggested that approximately 19% of the patients were not satisfied post operation. Only 72-86% patients were satisfied on the basis of pain relief. While 70-84% patients were satisfied for the functionality of the tibiofemoral joint for the daily activities. The study found the 1.9 times greater risk for postoperative complications leading to readmission in the hospitals.

Báča et al., (2018) assessed fractures of extremities, spine and pelvis in subjects with respect to mechanism, time of the incident and demography of subjects to propose preventive measures. The study includes 3,148 number of patients (out of which 53% were women) treated for 3,909 fractures with a mean age of 53 years. Most traumatized patients were from the age group of 30-40 years and 70-90 years. Male patients had higher multiple fractures problem. Study claimed most of the accidents occurred during day time on Saturdays during winter season. Car crash is one of the most frequent reason for spine or pelvic fracture. Radius and femur bone were the most frequently broken bones 18.5% and 11.1% respectively.

WANG et al., (2005a) attempted to calculate the peak stress and the stress levels on the hip joint surface. Researchers conducted the study based upon the established fact that intrinsic pathomechanical changes depends largely over local stress level, previous researches of the field focused more upon global joint loading. The stress level and peak stress level estimation are useful in treatment of osteoarthritis as abnormal mechanical stress on hip joint is one of the main reasons of it. In this work peak stress distribution of eight routine human activities for hip joint was calculated. These routine activity includes slow-walking, normal-walking, fast-walking, going upstairs and downstairs, stand up, knee bend and sitting down. It was observed from the results that the peak stress has highest and lowest value at fast walking and sit down conditions respectively. Also maximum peak stresses were found to be on higher side while going upstairs and downstairs. Minimum peak stresses were found at sitting down, standing up and knee bend cases. It was being quoted in the paper that average peak stress is 8.72 MPa and

Literature Review

the range of peak stresses is 5.317 MPa and 11.89 MPa in all the eight activities. Another important finding from this work is that double peak curves of peak stress distribution were found in walking cases. Hence from above research it can be concluded that the chances of hip injury is more while running fast.

The biomechanics of human movement can be analyzed by two conventional approaches, forward dynamics and Inverse dynamics. Buchanan et al., (2004) chosen forward dynamics method to calculate and anticipate muscle force and joint forces, Researchers in this paper presented forward dynamics neuro-musculo-skeletal model for the purpose. Electromyography signals were used as the inputs to the model and latterly inverse dynamics approach was used to verify the joint moments predicted by the model. In forward dynamics approach neural command is first measured and then is converted to joint moment by three steps that is muscle activation dynamics, muscle contraction dynamics and musculoskeletal geometry. In muscle activation dynamics a neural signal is converted to a measure of muscle activation. In muscle contraction dynamics conversion of muscle activation into muscle forces is carried out. In musculoskeletal geometry muscle forces were transformed to joint moments. After joint moments were found, joint moments were converted to joint movements. The model parameters include muscle moment arms and lengths, optimal fiber length, pennation angle, tendon slack length were calculated using models given by Delp et al. S.L. Delp et al., (1990) and cadaver studies. Some other parameters were calculated by comparing the forward dynamics and inverse dynamics approach. Experimental data (EMG) was collected for three subjects using surface electrodes and fine wire intramuscular electrodes. The EMG data collected for the trials on dynamometer and during gait. Joint moments were estimated from the EMG data of four muscles. Root mean square error of 1.4 N.M ($R^2 = 0.997$) is said to have occurred between the estimated moments obtained from forward dynamics and measured moments from inverse dynamics. From this work the researchers suggested that the joint moments can be accurately estimated by using neuro-musculo-skeletal model using EMG as input. The researchers further quoted that the model can aid in better understanding of tissue loading in joints, tensile ligament forces and compressive cartilage loads while performing the dynamic task.

Macker et al., (2011) attempted to study three dimensional knee kinematics of Middle East mohammedans during high flexion activities. Researchers also presented postoperative knee kinematics of the human subjects undergone TKA during high flexion activities. There are very less studies conducted on the range of motions of non-western cultural population. The researchers specifically focused on the population of Middle East, the activities in daily life include kneeling, squatting, and sitting cross-legged. In the contrary from western population

Literature Review

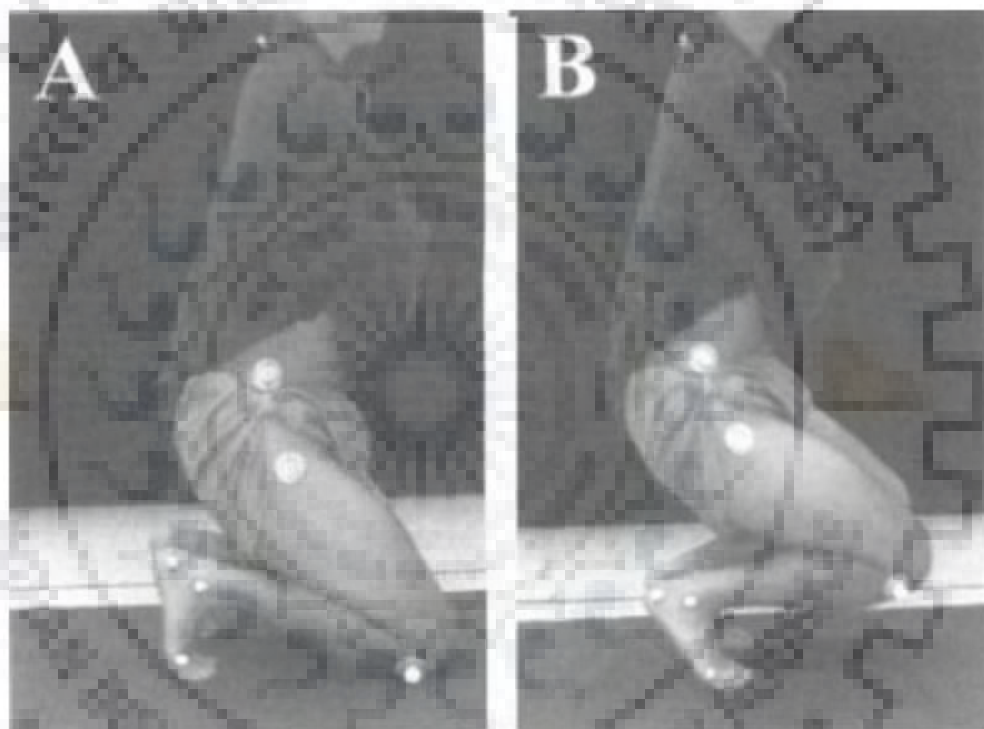
the Muslim subjects undertaken for the study expressed that they kneel 20 to 30 times a day for various activities like praying, eating, toileting and other works and could continue kneeling comfortably for more than an hour. The researchers quoted that nonwestern patients are often do not consider total knee arthroplasty as it limits their motion required for routine activities. Hence in countries like Saudi Arabia and the Middle East the TKA's performed are far less than western countries as its performance is highly dependent upon factors like implant design, surgical techniques and many patients' factors. The researchers collected data from male treated from total knee arthroplasty and 10 normal subjects following the Middle Eastern lifestyle. It was found that total knee arthroplasty patients were capable to make the kneeling, sitting cross legged, squatting and Muslim prayer. Out of these four activities researchers found significant difference in minimum flexion angle in three activities for the group of normal people and total knee arthroplasty patients. Researchers observed almost negligible difference in maximum joint angles between the group of normal and total knee arthroplasty patients.

With use of electromagnetic motion tracking system and a non-conductive force platform. Smith et al., (2008) attempted to determine axial tibiofemoral joint contact forces for high flexion that is squatting activities. The forces thus found were claimed to be useful in high flexion implant development during analysis. The model for tibio-femoral contact force developed in this study was based upon anthropometrics, ground reaction forces, calculated kinetics and measured kinematics having more focus on the axial joint contact forces working on tibia. This study can be considered as advancement over previous studies as in this researchers determine subject specific quadriceps and hamstrings moment arm magnitudes by using a scaling method. The scaling method was claimed to be non-invasive and it made direct measurements from the subject to a certain extent. Data was collected over nine Canadian subjects leading western lifestyle out of which six were males and three were females. Comparison was made of maximum tibio-femoral contact force between stair climbing and squatting activities, as far as squatting heel up activities and stair climbing was concerned, a significant static difference was found, although between squatting heels down activities and stair climbing no significant difference was found. Researchers claimed that the maximum contact forces are much higher in squatting heel up activity than stair climbing, though stair climbing is a single leg activity and squatting is double leg activity, hence it was expected that the maximum contact forces would be higher in stair climbing. These finding shows similarities with the study conducted by Nagura et al., (2002b) and D'Lima et al., (2011) During the chair rise as well the contact forces are higher in squatting. In this study the largest mean axial joint

Literature Review

contact force during squatting heels up activity was found to be 37.3 N/kg. The model proposed was claimed to be simple to apply and data collection require less time.

Nagura et al., (2002b) in this work attempted to study the biomechanics of deep knee flexion beyond 90° during squatting or kneeling. Previous to this study limited data was available on it. Nineteen subjects were studied to understand the dynamic loads on normal knee during deep flexion activities. The observations thus found was compared with walking and stair climbing. Out of 19 subjects 9 were women and 10 were men. The researchers used inverse dynamics approach to evaluate the kinematics and kinetics of the knee. The parameters involved during the work were limb segment size, body mass and ground reaction forces. The deep flexion activities carried out by subjects are shown in Figure 2.1.



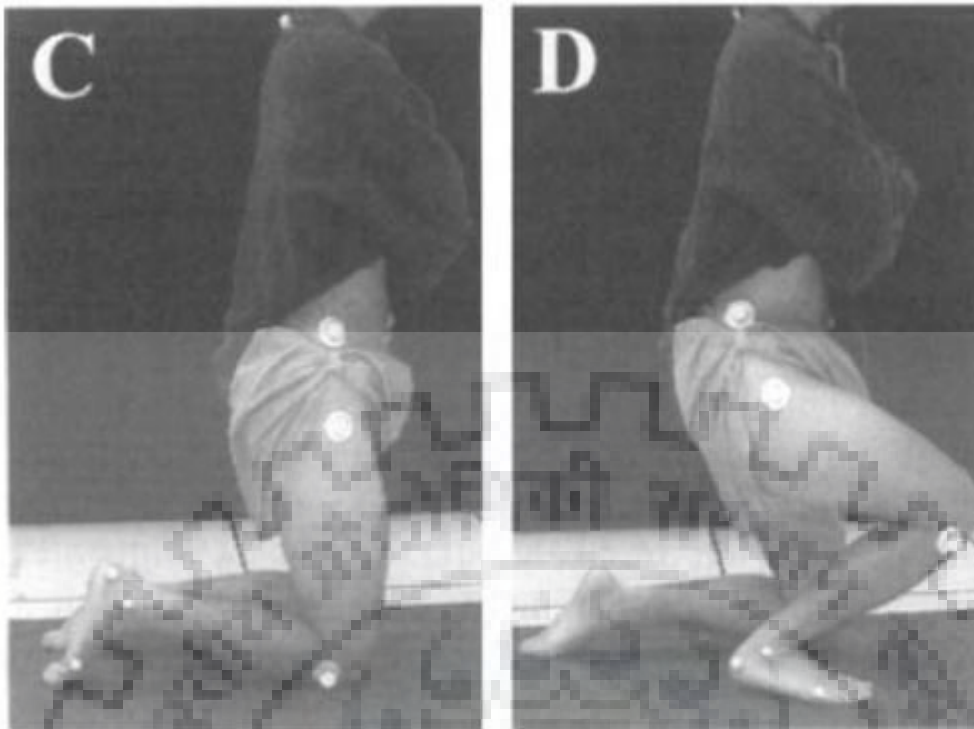


Figure 2.1 The deep flexion activities: (A) deep kneeling position in double leg motions, (B) rising/descending phase in double leg motions, (C) kneeling position in single leg motions, and (D) rising/descending phase in single leg motions.

The net quadriceps moments were found to be greater during deep flexion activities as compared to the routine activities. The net posterior forces were also found to be larger than the routine activities. At 90° and 150° of flexion, both net moments and posterior forces were maximum. These high moments and posterior force during deep flexion activities can enhance the stress on tibular tendon and joint contact forces. The posterior forces on the tibia were 50 % greater than the routine activities like walking, single leg rise etc. These forces in combination can likely cause strain to the structure providing posterior stability. In this study stair descending was not undertaken as well as the portion on force and moment taken by the thigh and the calf was neglected. Conclusively this study is useful for reconstructive process of knee pathogenesis and total knee arthroplasty patients.

Ipavec et al., (1999) attempted to develop a mathematical model focusing on contact stress distribution in the hip. The input data to this model is known resultant force and geometrical factors. The work was an extension to the work done by Iglıc et al., (1993). to the cases of an arbitrary direction from the resultant hip force. The mathematical model presented here was also aimed to simplify the already existed methods which were time consuming and researchers also claimed that this mathematical model can be directly apply to clinical practice of understanding stress distribution in most frequent body positions of everyday activities.

Literature Review

Researchers also indicated that as the weight bearing area changes the stress distribution and its peak value also change. The change in the weight bearing area is due to the variation in resultant force inclination. The minimum stress was found when resultant force is at right angles in the medial direction from acetabular borders. As the resultant force inclines away the stress increases due to decrease in weight bearing area. Though the model presented by researchers bear many assumptions, for example the cartilage was macroscopically defined. It was homogenous and linearly elastic. Researchers claim to give global averages rather than local contact stresses due to assumptions undertaken. The results by the mathematical model presented in this study find close values as found by experimentations conducted by Hodge et al., (1986) and Krebs et al., (1991).

Anderson et al., (2010) attempted to study hip morphology, cartilage mechanics and osteoarthritis by using computational model. The researchers attempted to incorporate varying degrees of simplified geometry as well as rigid bone material assumption, previous to this study researcher claimed that many other researchers consider hip joint to be a perfect ball and socket joint. The basis of the model was subject specific finite element model of a cadaveric hip joint. Bone – cartilage geometry used was either subject specific (irregular) or spherical or rotational conchoids, walking stair climbing and descending stairs. The contact stresses of simplified finite element model was compared with subject specific model. Sphere and conchoids geometries closely matches with native hip joint geometry. Underestimation of peak and average contact pressures were observed in models with conchoids and spherical bone geometry and smoothed articulate cartilage surfaces. Overestimated contact area was also observed in comparison to subject specific FE model. However, models having subject specific bone geometries with smoothed articulate cartilage uniform distribution of contact was observed, though underestimation of pressure is still there. Rigid bone models predicted higher pressure with respect to deformable bones. Conclusively bone material properties, cartilage interface and cartilage surface hold significant effect on the prediction of magnitude and distribution of contact pressures in hip joint.

Lamontagne et al., (2012) done their analysis on contralateral limb after total hip arthroplasty. Joint mechanics of lower limbs was investigated during sit to stand and stand to sit tasks. The subjects undertaken were 20 total hip arthroplasty patients out of which 10 were men and 10 were women. All subjects performed 3 trials of each sit to stand and stand to sit tasks from which the lower limbs kinematics and kinetics data was obtained. The results indicate that both total hip arthroplasty patients and healthy patients take same time in sit to stand and stand to sit tasks. Although there were some significant differences of kinematics and

Literature Review

kinetics of both THA patients and healthy subjects. During sit to stand THA patients had lower peak operated-hip extension moment at lower limbs. In addition to that lower peak hip flexion angle was also observed at the lower limbs of THA patients. Lower peak power was also generated. A different operated hip mechanism was observed in frontal and transverse plane of THA patients. During stand to sit several differences were again observed. A lower peak extension support moment was observed in THA patients. The tasks were performed with less flexion in THA patients. IN addition to these THA patients showed lower peak power absorption and lower hip abduction.

Self-adjusting file is an important instrument used by dentists. In this work, Nayak et al., (2018) attempted to analyze the forces and vibration during root canal shaping while using the self-adjusting file. Researchers claimed that the investigations carried out would be helpful in developing smart endodontic instruments. The material used during experimentation was forty square pillars, J shape endontic training blocks. During experimentation the blocks were held in a vice for rigidity. Force and vibration analysis is carried on it. Dynamometer and Accelerometer were simultaneously used to sense vibration and force signals. Total forty self-adjusting files were used. The largest amplitude of force and vibration was found at a frequency of 83.33 Hz. A correlation coefficient was found between force and vibration. The researchers found linear relationship between force and vibration amplitude. Hence during root canal shaping, vibration increases with the force. The peak value of vibration and forces were observed just before the fracture of self-adjusting file. Conclusively in this work forces between root canal and self-adjusting file were analyzed and this study showed the direct relationship of forces and vibration. Hence vibration analysis could be a method to predict forces during root canal and life of self-adjusting file.

Khas et al., (2018) attempted to treat clubfoot disorder in infants by using orthosis developed by them. Clubfoot is a disorder of foot in three dimensions and generally treated by a series of plasters (casts) over a period of time. Due to the plasters several infections were found in many cases like skin rashes, dehydration of skin, ulcers etc. By using this method, the medical professionals try to manipulate the position of infants' clubfoot. Researchers quoted that this process of treatment is not comfortable for infants as well as their guardians as multiple visit is required to the hospital. Researchers in this work presented an alternative to this clinical procedure by an orthosis developed by them. Orthosis was developed taking care of rotation of all three mutually perpendicular axis. Locks were provided in all three directions that is X, Y and Z. The cad model and actual prototype is presented in the Figure 2.2.

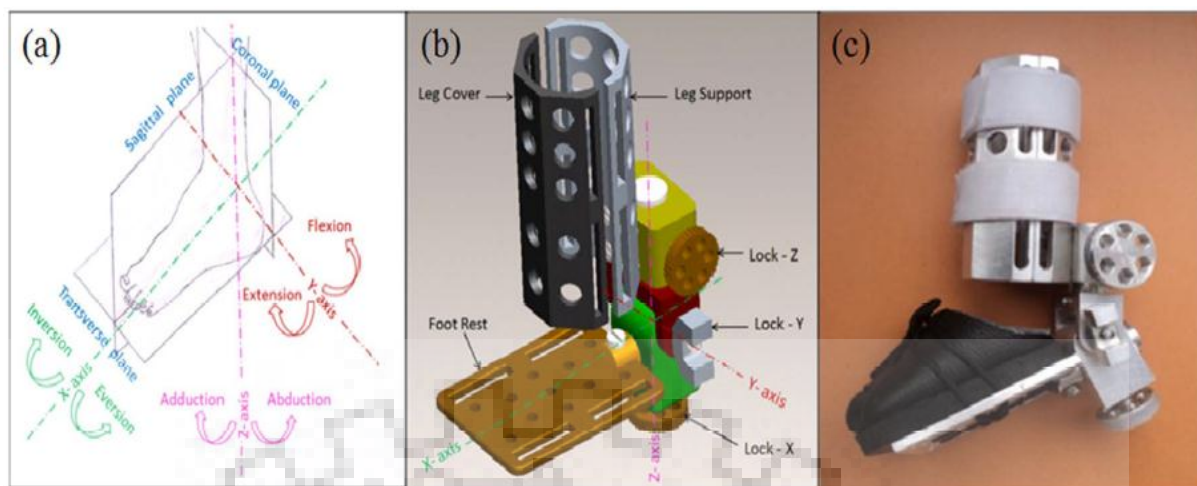


Figure 2.2 (a) Movement of foot in about three axes (lateral view, left foot) (b) Motion of orthosis about three axes (c) fabricated club foot orthosis (Khas et al., 2018)

The orthosis was applied to five infants' age under 30 days under the supervision of orthopedic doctor. The period of application of orthosis on each infant was one week and after than orthosis was removed. Comparison was made between the initial condition of clubfoot and the condition after the removal of orthosis. It was found that the clubfoot deformity was corrected to some extent after a week time and no infections like rashes, dehydration and ulcers etc. were evident. Conclusively by using orthosis for a week partial correction of clubfoot disorder was achieved. However, researchers recommended to use it for further more duration and more patients to ensure that orthosis can reliably treat clubfoot or to what extent it can treat the deformity.

Khas et al., (2013) conducted the biomechanical study for the assessment of natural club foot in order to design the orthosis. Orthosis is used for the treatment of clubfoot deformity in infants. In this paper a technique to replicate the natural clubfoot is discussed in which attempt is made to imitate the soft tissues and bones of natural clubfoot. Silicon rubber is used in place of soft tissues and polyamide material is used in place of bones for developing a heterogeneous model of clubfoot. Further the mechanical properties of this composite clubfoot is compared with the properties of natural clubfoot given by Mahmoodian et al., (2009) Computerized tomography (CT) scan data of a 5 days old infants clubfoot was obtained the data obtained was used in MIMICS and MAGICS software to prepare a 3D model of the clubfoot and the model is subsequently converted to STL files. Selective Laser Sintering machine was used to produce the prototype. The researchers developed twenty such models of composite clubfoot. The young's modulus and poisson ratio of the composite clubfoot were evaluated in a universal testing machine. The poisson ratio found was approximately equal to the poisson ratio of natural

Literature Review

clubfoot, but the young's modulus found was approximately 10 times of that of the natural clubfoot.

In this work, Khas et al., (2015) attempted to develop a device to measure the deformity of a clubfoot. Clubfoot is a deformity in which legs are not in proper shape and location. The existing device to measure the deformity is one dimensional and takes large time for measurement of the deformity. Researchers claimed that this new device is time efficient and effective. The device developed by the researchers can simultaneously read twist of adduction – abduction, twist of extension- flexion, and twist of inversion – eversion, twist of forefoot from hindfoot, can measure cavus, can measure rotation of forefoot from the hindfoot, can measure the length of the leg. The device can be used for both left and right leg. Three infants having clubfoot deformity were chosen for the study. The clubfoot deformity was measured by the proposed device as well as goniometer. The findings were almost similar from the proposed device as well as goniometer. The time taken for measurement through the new device is significantly less than that of the goniometer. The average time of measurement through proposed device was found out to be 2 minutes and average time of measurement from goniometer was 13 minutes. Conclusively the researchers claims that this new device can significantly reduce time and effort of measurement of club foot deformity.

Table 2.1 Kinetics and kinematics of lower extremity of the human body

Author(s) & Investigation	Highlights	Remarks
Hospital, (1996) Experimental	Impact direction influence on failure load and failure pattern of proximal femur Impact direction is independent to bone mineral density Longer the neck axis, higher the failure load	Trivial variation in line of action of impact force modifies failure load
Politis et al., (2013) Experimental	Analyzed strain patterns for variety of femur neck. Stresses are higher at anterior for anteverted neck and at posterior surface for retroverted neck	A custom-built fixture designed to reproduce loading conditions during the single-leg stance phase of walking
Bourne et al., (2010) Case study	1703 TKAs patients were cross examined in Ontario, Canada 81% patients were satisfied	Level of evidence, Level 2, prognostic study

Literature Review

Author(s) & Investigation	Highlights	Remarks
	72-86% satisfied with pain relief 70-84% satisfied for daily activities functionality	
Francis et al., (2012) Numerical	To predict bone morphology and tissue density, CAD models of 3 subjects viz 17, 32 and 40 years old males were created. Total deformation, Von Mises stress and max. principle stress increases with inclination angle. Safety factor decreases with increase in inclination angle	Inclination angle resembles change of direction of loading on femur head
Wagner et al., (2010) Numerical	Developed an automatic method for evaluation of forces during gait with the help of FEM. Used inverse dynamics method to calculate muscle forces and joint reaction forces and moments.	HU 801 and above for cortical bones while HU 800 and below for Cancellous bone
Masood et al., (2013) Numerical	The maximum deformation occurs at the point of application of load. Deformation reduces with the distance from the pressure application location. Maximum stresses and minimum deformations are located at the restraint end of femur bone	Unconventional method to develop 3D CAD model. Maximum deformation varies 0.04-0.56m and von Mises stress varies 57-66kPa
Birnbaum & Pandorf, (2011) Numerical	Calculated the hip centralizing forces of the iliotibial tract for different femoral neck angles. Higher compressive force on the femoral head for coxa valga and decreasing compressive force on the femoral head occurred for coxa vara	developed a hip joint model with different centrum-collum-diaphysis-angles of 115°, 128° and 155°
Lutz et al., (2016) Experimental	Mathematical equations for computing muscle forces of lower extremity for bone structure and by reducing load which causes bending of the patterns	Provides more accurate femoral stress strain patterns

Author(s) & Investigation	Highlights	Remarks
	bone to evaluate more accurate femoral stress-strain patterns.	
Hara et al., (2016) Experimental	The dynamic hip kinematics under four different movements osteoarthritis hip disorders just before total hip arthroplasty. The authors revealed OA patients could not flex their femurs deeply.	Deep flexion activities are still problem after total hip arthroplasty
Keyak & Rossi, (2000) Numerical	Authors compared nine failure theories to evaluate the performance of the femure bone for two different loading conditions.	Distortion energy theory and maximum shear stress theory are most robust for femoral fracture analysis
Hamai et al., (2009) Numerical	Analyzed knee kinematics during kneeling, squatting and stair climbing for healthy and medial osteoarthritis. The femoral external rotation gradually and increased with flexion for squatting and kneeling, and gradually decreased with extension for stair climbing in medial osteoarthritis knees	Study compares and quantifies the rotation in femur for healthy
Schileo et al., (2014) Experimental	The high speed videos used to monitor fourteen fresh frozen cadaveric femurs, seven for stance and seven for fall. FE models correctly identified the failure mode i.e. tensile in stance and compressive in fall.	Failure mode is tensile in stance and compressive in case of fall.
WANG et al., (2005a) Experimental	Instrumented implant and tested it for gait patterns to evaluate contact forces of hip joint for walking, climbing upstairs and downstairs. The load at hip joint is about 238% of the body weight when walking at about 4km/h and slightly less when standing on one leg.	Implants should be tested with loading conditions since load is above body weight

Literature Review

Author(s) & Investigation	Highlights	Remarks
Chowdhury & Kumar, (2013) Case study	<p>Authors formulated kinetic models of Human body is discretized in segments accurate measurement of segmental masses, to evaluate forces and acceleration, joint centers and moment of inertia moments at various acting at various joints.</p> <p>Inverse dynamic technique was used to compute the forces and moments with the help of free body diagrams and link segment model.</p>	points
Collins & O'connor, (1991) Case study	<p>Authors formulated a mathematical model for GAIT cycle considering femur, tibia and Anterior, posterior cruciate ligaments as links for four bar mechanism.</p> <p>Rolling and sliding of femur over tibia and ligaments directional change is considered in the mathematical model.</p>	The ligaments show a major role in load transmission
Yousif & Aziz, (2012) Numerical	<p>A 3D CAD model was developed by CT scan images to describe mechanical behavior of femur bone</p> <p>Authors investigated the behavior of human femur for one GAIT cycle of walking and standing up by providing hip contact forces.</p>	Stresses calculated are helpful for the orthopedic surgeons for evaluating severity of surgery and deciding bone prosthesis
Arnold et al., (2010) Experimental	<p>Authors developed a model to predict a relation between muscle fiber operating lengths and force and moment forces on muscles and joint moments over a wide range of body positions.</p>	Model predicts the force and moment generation capacity of the muscles about ankle, knee and hip.
Gullett et al., (2008) Study	<p>Authors studied differences in kinetics between front squats and back squats.</p> <p>Front squats produce lower maximal joint compressive forces at the knee and reduced stress at lumbar as compared with back squats</p>	Front squats produce comparatively less

Author(s) & Investigation	Highlights	Remarks
Shireesha et al., (2013) Numerical	A 3D CAD model of proximal human femur bone under physiological load conditions. Two implant material viz Ti-6Al-4V and stainless steel were compared. Titanium alloys implant gave less deformation on static loading.	Titanium alloys are low density hence have less weight and are biocompatible
Kirkwood et al., (2007) Numerical	Range of motion, power, force momentum and mechanical work are analyzed for studying the performance of hip and knee joints of human load subjects.	Sagittal plane shares major portion of the load
Sowmianarayanan, (2003) Experimental	Author positioned a fracture 30 mm below lesser trochanter in transverse direction for a nonlinear contact analysis of a fractured femur and implant assembly.	Contact surface should be adequately stressed for faster healing
Nareliya, (2011) Numerical	Authors investigated stress distribution, total deformation and fatigue failure of femur for a healthy male with 75 kg weight.	No general method available to evaluate stresses on femur
Duda et al., (1998) Experimental Numerical	Authors calculated stresses and strains of the femur, thigh muscle forces and hip joint contact forces on a finite element model of the lower extremity.	For modeling diaphyseal bone, three vastus muscles should be considered while modeling distal femur should account gastrocnemius muscle
Schoenfeld, (2010) Case study	Compared postures of power lifters for low and high bar positions. It was suggested that because of greater forward inclination of the upper torso, low bar position of power lifters produces high hip extensor torque while high bar squat produces less knee extensor torque.	Athletes must avoid the low bar or high bar positions as per the nature of injury.

Author(s) & Investigation	Highlights	Remarks
Singh et al., (2015) Experimental	<p>Authors deposits nano sized (25-30nm) hydroxyapatite (nHA) on titanium based orthopedic implants by electrostatic spray deposition method.</p> <p>nHA was investigated for surface qualities (atomic force microscopic images), Hydroxyapatite coating morphology (SEM) and corrosion resistance (XRD).</p>	<p>Hydroxyapatite has similar structure, biocompatibility and composition as of natural bone.</p> <p>improves corrosion resistance of Ti implant.</p>
Bourne et al., (2010) Case study	<p>Authors examined 1703 patients of TKA for satisfaction level after surgery</p> <p>One out five patients was unsatisfied post operation.</p> <p>72-86% patients were satisfied for pain relief.</p> <p>70-84% patients were satisfied for the functionality of the knee joint for routine activities</p>	<p>Patients situation will be tougher for Asian subcontinent population being complex routine activities.</p> <p>Level of evidence, Level 2, prognostic study.</p>
Bergmann et al., (2001) Experimental	<p>Authors calculated peak stress and stress level on the hip joint surface for eight routine activities viz slow, normal and fast walking, upstairs and downstairs, stand up and sitting down and knee bend.</p> <p>Max. stress was observed for walking fast than upstairs, down stairs.</p>	<p>Hip injury is more higher inertia cases</p>
Buchanan et al., (2004) Mathematical	<p>Authors used forward dynamics method to calculate muscle forces and joint forces</p> <p>Neural signal obtained from EMG was converted in to a measure of muscle activation.</p>	<p>The joint moments can be accurately estimated by using neuro-musculo-skeletal model using EMG as input</p>

Author(s) & Investigation	Highlights	Remarks
Macker et al., (2011) Case study	<p>Authors presented postoperative knee kinematics of patients of total knee arthroplasty during high flexion activities of middle east population.</p> <p>Authors claimed that non-western patients often don not consider TKA as it limits their motion required for routine activities.</p>	<p>Authors claimed very few studies about range of motion for non-western TKA patients.</p> <p>Eastern population avoid TKA as it limits the range of movement for routine activities.</p>
Smith et al., (2008) Experimental	<p>Authors examined nine Canadian subjects on an electromagnetic motion tracking system and a non-conductive force platform to determine axial knee joint contact force for high flexion activities viz stair climbing and squatting.</p>	<p>Squatting activity generates more contact force at knee joint</p>
Nagura et al., (2002b) Experimental	<p>Authors studied 19 subjects to understand the dynamic loads on normal knee during deep flexion (beyond 90°) activities viz squatting and kneeling.</p>	<p>Greater muscle moments lead to larger stress and joint reaction force</p>
Ipavec et al., (1999) Mathematical	<p>Authors simplified the mathematical model developed by Iglic et al (1993) to reduce time of calculation and to be useful directly to clinical practice for calculation of stress distribution in most frequent routine activities.</p>	<p>Resultant forces and geometrical factors were used as parameters.</p> <p>The mathematical model gives global averages rather than local contact stresses.</p>
Anderson et al., (2010) Numerical	<p>Authors developed a subject specific finite element model of cadaveric hip joint.</p> <p>The study compares the subject specific (irregular) model with the simplified hip joint (ball and socket) model for walking, stair climbing/descending.</p>	<p>Hip joint can be tested by considering it a ball and socket joint.</p>

Author(s) & Investigation	Highlights	Remarks
Lamontagne et al., (2012) Experimental	Analyzed joint mechanics of contralateral limb after THA of 20 subjects for sit to stand and stand to sit tasks up to chair level posture. Each subject undergone three trials and found time taken by normal persons and THA patients were approximately same.	Material properties plays significant role in stress distribution. Time taken for sit ups by healthy persons and THA patients were approximately same.
Nayak, Jain, & Kankar, (2019) Experimental	The forces and vibration during root canal shaping while using the self-adjusting file to develop smart endodontic instruments by using square pillars J shape endodontic training blocks.	Vibration analysis could be a method to predict forces during root canal and life of self-adjusting file.

2.1. Research Gaps

A huge amount of literature related to femur modeling, femur stress analysis, hip joint force analysis and their anthropometry is available. The contemporary studies and computational analysis concluded that for the analysis of femur, hip joint, knee joint etc., a model is required. That model can be real physical model (man-made) or the computational model with the help of some software or by scanning the CT/MRI images and use any medical imaging software like MIMICS that converts 2D model into 3D model. Literature survey presented above reveals that very few attempts have been made for analyzing squat positions and moreover those attempts are dedicated to sports arena such as weight lifting or power lifting. There has been no attempt appears to be made for squat position or floor level postures as a routine activity which are very common among most of the south Asian population.

The available literature discloses that most of the work in this area has been done for stance and swing positions during standing up and sitting down, slow walking and fast walking, upstairs and downstairs, knee bend etc. The range of motion is from 0° (vertical to the ground) to a maximum of 90° (sitting on chair). No work has been observed yet about effect of implant after surgery for body postures where thigh-shank angle is above 90°. No evidences were found for evaluation of routine activities of the subjects undergone with hip implant.

2.2. Proposed research work

The present study is focused on the hip-joint's kinematic constraints and their impact on the bone strength and bone life while performing a successful deep squat (a routine activity among South-Asian population). After an exhaustive literature survey presented in the next chapter, following objectives are proposed to carry out the research work. Each joint viz., Shoulder joint, knee joint, hip joint, ankle joint, wrist joint takes part in stability of the body movements and forms different body postures. The present study is related to hip joint which is one of the most complex as well as vulnerable as each hip joint has to bear a continuous variation in load while walking, jogging, climbing and sitting etc.

2.3. The Objectives

The following objectives are meant to fill a few research gaps found from the exhaustive reviews.

- To reveal mechanical failure behavior of the CAD model of human hip-joint under different loading conditions
- To propose the implant material and design intended to fabricate and test the same under different loading conditions
- To propose a mathematical model to predict the design stress of a femur bone and the same to be used for the fabrication of implant

3.1. Numerical methodology

A smooth and void less physical domain i.e. 3D CAD model of a femur has been chosen to perform the numerical simulation. The solid domain has been discretized into finite number of tetrahedron elements as shown in Figure 3.1. The discretized model is simulated for different postures of body viz. standing, knee bend, chair, pre-squat and deep squat. The discretized 3D CAD models of different configurations of the human body have been presented in the appendix A. The refined mesh comprises of 3333790 number of tetrahedral elements and 4650539 number of nodes. The boundary conditions, resolution of force components, and assigning the material properties are described in the following sections.

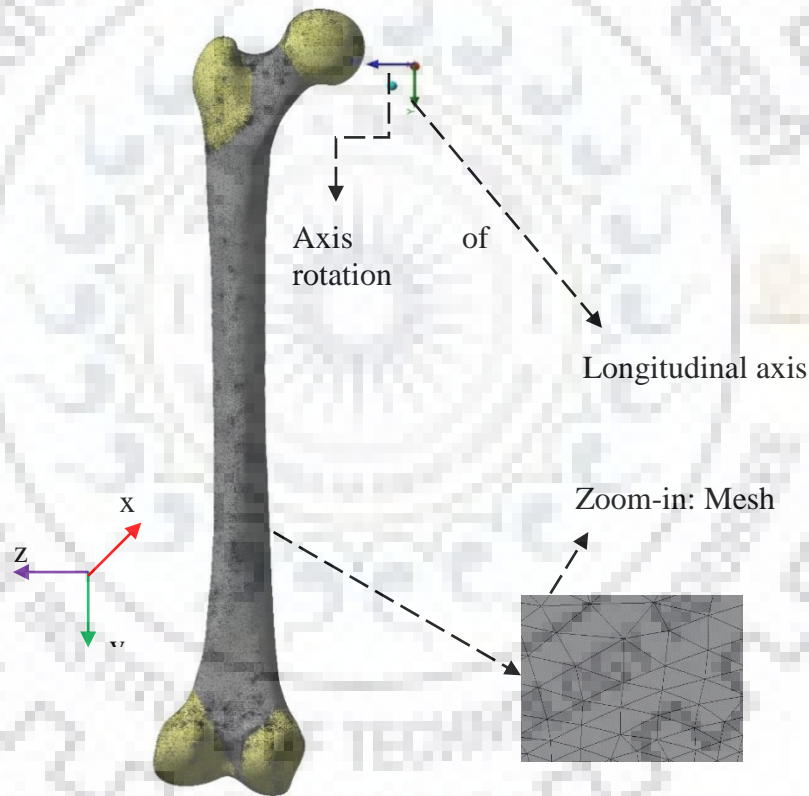


Figure 3.1 A discretized 3D CAD model of a femur

3.1.1 Boundary conditions

A solid model of a femur has been made and fitted into a Cartesian coordinate system. The resultant force is applied at the femur head for all the postures considered in this study during a successful squat. The geometry and static behavior of true postures considered in this study are revealed in the later sections. The contact area between pelvis and femur head is considered

as the area through which the load transfers. Because of an irregular shape of the femoral head as well as acetabulum cup, the change of contact area is observed while making a squat.

There are no standard analytical procedures or values universally to determine the effective contact area and thereby approximation has been taken in this study. The distal end of the femur forms a lower pair with proximal tibia and allows a simple tangential motion always. This tangential motion is constrained by the medial condyle, lateral condyle and femoral patellar surfaces. A single degree of freedom is obtained as the rotation of femur about its longitudinal axis is significantly minimum and neglected. Also, medial condyle, lateral condyle and femoral patellar surfaces were fixed with respect to posture.

3.1.2 Free body diagram

A static structural model has been developed for stress analysis in the present study and its isometric view is shown in Figure 3.2. The physical model has been put into a proper coordinating system to ensure the correct nature of the loading.

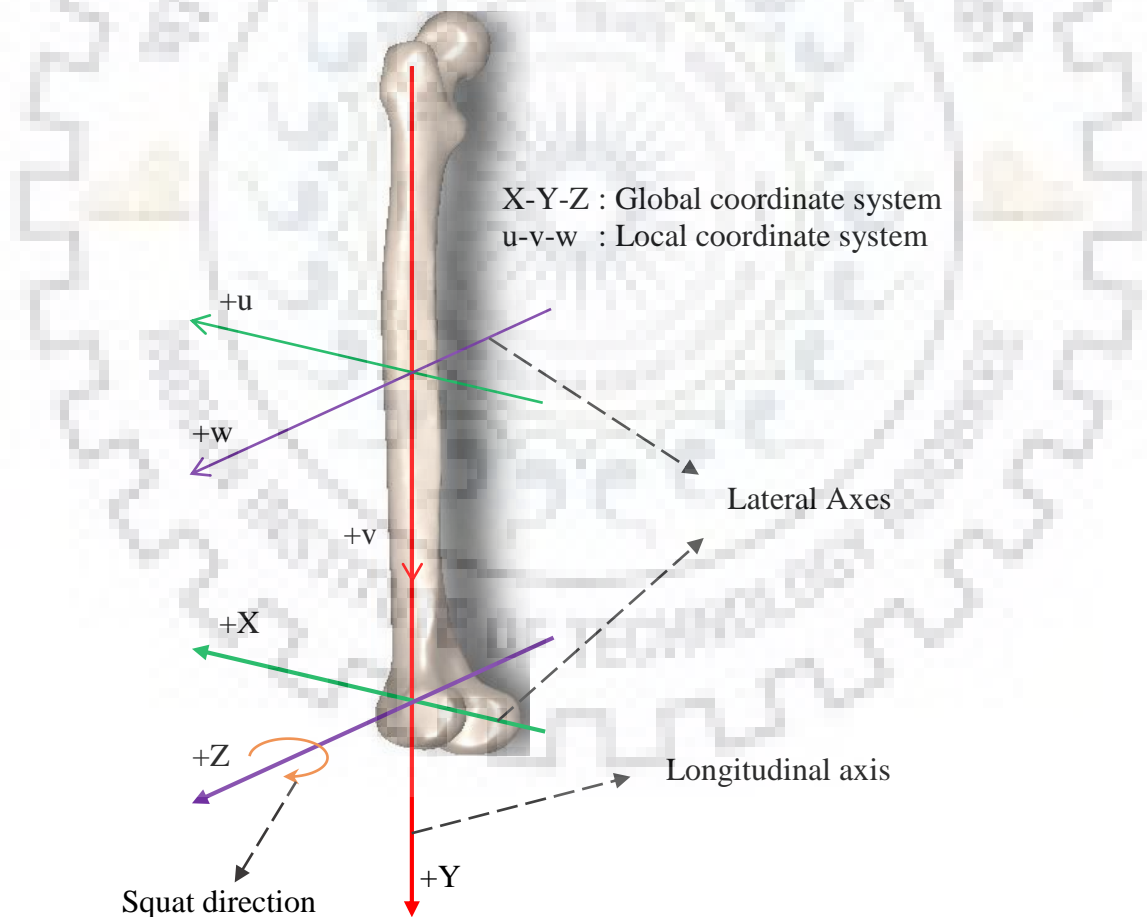


Figure 3.2 An isometric view of a femur showing the orientation towards squat with respect to global coordinate system

The coordinating system is divided into global and local coordinate systems, so that the orientation of femur could be well defined while performing squat. The weight of the body considered in the present study is 60 kgs \approx 600 N. The total load 600 N is shared equally by the two limbs i.e., 300 N each. In case of walking, a load of 2.5 times the shared load among the limbs is observed to be acted upon the femur head Susan Standring, (2016).

It is assumed that the same amount of load occurs in all the postures of a human body. Hence, a constant resultant load of 750 N is applied at the contact portion of femur head and the acetabulum of pelvis for all the cases. The resolution of such load on femur has shown in Figure 3.3. The magnitude of all the component of applied load is presented in Table 3.1. The Figure 3.3 shows the variation of longitudinal and lateral component of forces with respect to the angular displacement of femur on XY-plane. A simple Pythagoras technique has been applied to obtain the cosine and sine components of a resultant force on femur head. It is evident that the resultant force always acts in the direction of gravity. The resultant load is divided into two components all the time except in the direction of gravity and perpendicular to it. Therefore a direct and full load could be observed in standing and chair postures as shown in Figure 3.3(a). The components of a resultant load in all other positions causing the femur to have translation and rotational motion as well. This translation and rotational motion of a femur leads to a successful squatting of a hip joint.

Table 3.1 The component forces of a resultant force with respect to knee flexion angle

Posture	Knee Flexion angle	Magnitude of load (N)	
		Axial component (y)	Lateral component (x)
Standing	0°	750	0
Knee bending	45°	530.33	-530.33
Chair	90°	0	-750
Pre-squat	126°	-440.84	-606.76
Deep squat	160°	-704.77	-256.51

The magnitude of component forces acting on femur head with respect to the knee flexion angle has been shown in Table 3.1. The simulation has been carried out for the five familiar positions as shown in Figure 3.3(a-e). The direct resultant load is observed to be act vertically downwards in the initial or standing position represented in Figure 3.3(a). The reaction from the ground through the hip joint causes the upper portion of body to rest on femur with an equilibrium condition. The immediate next position to the standing is knee bending represented in Figure 3.3(b). A compressive load on femur could be observed from the standing position

Numerical methodology

till before chair position. A vertical resultant load causing the femur to experience shear, has been observed in chair position represented in Figure 3.3(c). The pre-squat and deep squat positions are represented in Figure 3.3(d) and Figure 3.3(e) respectively, causes the femur to undergo a tensile load.

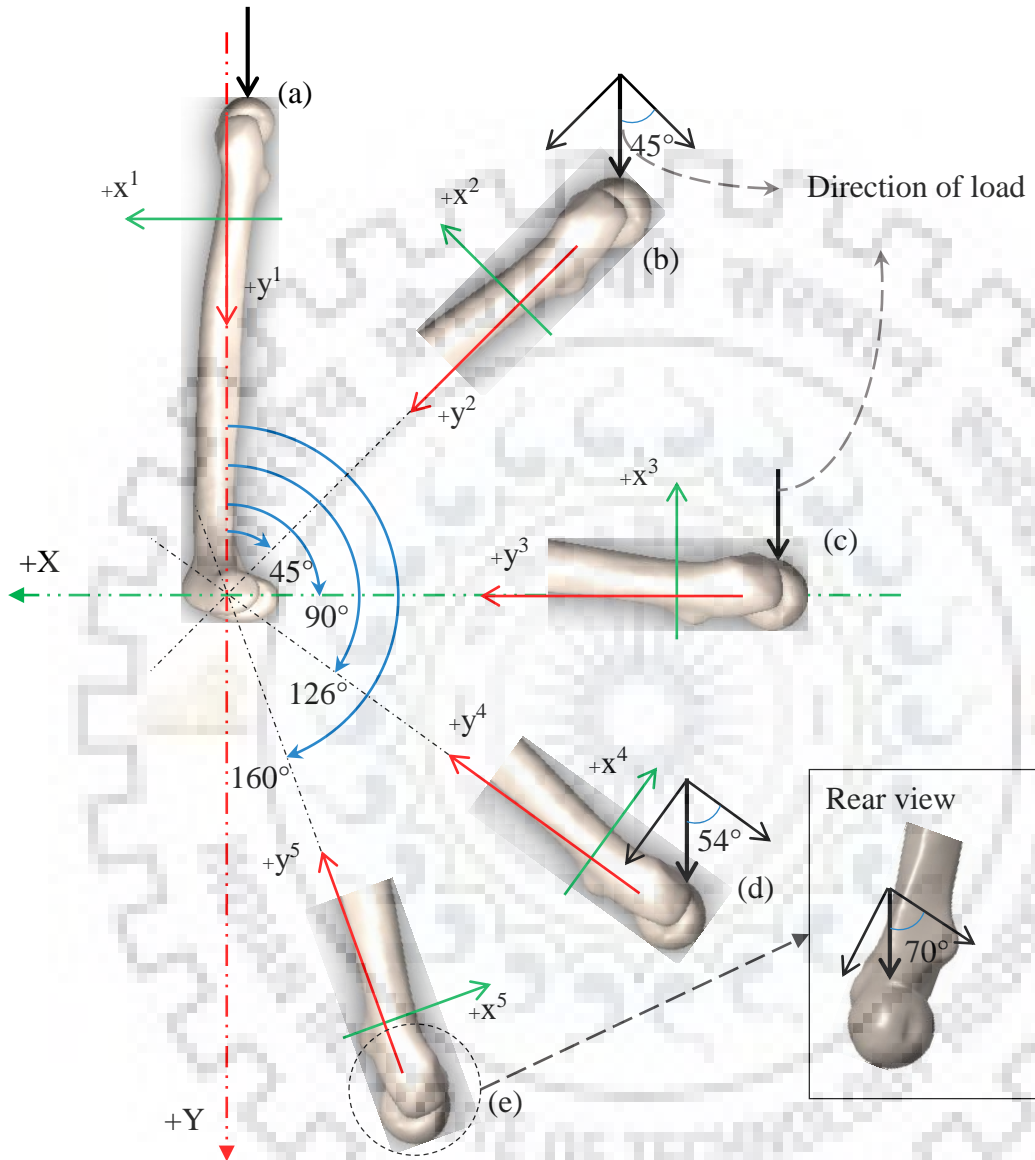


Figure 3.3 Free body diagram of the femur for different posture styles (a) Standing (b) Knee bend (c) Chair (d) Pre-squat (e) Deep squat

3.1.3 Material definition

A material is characterized with well-defined physical properties viz. density, Modulus of elasticity, etc. A 3D CAD model has been made and assigned with the physical properties of a human bone. The model with physical properties becomes realistic and simulation if such model could predict the characteristics of a joint. These physical properties ultimately define the mechanical properties of a material/model viz. ultimate strength, shear strength, toughness, etc.

In case of bones, the density is affecting the mechanical properties significantly and varies for cortical and cancellous bones. The Hounsfield unit for cortical and cancellous bone is about 2200 and 800 Wagner et al., (2010) respectively. The bone density is calculated on the basis of Hounsfield unit from the empirical linear relation Eq. 3.1 Baca et al., (2008); Dash et al., (2013); Kourtis et al., (2008). It is difficult to assign the properties of a bone due to its heterogeneity and nonlinear nature.

Table 3.2 Physical properties of femur Yousif & Aziz, (2012)

Physical properties	Hounsfield unit	Density (g/cm ³)	Modulus of elasticity (MPa)	Modulus of rigidity (MPa)	Poisson's ratio
Cortical bone	2200	2.0208	E ₁ =6982.88	G ₁₂ =4690	ν ₁₂ =0.4
			E ₂ =6982.88		
			E ₃ =18154.61		
Cancellous bone	800	1.3712	E ₁ =2035.84	G ₂₃ =5610	ν ₂₃ =ν ₃₁ =0.25
			E ₂ =2035.84	G ₃₁ =7680	
			E ₃ =3195.30		

*Where 1, 2, 3 stand for the medial-lateral, anterior-posterior and superior-inferior axes respectively

The model is assumed to be elastic and homogeneous in this study Amornsamankul et al., (2010); Baca et al., (2008); De Vos et al., (2009); Kourtis et al., (2008); Yousif & Aziz, (2012). There is no standard procedure to calculate the Young's modulus of orthotropic materials Nareliya, (2011). However, the empirical correlations developed based on the realistic model simulations are available and given below Eq. 3.2-3.5.

$$\rho = 4.64 \times 10^{-4} HU + 1 \quad 3.1$$

$$E_{1c} = E_{2c} = 2314 \times \rho^{1.57} \quad 3.2$$

$$E_{3c} = 2065 \times \rho^{3.09} \quad 3.3$$

$$E_{1t} = E_{2t} = 1157 \times \rho^{1.79} \quad 3.4$$

$$E_{3t} = 1904 \times \rho^{1.64} \quad 3.5$$

In general, the bone comprises of two portions named cortical (outside portion) and cancellous (inside portion) based on strength and density. Normally the cancellous dominants at joints and through which load is supposed to be transferred and they are highly flexible in mobility. The remaining portion of the bone is dominant by cortical and which is high dense and strength in nature. In the present study for the purpose of simulation the greater trochanter, femur head, and medial and lateral condyle are considered as cancellous. The femur shaft is

Numerical methodology

considered as pure cortical as shown in Figure 3.4. Table 3.2 shows the physical properties of a typical femur obtained from empirical correlations.

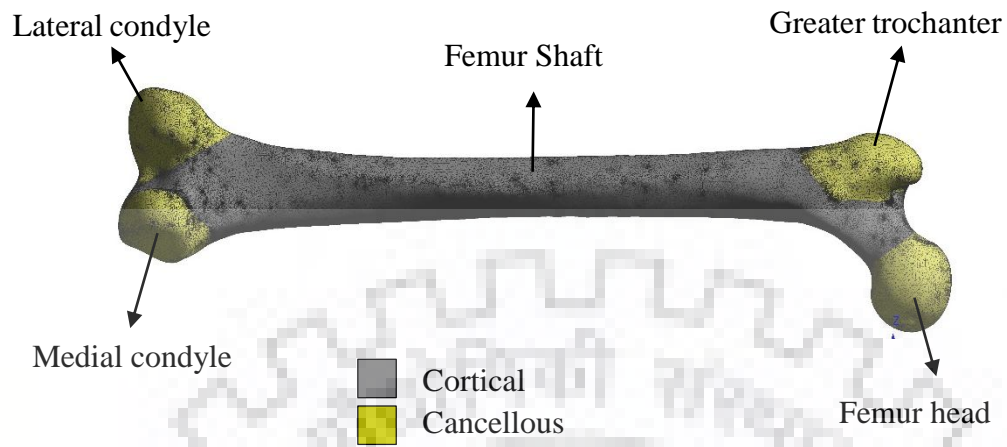


Figure 3.4 Defining the properties of femur based on the inner structure of a human bone

4.1. Experimental Test-Rig

The experimental set-up has been developed as a part of the present study, an experimental set-up to conduct the experiments on the femur bone and pelvis bone was designed and built as shown in Figure 4.1. The experimental set-up was built to produce the kinematic constraints of human hip-joint. The physical configuration of test section after fixing on the experimental set-up, resembles the human hip-joint allows 1-rotation and 1-vertical movement. The experimental set-up was developed on a rigid base in order to avoid the small vibrations while performing the experiments.

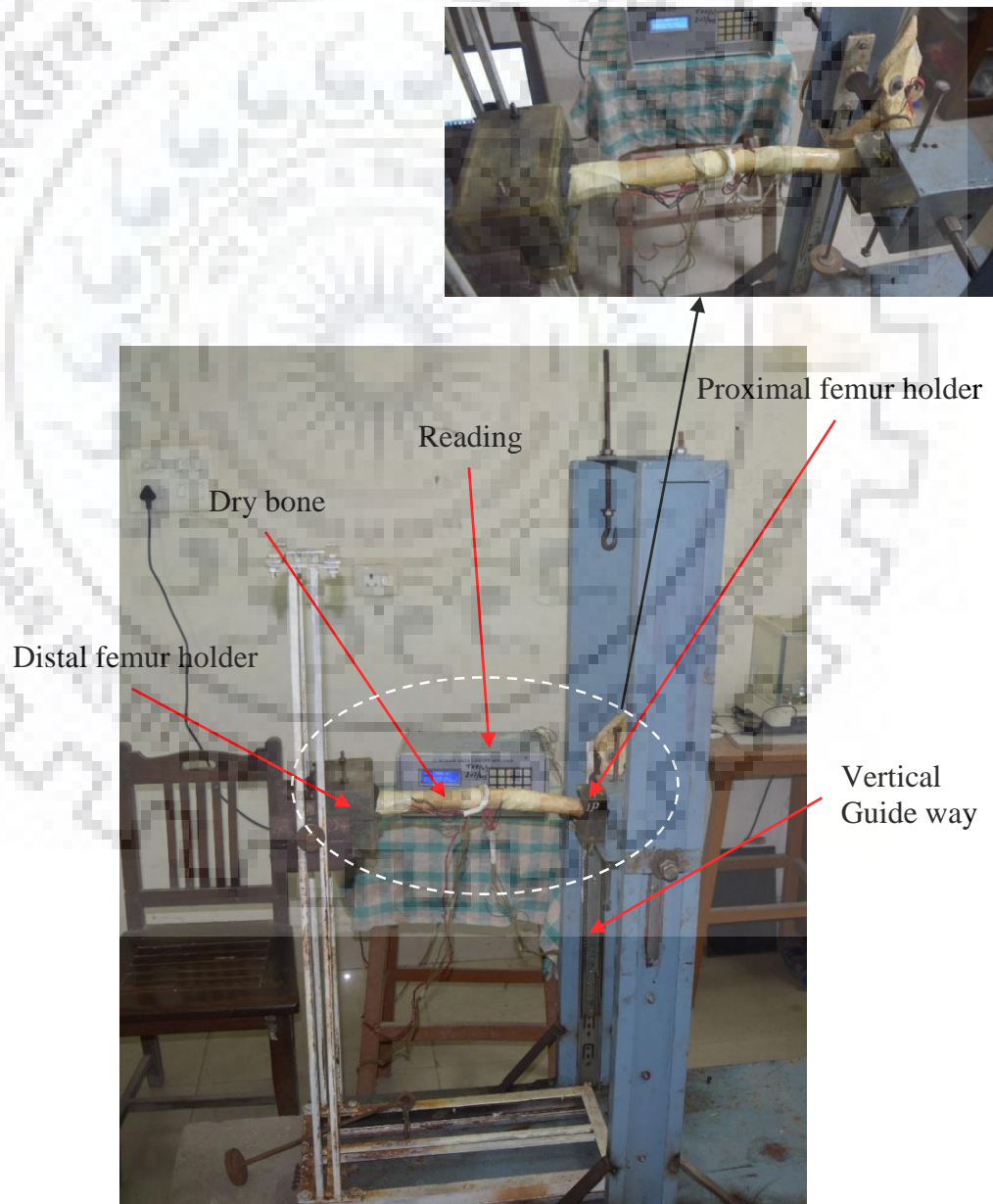


Figure 4.1 Photographic view of an experimental set-up

Experimental set-up

4.1.1 Pelvis holder

The structure of pelvis and its holder together was developed by a systematic process applied to different elements viz., nut & bolt, steel plate, pelvis bone and screw. A thick steel plate screwed to pelvis bone at “sciatic buttress” at one end and “superior pubic ramus” of the pelvis bone at other end as shown in Figure 4.2. Therefore, the steel plate become an integral part of the pelvis bone. This is to make the pelvis bone to be able to transfer the load on the femur head. An internally threaded nut was welded to a plate attached to pelvis bone. The pelvis thus make a bolted joint mounted on the fixed vertical frame through a vertical guide way mechanism. The vertical guide way allow the pelvis bone system to move up and down.

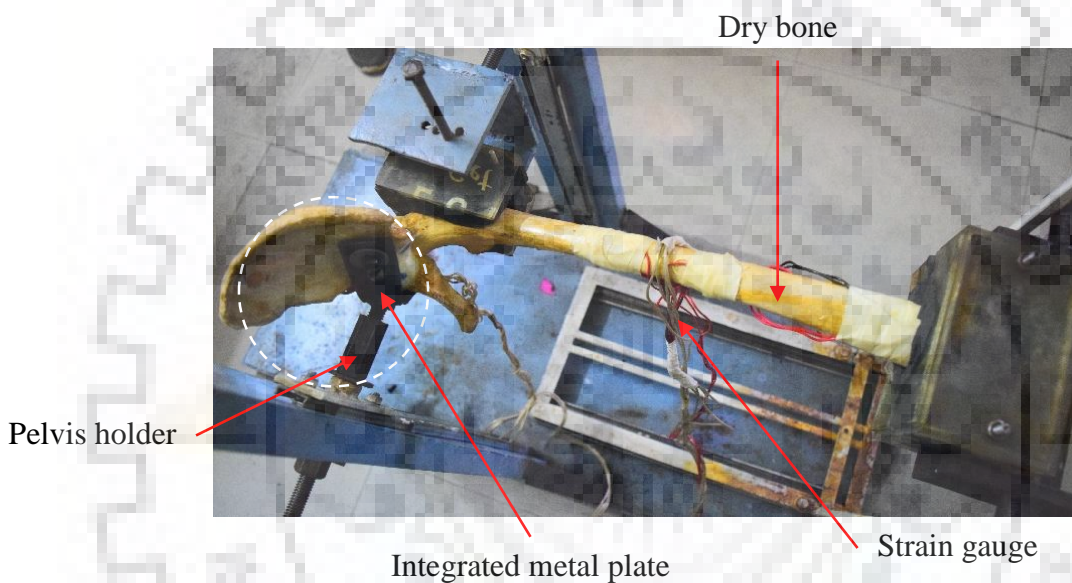


Figure 4.2 Photographic view of ‘pelvis holder’

4.1.2 Proximal femur holder

A ‘C’ – clamp was fixed to a rigid vertical frame as shown in the Figure 4.3 (side view). This is to hold the proximal femur (near trochanters) firmly. The trochanters have been supported by uniformly distributed compression load through a distinct material of epoxy. The ‘silica powder’ mixed with ‘epoxy resin’ in one part of the clay and ‘poly amide hardener’ in other part of the clay mixed together to form a glue. This glue was filled in mold box made up of acrylic sheets. The mold box here is a misnomer as the lower box could not be dragged as of casting mold box. The lesser trochanter was put in drag box to make imprint in the epoxy glue, while the greater trochanter was placed in cope box. The glue along with the trochanters left for a while to get solidified. The whole structure together ensure that, there is always a smooth and precise contact between the femur head and the acetabulum cup for all the body postures as shown in the Figure 4.3.



Figure 4.3 Photographic view of ‘proximal femur’ holder

4.1.3 Distal femur holder

Another fixture was fabricated in the same way for supporting the distal femur. The lower part of the box gets impression of medial and lateral condyles while the upper part of the box for patella femoral groove and anterior femur epiphysis. These fixtures ensures femur to be stable and having a stable assembly at hip joint when femur head articulates in acetabulum cup.

4.1.4 Horizontal guideway

The fixture at distal end of the femur is mounted at another frame (painted white as shown in figure) is allowed to move to and fro relative to fixed frame. This frame travels on a guide way such that the knee joint shifts according to hip joint by maintaining the rigidity of the experimental set up without hindering the successful squat. The range of movement of movable frame was given such that it duplicates the position of knee joint for any position of hip joint during the squat. The farthest it can move when the posture symbolizes chair sitting. At this position the distance between movable frame and fixed frame was equal to femur length while shortest distance was during standing posture when movable frame almost approaches underneath fixed frame but with slight eccentricity as we have in healthy human standing posture. The movable frame that embraces distal femur, the fixture that clenches trochanters at proximal femur and fixture that holds pelvis bone uses rectilinear guideways for the motion.

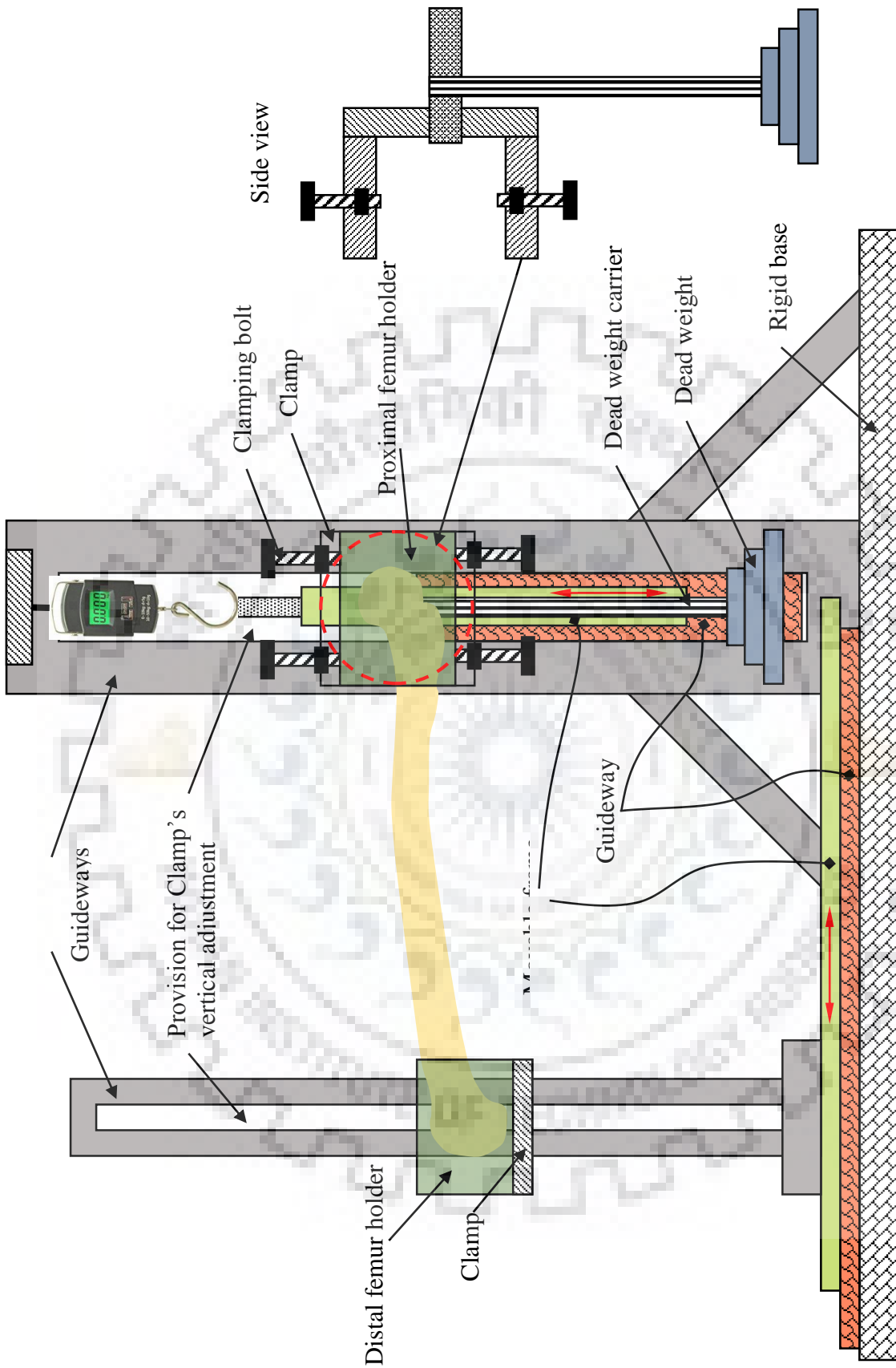


Figure 4.4 Schematic view of an experimental set-up

Experimental set-up

Rectilinear guideways provide linear motion by re-circulating rolling elements between a profiled rail and a bearing block. The coefficient of friction on a linear guideway is negligible compared to a traditional slide and they are able to take loads in all directions. With these features, the rectilinear guideway achieved great precision and significantly better moving accuracy. A schematic sketch of the experimental set-up has been shown in Figure 4.4.

4.2. Design Specifications and Considerations

The rig was designed to replicate all the possible postures of a squat. The dimensions of the system was considered on the basis of general South Asian human physic. The test rig is very much efficient to evaluate strain generated in any pelvis and femur bone of South Asian subjects. The apparatus used was successfully able to stabilize the test section during any instant of experiment.

4.2.1 Width of space

The whole system stands on the rigid iron base of dimension 1020 x 450 x 40 mm. The height of the fixed frame was 1130 mm and rectilinear guideways allows a high range of vertical movement of clamps and pelvis bone. The movable frame translates 480 mm with the help of the guideways situated in the width of 360 mm between two columns of the fixed frame. This design of the test rig makes it the generalized system for evaluating forces and stresses generated in lower extremity of Indian sub-continent population. The clamps, with nut and bolt arrangement, used to stabilize the test section between the fixed frame and movable frame were capable to clench the different sizes fixtures. Though, both the fixtures were subject specific and especially fabricated for available femur bone. Similar fixtures can be easily fabricable as per the availability of the human lower extremity for testing on the rig designed.

4.2.2 Length of the base

The effective length of the base is described as the extreme positions of femur and pelvis bone together. However, the experimental set-up was built to adjust its effective length based on the size of the femur and pelvis bone together. This provision helps to test bones of different size. The maximum length of the bone i.e. maximum test section length that could be tested is 48.6 mm.

4.2.3 Maximum weight could be tested

Dead weights were used to load the hip joint for each posture considered in the squat. The range of dead weights to be used was estimated by conducting the pilot experiments as per the

Experimental set-up

feasibility of the test section. A very small incremental load was applied to test the capability of the dry bones used. Thus evaluated that the maximum capability of the test section to bear the load was sufficient to measure normal weight range of the healthy adults of the subcontinent. The squat was discretized in five postures viz standing being the first, knee bending, chair posture, pre squat and deep squat posture being the last. The strain was measured for five weight categories for each posture. The magnitude of the load applied was uniformly distributed among the range selected viz 30 kg, 45 kg, 60 kg, 75 kg and 90 kg. The load was applied as near as possible to femur head and acetabulum cup assembly.

4.3. Dry bone

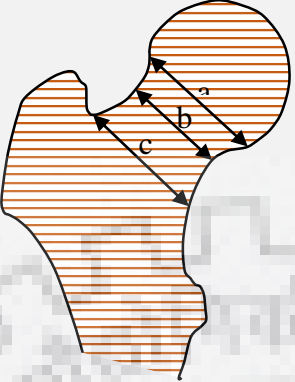


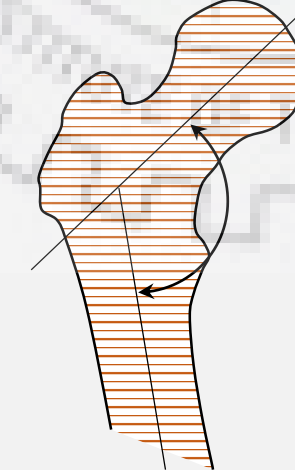
The dry bone was procured from an authentic supplier located in Kolkata. The set includes disarticulated left side original pelvis and femur bones. Both the bones are dry, healthy and free from contamination. The set of pelvis and femur shown in Figure 4.5 belongs to a healthy male subject of age about 51-55 years. The subject had an athletic routine i.e. high amount of physical activities. The bones when procured had few holes for being used as articulated human skeleton.

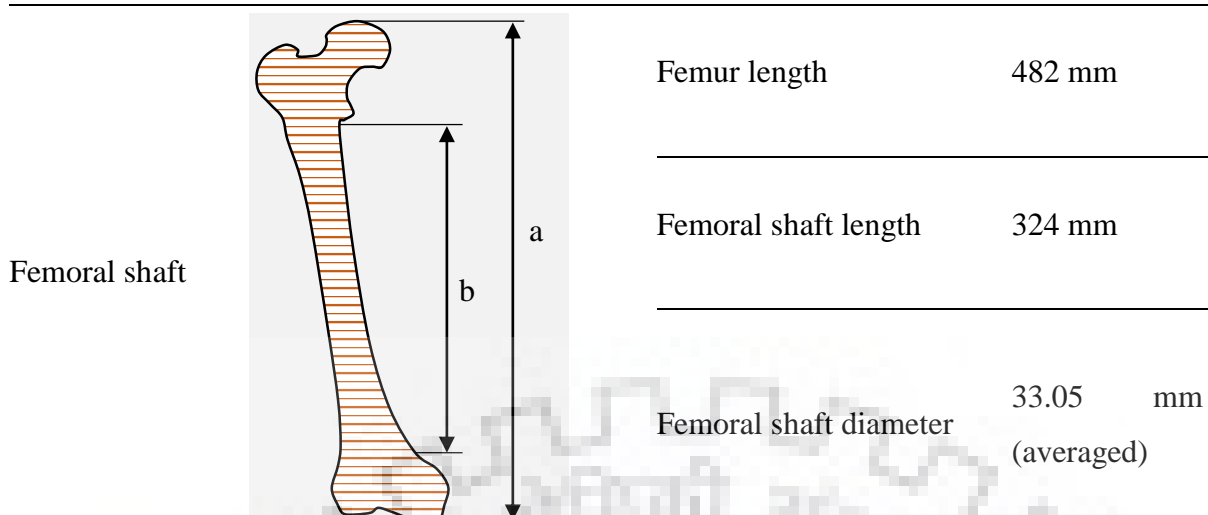


Figure 4.5 Dry bone set

Specifications: The dimensions of the femur bone is shown in Table 4.1. The femoral head lateral medial diameter has a maximum of 45.3 mm. The neck of the bone has a sub capital, midcervical and basilar diameter of 41.23 mm, 31.43 mm and 55.5 mm respectively. The length of sub-trochanteric apical axis is 93.24 mm with an angle of inclination 127.8° to the femoral shaft axis. The femoral shaft length includes metaphysis and diaphysis regions has a magnitude of 324 mm with a total length of 482 mm which includes proximal and distal epiphysis regions. The average femoral diameter at proximal metaphysis region is 27.3 mm and medio-lateral and anterior posterior femoral diameter at distal metaphysis region are 40.55 mm and 32.4 mm respectively. The least crosssectional diameter (assumed circular) is 25.4 mm. The acetabular cup of the pelvis bone is assumed hemisphere has a diameter of 48.3 mm.

Table 4.1 Specifications of the Femur bone

Portion of Femur bone	Graphical Terminology	Parameter	Dimension
Neck		a. Subcapital	41.23 mm
		b. Midcervical	31.43 mm
		c. Basilar	55.5 mm
Femur head		Latero-Medial diameter	45.3 mm
Sub-trochanteric apical axis		Sub-trochanteric axis length	93.24 mm
Angle of inclination		Angle of inclination	127.8°



Note: Digital Screw gauge and Vernier caliper were used to measure the above dimensions

4.4. Instrumentation

The following instruments were used in the present experimental investigation. The details of individual instruments have been explained in the following sections.

4.4.1 Strain gauge

A Strain gauge Figure 4.6 is a device whose resistance varies with applied force. It transforms force, pressure, tension, weight, etc., into a change in electrical resistance which can then be measured. Strain and stresses are the effects whenever any external forces applied on some object. The strain gauge is a sensor which measures tensile and compressive strain distinguished by positive and negative sign.



Figure 4.6 Strain gauge used for measuring strain (BKNIC-20)

Experimental set-up

The strain of an object is produced by an external impact or an internal effect such as moments, pressures, forces, heat, structural changes of the material etc. In a constraint environment, the magnitude of the influencing quantity can be assessed from the measured strain value. In order to evaluate the strain, the strain gauge must be connected to an electric circuit as shown in Figure 4.7. It is capable of quantifying the minute variations in resistance corresponding to strain. This electric circuit is called as Wheatstone bridge which is a divided bridge circuit used for measurement of electric resistance.

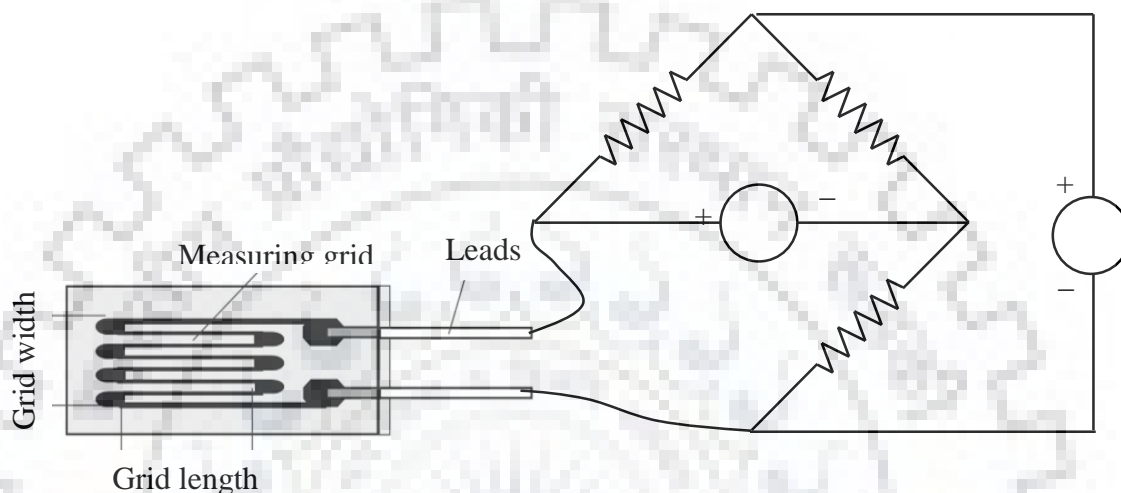


Figure 4.7 Strain gauge connection

Four set of strain gauges were equipped in the present study. Three of them mounted on femur bone while one at pelvis bone. The set of strain gauges mounted on the pelvis bone was used to measure the bending stress on pelvis due to reaction force generated by femur head at hip joint. The strain gauge mounted at metaphysis - near the trochanters measure the torsional effect on the femur while making the squat while the set of strain gauges at diaphysis shaft – minimum cross-sectional area and at metaphysis region of distal femur measures bending stresses.

4.4.2 Data logger

Data loggers are the equipment which automatically monitor and record parameters over time. Data logger receives the information to measure, document, analyze and validate according to the conditions provided to it before transferring it to storing device such as computers. The data loggers measure electronic information more accurately, effectively and with better reliability in comparison to manual recordings.

4.4.3 Weight measurement

The fixed frame includes an arrangement for mounting a spring balance at the top of the frame above the pelvis bone. The spring balance ensures stable position of pelvis for a posture by holding the nut attached to pelvis. By nullifying the self-weight of the pelvis-nut arrangement the spring balance confirms that only the load applied for testing contributes in strain calculation. The capacity of spring balance was to measure weight up to 150 Kg. The test rig was designed to evaluate the effects of human body weight on hip joint. Habitually, in south Asia, a healthy human adult weighs from 40 Kgs to 110 Kgs and each hip joint shares half of the body weight. Therefore, the range of weight used for the experiments was 20 Kg to 60 Kg. The dead weights were used to provide load at femur head acetabulum joint. The experimental set up tested 5 postures with 5 set of dead weights for the successful squat.

4.5. Experimental Procedure

The built in experimental set-up was used to perform the experiments to evaluate the strength of the femur and pelvis bone through the strain outcomes. The following procedure was practiced to achieve the objectives. The experiments conducted on the dry bone under different physical configurations with different body weights. The test rig has been located in the enclosed part of machine tool laboratory, IIT Roorkee.

- Preliminary experiments were conducted to verify the feasibility of the test rig and the test section under the range of load to be applied for experiments.
- The range of operating parameters under which the dry bone has to be tested had been specified before performing the experiments. The knee flexion has been changed from 0° to 155° in steps of 45° , 90° , 135° and 155° .
- The first posture was standing and the body weight distributes over the hip joints: The movable frame stay closed to fixed frame.
- The proximal fixture at trochanters was clamped such that the femur head and acetabulum cup stabilize themselves to allow the body weight on the hip joint.
- The pelvis bone was dangled by a spring balance attached to the top of the fixed frame. Test section was clamped at condyles with the help of distal fixture.
- A dead weight having load of 30 Kg hung just near the hip joint.
- The load replicates the half of the body weight of a 60 Kg human on his right side hip joint. Thus, the hip joint bears the body weight through the contact between the two bones.

Experimental set-up

- The posture was left for 10 seconds to stabilize the readings obtained by the data logger through attached strain sensors.
- The experiment was repeated thrice for having an average value of the strain generated at marked positions of the test section.
- Every new loading of the set up was done once the reading in the data logger reaches to zero.
- For evaluating strain values during second posture of the squat, the movable frame was adjusted such that the longitudinal axis of the femur makes an angle of 45° with the axis perpendicular to the normal to ground in the sagittal plane.
- The posture ensures the contact area between femur head and acetabulum cup for the posture. The test section was clamped through the fixtures to maintain the rigidity during strain evaluation.
- The standing posture was then loaded with another set of dead weights. The load of 45 Kg was applied to evaluate the change in strain readings and the data recorded when reading in logger stabilized.
- The system was unloaded and remained free so that wheat-stone bridge reaches to zero value. The observation process repeated for three readings further to be averaged.

Similarly, other three postures were evaluated. The movable frame was adjusted to its maximum possible location with the mounted test section for making chair posture i.e. 90° from the vertical axis of the sagittal plane. For pre squat and deep squat postures the movable frame was adjusted in such a way that the test section remains in 135° and 155° from vertical axis of the sagittal plane.



5.1. Mathematical model

In order to validate the above numerical and experimental results the mathematical model has been developed through kinematic approach. In this section the agreement of mathematical model prediction to the experimental and numerical results has been discussed.

5.1.1 Physical analogy

The present study was started with treating the human bones as kinematic links, through which the load is being transferred. The direction of load is defined by the kinematic structure of the linkages at different positions. The lower extremity of the body is analogous to a four bar mechanism. In the present study the four links are Tarsus (fixed), Tibia, Femur and Pelvis. The above four links undergo different positions while performing a successful deep squat. The tarsus through ankle joint is assumed to be fixed. The tibia experiences an oscillatory motion for multiple successful deep squats. While the femur and pelvis experiences the rectilinear and curvilinear motions respectively as shown in Figure 5.1.

There is no standard constrained motion of the pelvis in case of human subjects. However, in order to reduce the complexity, the motion of the pelvis is assumed to be a curved path as shown in Figure 5.1 defined by the physical dimensions and the angular positions of a tibia and femur. The pelvis follows the path traced by the point P (x_1, y_1). The path of the point P (x_1, y_1) is obtained by applying physical laws to individual links.

5.1.2 Kinematic constraints of individual links/joints:

Each link of the four bar mechanism considered in the lower extremity of human body has a constrained motion to perform a successful squat.

5.1.2.1 Tarsus

The tarsus is fixed link formulated when distal tibia joins talus to form a talocrural joint. The talocrural joint is a synovial hinge joint, that connects the distal ends of the tibia and fibula in the lower limb with the proximal end of the talus. Since the talocrural joint is a hinge type, the degree of freedom of ankle or talocrural joint is 1. In the present study, it is assumed that the tibia attains a maximum angle of 20° Norikin & White, (2009) and the corresponding maximum knee flexion is about, $\varphi = 155^\circ$ Norikin & White, (2009).

5.1.2.2 Tibia

As stated above, the distal end of tibia is hinged with tarsus and therefore the tibia can only oscillate about ankle joint. Thus the tibiofemoral joint, $K (x_1, y_1)$ oscillates about the talocrural joint as shown in Figure 5.1. The tibiofemoral joint is a modified hinge joint to permit the flexion and extension as well as slight internal and external rotation. In the present study, a negligible internal and external rotation of tibiofemoral joint is assumed to avoid the complexity of kinematic analysis.

Mathematically,

$$\theta_{1t} = \theta_0 + \theta_0 \sin(\omega t);$$

$$\omega_{1t} = \theta_0 \omega \cos(\theta_{1t});$$

5.1

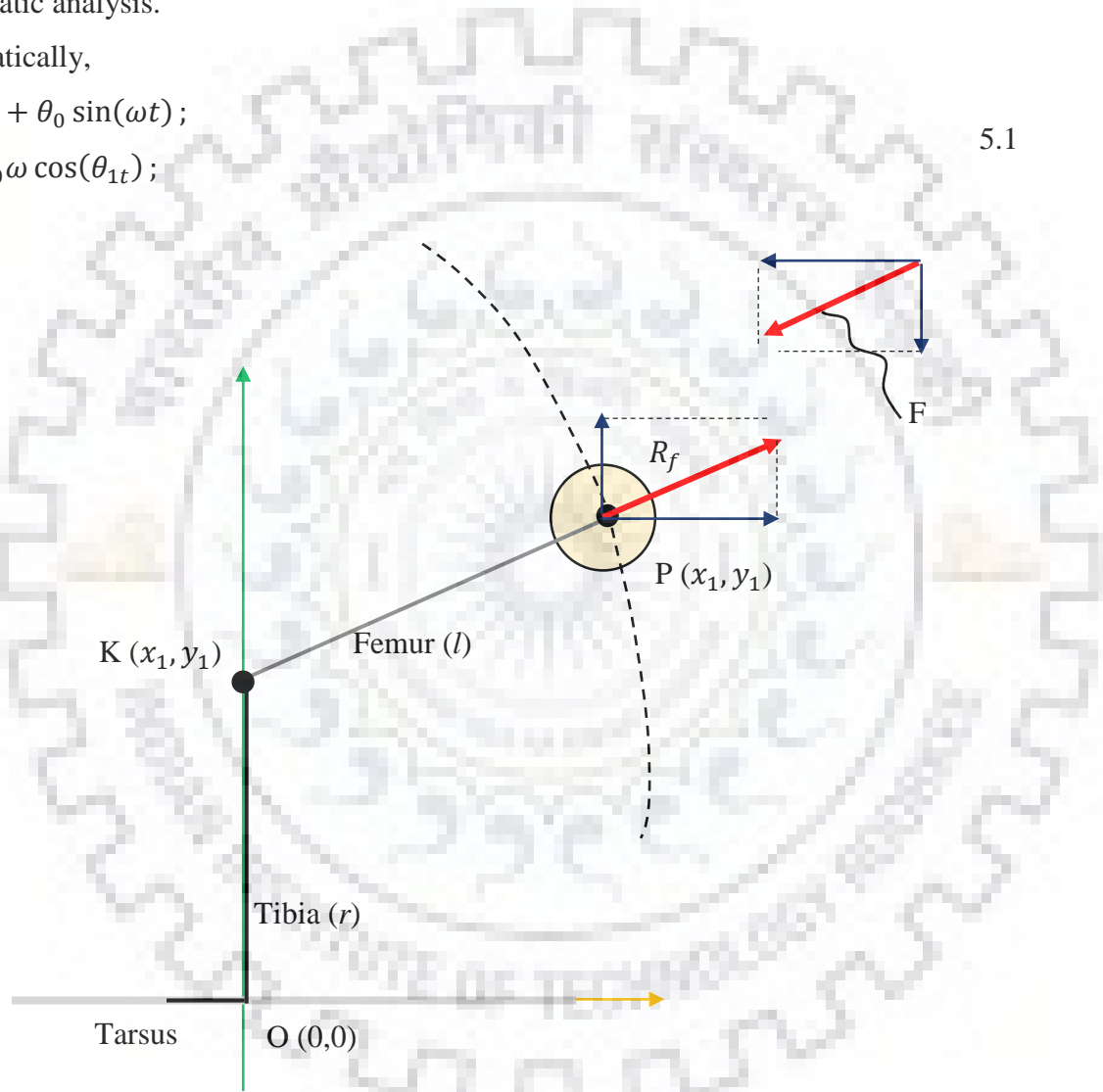


Figure 5.1 Path traced by hip-joint while performing a successful deep squat

5.1.2.3 Femur

The modified hinge type tibiofemoral joint causes the femur bone to exhibit a trans-rotational motion. However, the flexion and extension limited by the ligaments surrounded to the knee. The angular position of femur, θ_2 is inhibited by the angular frequency of the tibia while performing a successful deep squat.

Mathematical model

Mathematically,

$$\begin{aligned}\theta_{2t} &= (k - 1) \times \theta_{1t}; \\ \omega_{2t} &= (k - 1) \times \omega_{1t};\end{aligned}\tag{5.2}$$

Where the constant 'k' is given by,

$$\therefore k = \frac{\varphi_{max}}{\theta_{1,max}};\tag{5.3}$$

5.1.2.4 Pelvis

The pelvis bone is connected to femur bone to form hip-joint. The upper torso along with arms and head rests on hip-joint/pelvis. The hip-joint is a ball and socket type of joint Anderson et al., (2010); Arnold et al., (2010). connecting the upper half body to lower extremity. The hip-joint has three degrees of freedom. However, the flexion (100°) and extension (30°) are predominant as compared to lateral rotation (40°) and medial rotation (50°) and abduction (40°) and adduction (20°) around sagittal axis Norkin & White, (2009). Therefore, the rotation about longitudinal axis and sagittal axis has not been considered for the kinematic/dynamic analysis. The pelvis exhibits a curvilinear motion with two components of acceleration viz. tangential and radial or normal. The pelvis experiences a torque when the torso leaves the standing posture i.e. when the pelvis move away from the center of gravity line through which the line of action of force acts. In case of a slider crank mechanism the motion of the slider is constrained to a fixed path. However, the upper extremity body (analogous to slider) is kinematic ally constrained to move along the path traced by the mechanism of the femur bone, pelvis bone, tibia, tarsus and their joints.

5.1.3 Development of Mathematical model

In order to understand the relative motion between the links, a kinematic model has been developed for the configuration shown in Figure 5.2. The location of the pelvis is defined by the angular positions of the Tibia and Femur and their physical lengths. The random location of the pelvis is given by the point P (x_2, y_2).

Where,

$$x_2 = l \sin \theta_{2t} + r \sin \theta_{1t};\tag{5.4}$$

$$y_2 = l \cos \theta_{2t} + r \cos \theta_{1t};$$

As the Tibia is always allowed to oscillate, the motion is considered to be a simple harmonic motion (SHM). Although the motion of tibiofemoral joint is purely depending on the

Mathematical model

metabolism of an individual, a constrained SHM is assumed for the simplicity of kinematic analysis. Thus the angular displacement of Tibia at any instant is given by,

$$\theta_{1t} = \theta_0 \sin(\omega t); \tag{5.5}$$

θ_0 = Maximum amplitude = 20° ; ω = Angular frequency of the sit-up; t = Time instant;

Let, the knee flexion is directly proportional to the angular displacement of the Tibia and therefore we have, $\varphi = C \cdot \theta_{1t}$. Where the constant ‘C’ is defined by the maximum possible knee flexion and tibia dorsiflexion. In the present study, $\varphi_{max} = 155^\circ$ & $\theta_{1t,max} = 20^\circ$; Also,

$$\theta_{1t} + \theta_{2t} = \varphi_t; \tag{5.6}$$

The acceleration of Pelvis along the X&Y directions are given by,

$$\begin{aligned} a_{P_x} = \ddot{x}_2 &= -\omega_{2t}^2 l \sin\theta_{2t} - \omega_{1t}^2 r \sin\theta_{1t}; \\ a_{P_y} = \ddot{y}_2 &= -\omega_{2t}^2 l \cos\theta_{2t} - \omega_{1t}^2 r \cos\theta_{1t}; \end{aligned} \tag{5.7}$$

Where, ω_{1t}^2 and ω_{2t}^2 represents the angular accelerations of the tibia and femur respectively.

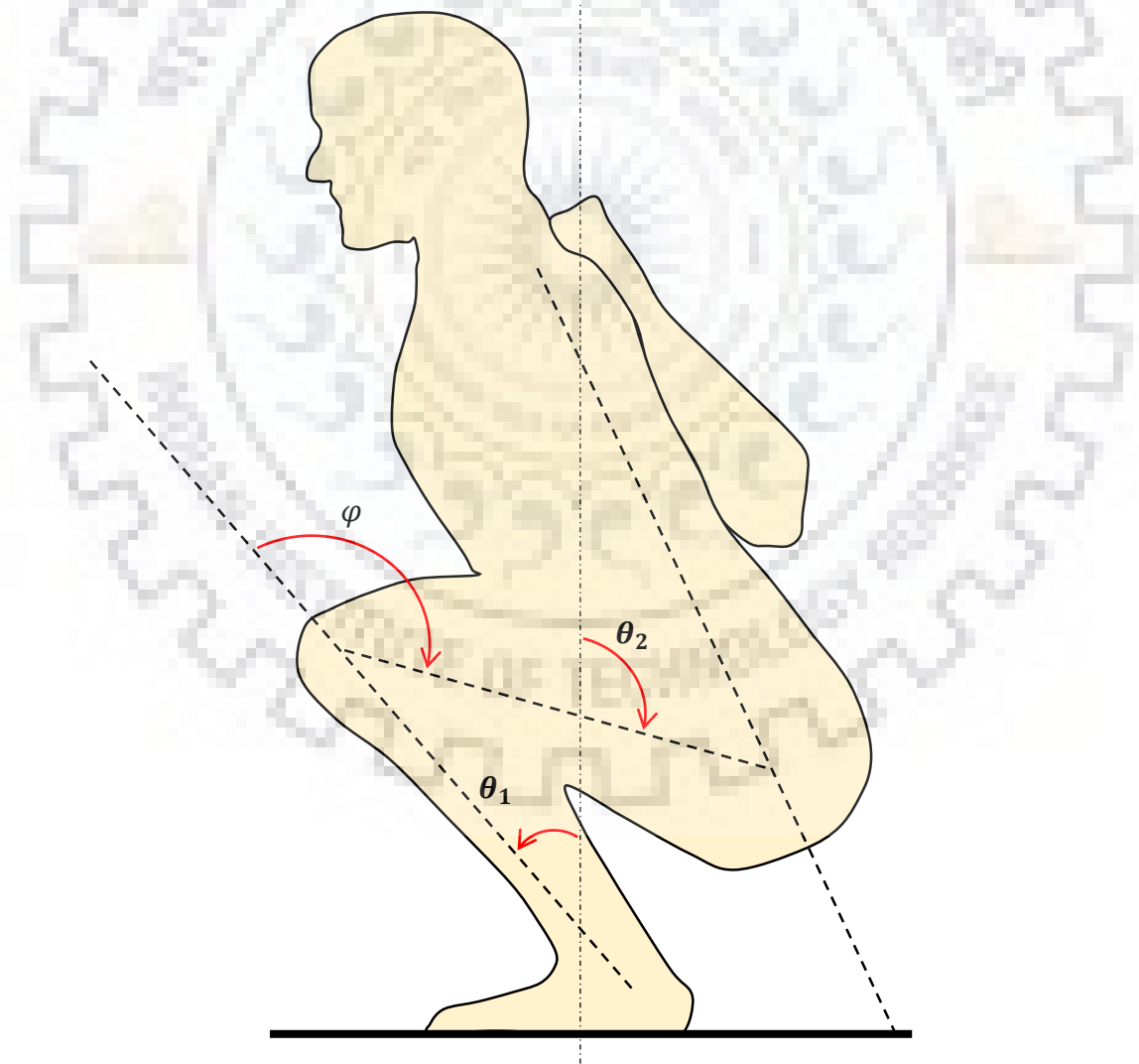


Figure 5.2 Kinematic movement of a Human hip-joint under deep squat posture

Mathematical model

The dynamic analysis was done on the kinematic model to obtain the joint reaction forces. The reaction force from the femur bone towards the hip joint is obtained the following sections. The force acting on joint due to acceleration of upper extremity body mass (m), is given by the product of mass and acceleration of mass towards the earth. There would be a reaction force from the femur bone, due to the load causing the motion. The resultant force acting on the femur head is given by,

$$F = m \cdot \sqrt{a_{P_x}^2 + a_{P_y}^2} \quad 5.8$$

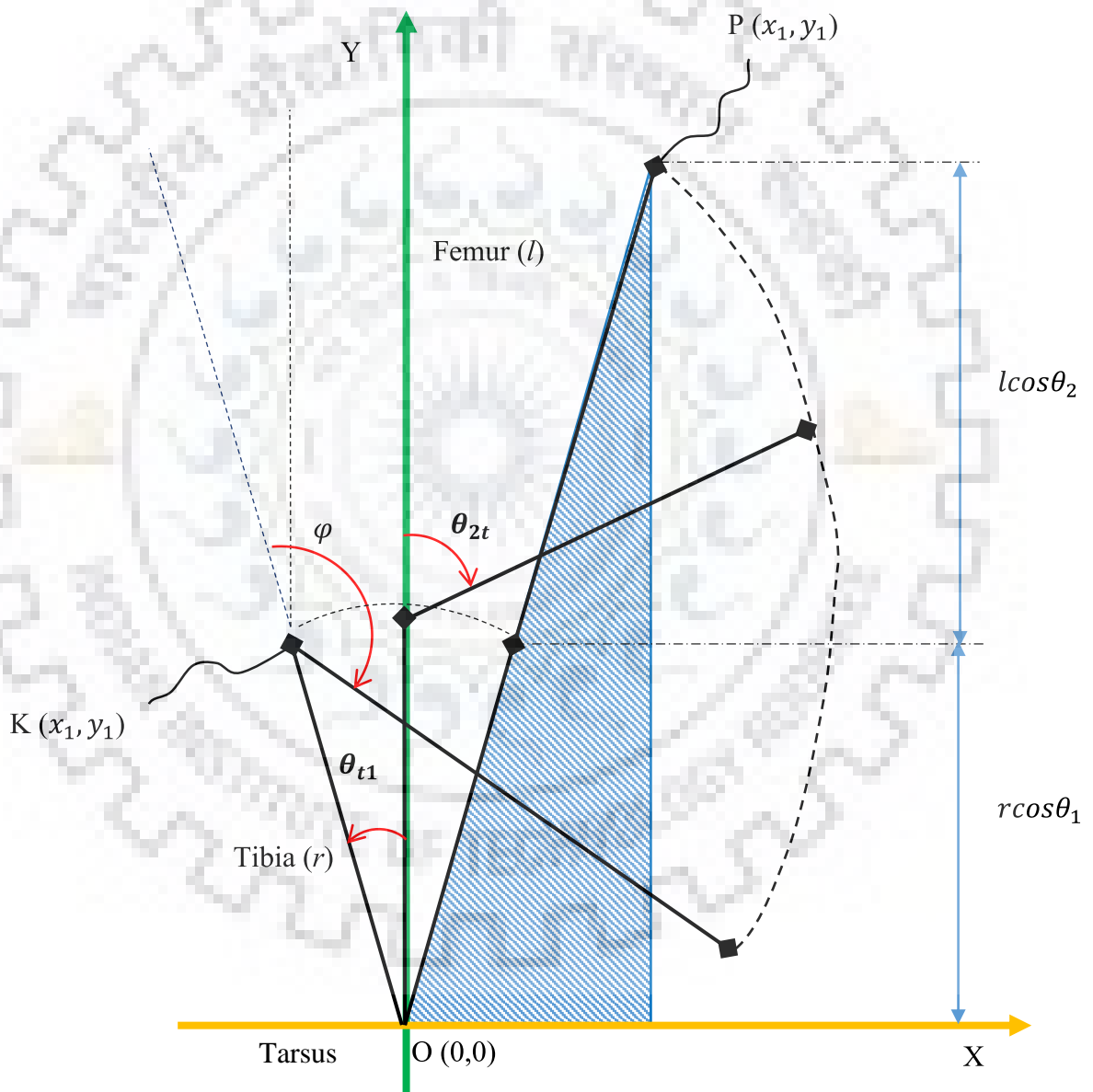


Figure 5.3 Kinematic constraints of a Human hip-joint with different knee flexion

Mathematical model

Sitting-down: The reaction force along the femur bone is given by the addition of weight to the force due to acceleration of upper extremity body towards the earth gravity, while performing a sitting-down activity.

Mathematically,

$$R_{f,down} = F + m. g. \cos\left(\frac{\pi}{2} - \theta_{2t}\right) \quad 5.9$$

Standing-up: The reaction force along the femur bone is given by the subtraction of weight to the force due to acceleration of upper extremity body against the earth gravity, while performing a sitting-down activity.

Mathematically,

$$R_{f,up} = F - m. g. \cos\left(\frac{\pi}{2} - \theta_{2t}\right) \quad 5.10$$

The evaluation of stress in three major portions viz., Femur head, Neck and Shank of femur bone was done by the following expressions. The direct normal stress is considered in neck and shank of femur bone. While direct compression or crushing stress was considered in femur head. The direct compressive stress between the femur head and acetabulum cup was obtained by taking analogy of “the stress between the solid sphere inside the hallow sphere”. Therefore, the Hertz’s Bhandari, (2010); WANG et al., (2005b) is to be considered to evaluate the compression stress.

Neck and Shaft:

$$\sigma_{c,Neck} \& \sigma_{c,shaft} \quad 5.11$$

$$= \frac{m. \sqrt{\left(-\omega_{2t}^2 l \sin \theta_{2t} - \omega_{1t}^2 r \sin(\theta_0 \sin(\omega t))\right)^2 + \left(-\omega_{2t}^2 l \cos \theta_{2t} - \omega_{1t}^2 r \cos(\theta_0 \sin(\omega t))\right)^2} \pm m. g. \cos\left(\frac{\pi}{2} - \theta_{2t}\right)}{\frac{\pi}{4} d^2};$$

Femur head:

$$\sigma_{c,Femur\ head} = \frac{F}{\pi * \left[\sqrt[3]{\frac{3F \left\{ \left(\frac{(1-v_1)^2}{E_1} \right) + \left(\frac{(1-v_2)^2}{E_2} \right) \right\}}{\left(\frac{1}{d_1} - \frac{1}{d_2} \right)}} \right]^2}; \quad 5.12$$

Further simplifying,

$$\sigma_{c,Femur\ head} = \frac{F}{4\pi} \left[\sqrt[3]{\frac{3d_1 d_2 F (E_2 (v_1^2 - 1) + E_1 (v_2^2 - 1))}{(d_1 - d_2) E_1 E_2}} \right]^2; \quad 5.13$$

Where, F is reaction force by femur, ‘v’ is Poisson’s ratio, ‘E’ is young’s modulus, ‘d’ is diameter; 1 represent femur head and 2 represent acetabulum cup

5.1.4 Operating Parameters

The following parameters has been considered for the purpose of kinematic study of the hip joint. The operating parameters are detailed in the following sections and their range is shown in Table 5.1.

5.1.4.1 Tibia flexion/extension, θ_{1t}

Tibia bone is the link adjacent to fixed link tarsus. Distal tibia bone with reference to ankle joint oscillates with a maximum range of movement of 20° Norkin & White, (2009). For making a successful squat, tibia moves anteriorly to flex ankle when body sits down and moves posteriorly to extend the ankle when body stands up. The angular displacement of the tibia flexion or extension is measured while performing the successful deep squat.

Mathematically, $\theta_{1t} = \theta_0 \sin(\omega t)$;

5.1.4.2 Angular displacement of femur bone on xy-plane, θ_{2t}

The angular displacement of femur bone is measured in the xy-plane with reference to y-axis, as shown in Figure 5.3. The angular velocity of femur bone is mathematically related to tibia's angular velocity as given below.

Mathematically, the angular velocity of femur bone, $\theta_{2t} = (k - 1)\theta_{1t}$;

5.1.4.3 Knee flexion/extension, φ

Femur bone is the third limb of the kinematic links in the four bar mechanism analogy of the present study. Distal femur rotates with respect to knee with a maximum range of movement of 155° Norkin & White, (2009) by flexing the knee joint during sitting down to make the deep squat. While knee extends during the second half of the squat when femur head rotates back to raise the hip and torso. The angular displacement of the knee flexion or extension with respect to tibia flexion or extension is measured while performing the successful deep squat.

Mathematically, $\theta_{1t} + \theta_{2t} = \varphi_t$;

5.1.4.4 Time period, T

In the present study, healthy human subjects were instructed to do deep squats calmly and uniformly within the comfort level of the individual subjects. All the human subjects of different age, weight, gender and routine categories performed squats in four sets with 10 squats in each. Time period for each set was observed. The duration was averaged for the sets and further for the total data collection of the individuals. The time period thus obtained for one squat was called the duty cycle of each squat.

5.1.4.5 Length of the femur/tibia

The length of the femur bone and tibia bone were estimated based on the ratio of length of the bone to the total height of the human subject. The aspect ratio of the length of the bone to the height of the human subject was standardized based on the X-ray scanning results of 10 human subjects. The standardized ratio would assist to estimate the length of the bone based on the height of the human subject.

5.1.4.6 Radius of the femur head, R

The present study has medical limitations, therefore, the femur head diameter was estimated based on the aspect ratio of the dimensions of the dry bone used in the experimental investigation.

Table 5.1 Range of operating parameters

Parameter	Range	Measures in
Ankle flexion/extension, θ_{2t}	0-20	degrees
Knee flexion/extension, φ	0-155	degrees
Time period, T	0.508-1.008	seconds
Length of the femur	370-540	mm
Length of the tibia	260-450	mm
Radius of the femur head, R	43-47	mm

6.1. Numerical model

The numerical simulation has been carried out to evaluate the stress distribution and the deformation along the femur bone. The simulation of a femur bone is analogous to the study of a cantilever beam with one end fixed and the other is free end. The maximum stresses and minimum deformations are originate at the condyle end of femur bone described by Masood et al., (2013). The free end is superior femur and the distal end acts like fixed support. The change of direction of stress components i.e., x, y-components were presented earlier. This change of nature of stress components results in change of magnitude of deformation and maximum distortion stress as well. The simulation was run for all the postures of a successful squat with shear strain energy theory applied to it. The von Mises criterion is chosen for the progression of simulation, due to consistent robust performance could be obtained under different loading conditions Keyak & Rossi, (2000). According to this theory the material fails when the von Mises stress exceeds the yield stress of the material.

The most reliable characteristics of failure of a mechanical object could be explained by the von Mises criterion. Based on this theory, the strain energy stored in a body due to the applied load is expressed in terms of hydrostatic/volumetric stress tensor and deviatoric/distortion stress tensor. Hydrostatic stress tensor component is responsible for deformation as well as dilation, while the deviatoric stress tensor component causes distortion of the body Bhandari, (2010).

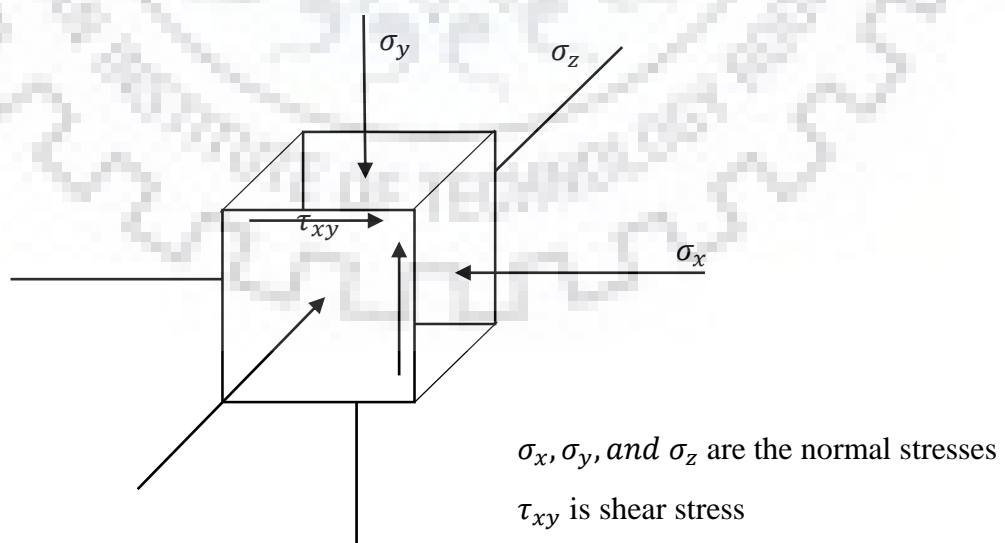


Figure 6.1 Stress boundary conditions

Results and Discussion

The normal stress is generated in femur with the application of load unidirectional i.e. x-direction, while the normal stresses in other two directions viz. y, z- directions are zero. The stress boundary conditions are shown in the Figure 6.1, referred to Bhandari, (2010). The principal stresses σ_1 and σ_2 were evaluated from Eq. 6.1 and thereby von Mises or deviatoric stresses determined by using Eq. 6.2 Bhandari, (2010).

$$\sigma_{1,2} = \left(\frac{\sigma_x + \sigma_y}{2} \right) \pm \sqrt{\left(\frac{\sigma_x - \sigma_y}{2} \right)^2 + \tau_{xy}^2} \quad 6.1$$

Where $\tau_{xy} = \tan 2\theta \left(\frac{\sigma_x - \sigma_y}{2} \right)$;

Where $\sigma_x = \frac{750}{a}$, $\sigma_y = 0$, $\sigma_z = 0$, and $\theta = 45^\circ$;

The von Mises stress is given by,

$$\sigma_v = \sqrt{\left[\frac{(\sigma_1 - \sigma_2)^2 + (\sigma_2 - \sigma_3)^2 + (\sigma_3 - \sigma_1)^2}{2} \right]} \quad 6.2$$

6.1.1 Deviatoric stress

This deviatoric stress component has been evaluated for each posture of successful squat. Figure 6.2 shows the distribution of deviatoric stress of a femur for different knee flexion. An increase of stress in the femur has been observed with increase of knee flexion angle. However, a maximum stress is observed, when the knee flexion angle is 126° . This could be due to the gradual increase of the force in lateral direction at femur head. The shifting of patella from femoral groove to mid of the condyles also might be reason for the same. The lateral component at the proximal femur tends to rotate it at the tibial plateau and since distal femur is constrained, condyles undergo maximum stress at anterior portion of the bone for whole squat until it reaches to high knee flexion region for deep squat.

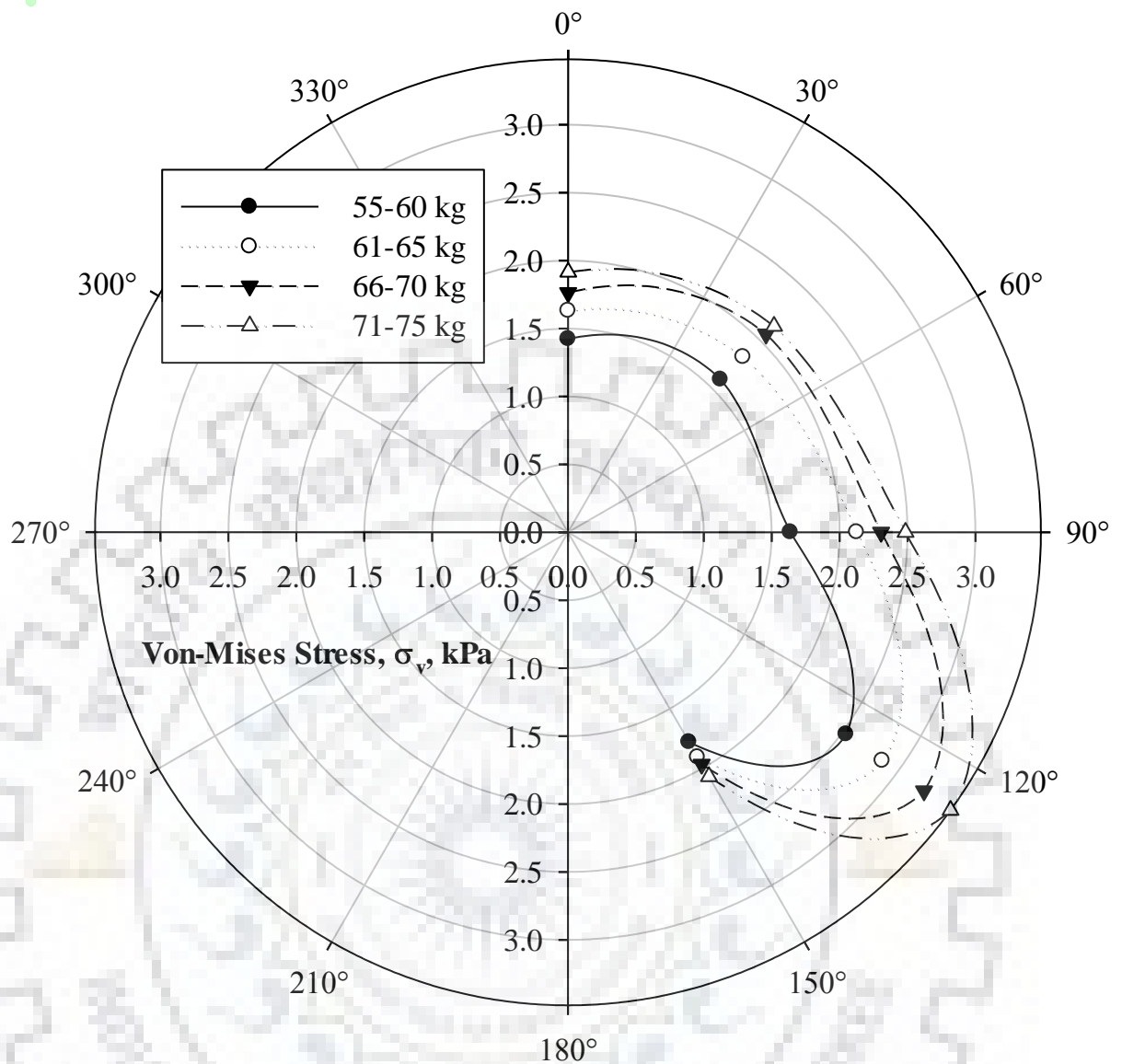


Figure 6.2 Effect of loading on Distortion stress for different postures of the body

6.1.2 Total deformation

The maximum deformation is observed at the superior femur and greater trochanter for all the postures. The variation of total deformation for different postures obtained from static structural analysis of femur with specified body weight is shown in Figure 6.3. The maximum deformation is observed for the chair posture followed by knee bend and pre-squat postures. It could be due to the change of nature of axial and translating force components at contact surface of femur head inside the acetabulum cup.

In addition to the above the kinetic load significantly affects the deformation. This kinetic load is due to the inertia of a body against gravitational effect causes the femur to rotate with finite velocity. A minimum or negligible kinetic load could be observed at standing and deep

Results and Discussion

squat postures. The femur head experiences minimum deformation because of this little kinetic effect for standing and deep squat postures.

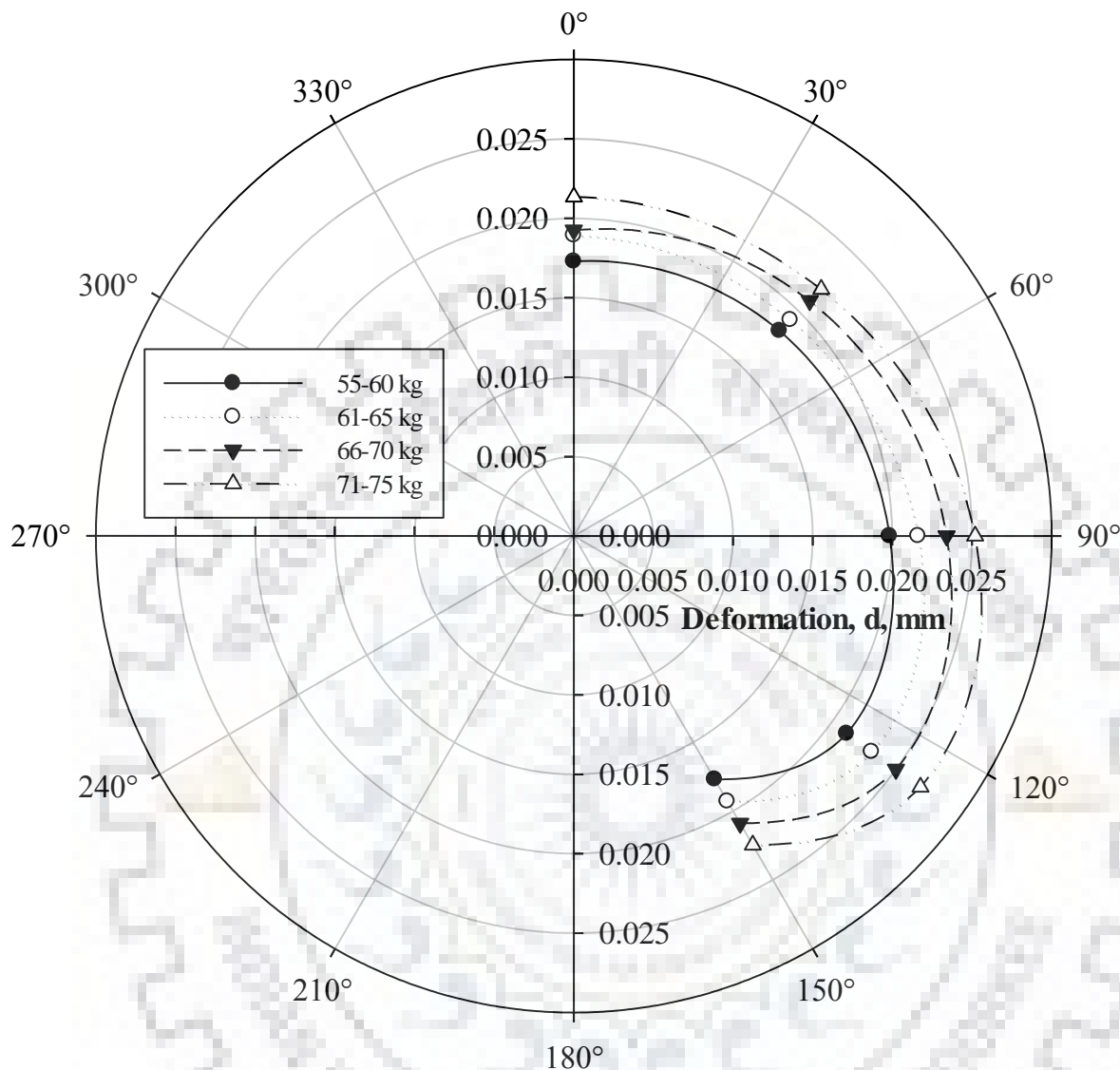


Figure 6.3 Effect of loading on Deformation

The axial/lateral component of the applied load acting at anterior to posterior direction results the femur to rotate towards the deep squat posture. An increase of femoral head deformation is observed till pre-squat posture. This deformation is gradually decreased after the pre-squat posture till the deep squat as shown in Figure 6.3. This could be due the lateral force is observed to be less as compared to axial load in deep squat posture. A ground support is obtained from distal joint through the tibial plateau and is equivalent to the resultant force. This ground support helps the bone to have stable and balanced posture.

Results and Discussion

6.1.3 Location of max. stress and deformation

The deformation of femur bone under different configurations of the femur bone has been evaluated through numerical simulation. All the posture was simulated under the static load i.e., body weight varied from 55-75 kgs. The simulations were carried by treating the lateral and medial condyles as rigid support. The femur bone was loaded at femur head as point load of body weight. The total deformation of the femur bone for different configurations of the human body has been discussed in the following sections. In addition to the deformation, the location of maximum stress in the femur bone is also been shown for the different postures.

6.1.3.1 Standing posture

The deformation of the femur bone in standing posture with body weight of 55-60 kg is shown in Figure 6.4. The femur head possesses highest deformation, while moving to the condyle a reduced deformation was noticed. The standing posture exhibits an increase of deformations with the body weight. When the range of body weight increases from 55-60 to 61-65 kgs, the highest deformation in femur bone was raised by 9 percentage. When the range of body weight increases from 61-65 to 66-70 kgs, the highest deformation in femur bone was raised by 2 percentage. Similarly, when the range of body weight increases from 66-70 to 71-75 kgs, the highest deformation in femur bone was raised by 10 percentage.

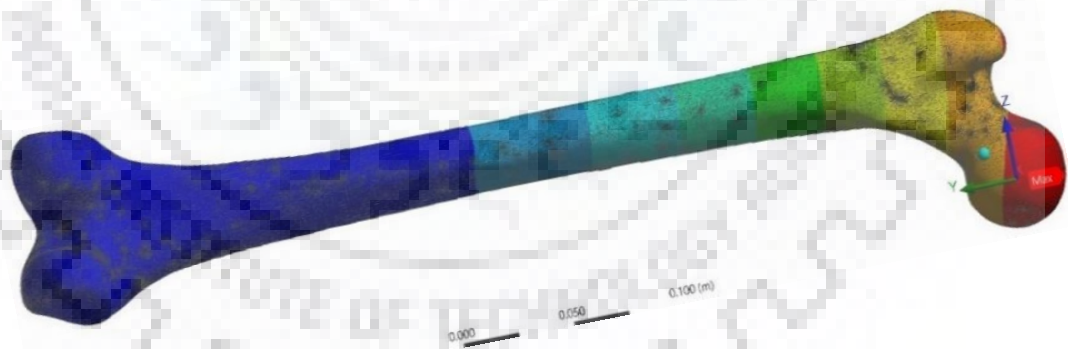


Figure 6.4 Total deformation in a femur bone with knee flexion under different body postures (M = 60 kgs)

On the other hand, the maximum stress in the femur bone was noticed to vary its location based on the body posture. This non-uniform distribution of the stress along the femur bone is due to irregular geometry, the change of bone properties and the physical configuration of the femur bone viz., one end fixed and other is loaded. The maximum stress is observed at the

Results and Discussion

“medial epicondyle”, which could be seen in the anterior view of the femur bone as shown in Figure 6.5.

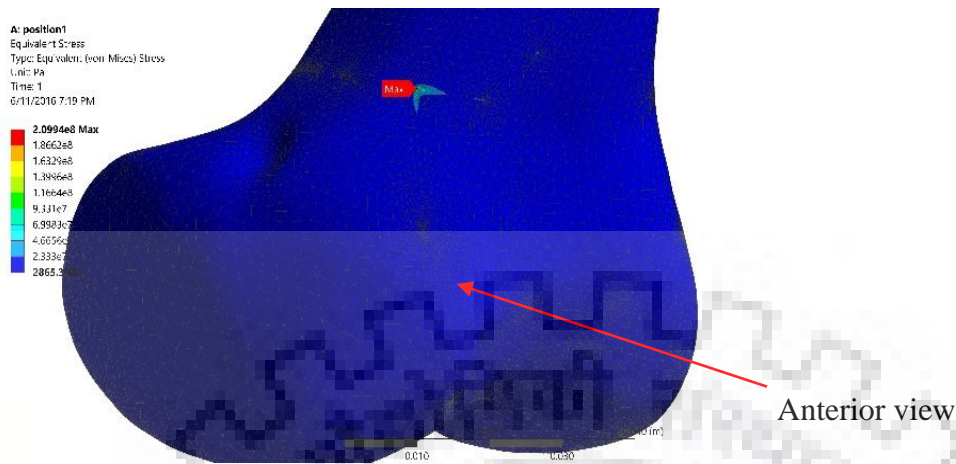


Figure 6.5 Location of maximum stress for different posture

6.1.3.2 Knee bend posture

The deformation of the femur bone in standing posture with body weight of 55-60 kg is shown in Figure 6.6. The femur head possess highest deformation, while moving to the condyle a reduced deformation was noticed. The knee bend posture exhibits an increase of deformations with the body weight. When the range of body weight increases from 55-60 to 61-65 kgs, the highest deformation in femur bone was raised by 4 percentage. When the range of body weight increases from 61-65 to 66-70 kgs, the highest deformation in femur bone was raised by 8 percentage. Similarly, when the range of body weight increases from 66-70 to 71-75 kgs, the highest deformation in femur bone was raised by 5 percentage.

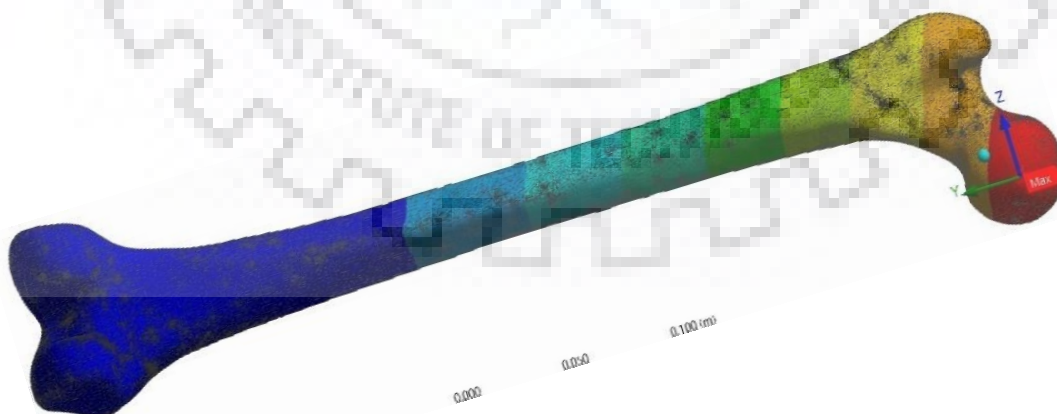


Figure 6.6 Total deformation in a femur bone with knee flexion under different body postures (M = 60 kgs)

Results and Discussion

On the other hand, the maximum stress in the femur bone was noticed to vary its location based on the body posture. The maximum stress is observed at the “patellar surface - close to lateral epicondyle”, which could be seen in the anterior view of the femur bone as shown in Figure 6.7.

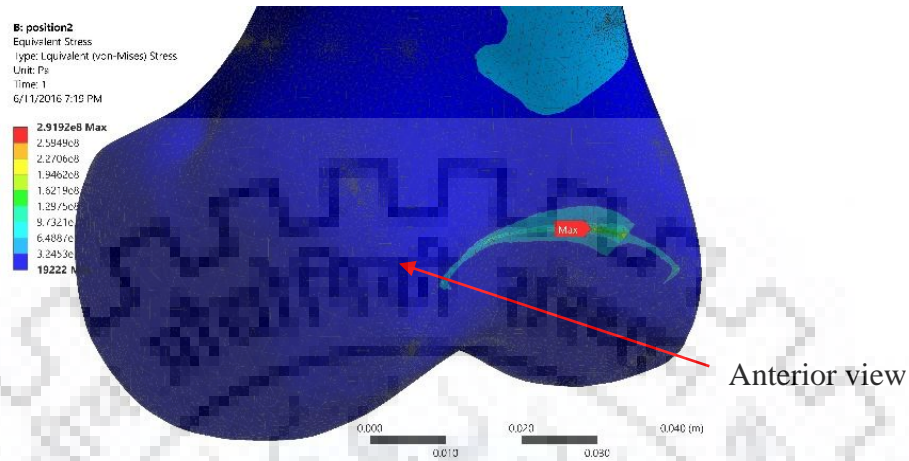


Figure 6.7 Location of maximum stress for different posture

6.1.3.3 Chair posture

The femur head possess highest deformation, while moving to the condyle a reduced deformation was noticed as shown in Figure 6.8. The chair posture exhibits an increase of deformations with the body weight. When the range of body weight increases from 55-60 to 61-65 kgs, the highest deformation in femur bone was raised by 9 percentage. When the range of body weight increases from 61-65 to 66-70 kgs, the highest deformation in femur bone was raised by 8 percentage. Similarly, when the range of body weight increases from 66-70 to 71-75 kgs, the highest deformation in femur bone was raised by 7 percentage.

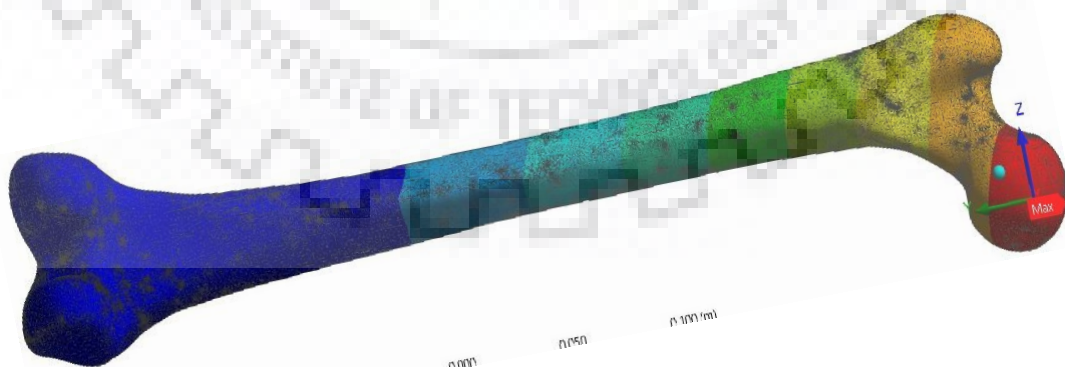


Figure 6.8 Total deformation in a femur bone with knee flexion under different body postures (M = 60 kgs)

Results and Discussion

On the other hand, the maximum stress in the femur bone was noticed to vary its location based on the body posture. The maximum stress is observed at the “patellar surface – close to medial epicondyle”, which could be seen in the posterior view of the femur bone as shown in Figure 6.9.

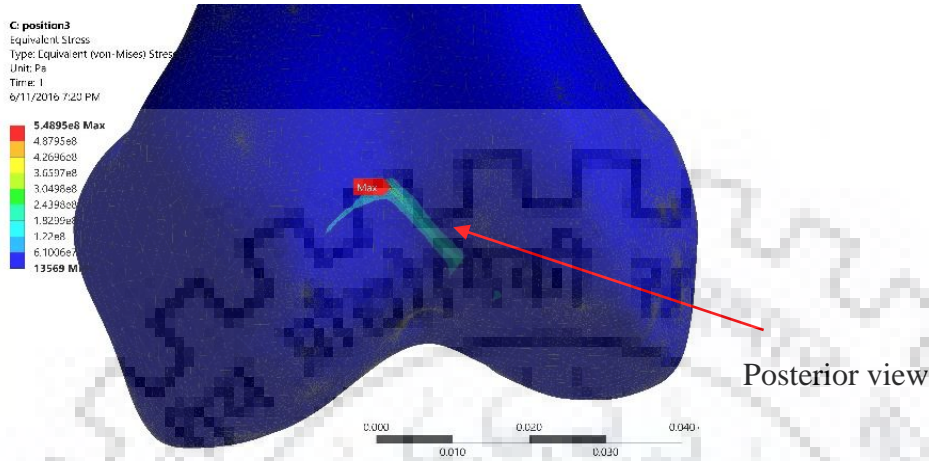


Figure 6.9 Location of maximum stress for different posture

6.1.3.4 Pre-squat posture

The femur head possess highest deformation, while moving to the condyle a reduced deformation was noticed as shown in Figure 6.10. The pre-squat posture exhibits an increase of deformations with the body weight. When the range of body weight increases from 55-60 to 61-65 kgs, the highest deformation in femur bone was raised by 8 percentage. When the range of body weight increases from 61-65 to 66-70 kgs, the highest deformation in femur bone was raised by 8 percentage. Similarly, when the range of body weight increases from 66-70 to 71-75 kgs, the highest deformation in femur bone was raised by 7 percentages. A tensile nature of stress has been observed after chair posture. This is due to the sign change of a component of resultant load along the longitudinal axis. The maximum deviatoric stress of 2.86 GPa is generated at anterior portion of femur in pre-squat posture.

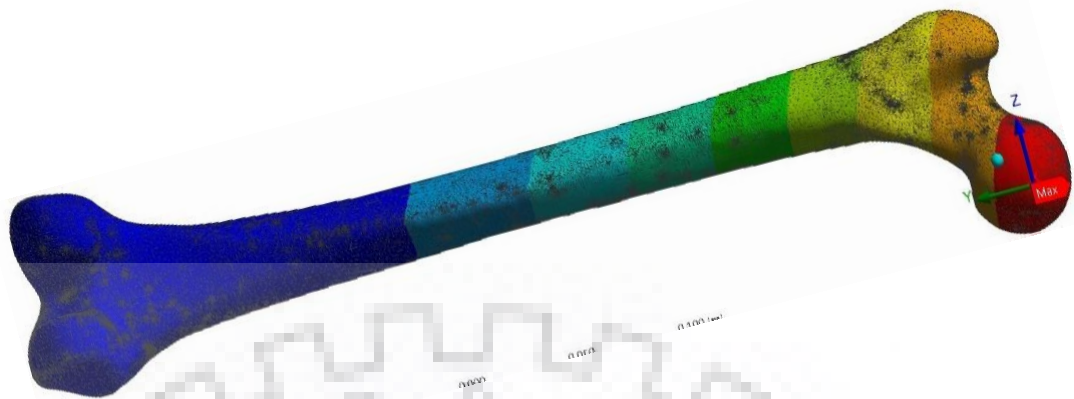


Figure 6.10 Total deformation in a femur bone with knee flexion under different body postures (M = 60 kgs)

On the other hand, the maximum stress in the femur bone was noticed to vary its location based on the body posture. The maximum stress is observed at the “patellar surface - close to lateral epicondyle”, which could be seen in the posterior view of the femur bone as shown in Figure 6.11.

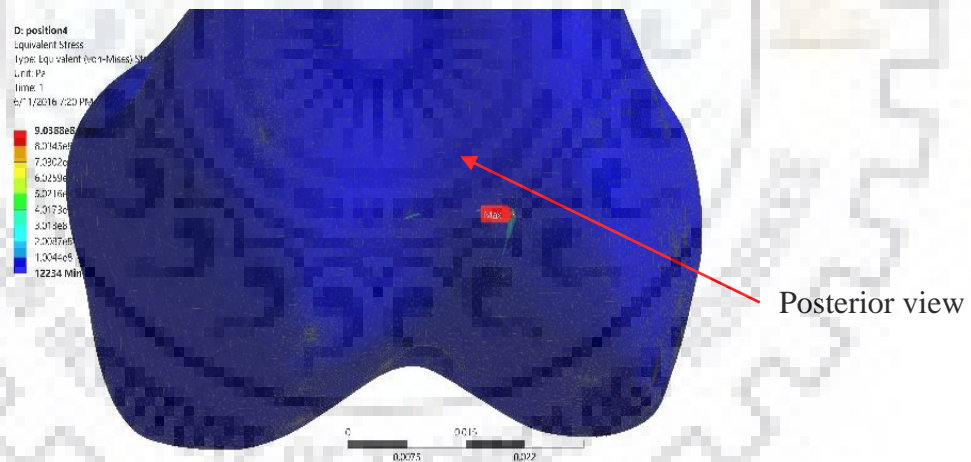


Figure 6.11 Location of maximum stress for different posture

6.1.3.5 Deep-squat posture

The femur head possess highest deformation, while moving to the condyle a reduced deformation was noticed as shown in Figure 6.12. The deep squat posture exhibits an increase of deformations with the body weight. When the range of body weight increases from 55-60 to 61-65 kgs, the highest deformation in femur bone was raised by 9 percentage. When the range of body weight increases from 61-65 to 66-70 kgs, the highest deformation in femur bone was raised by 8 percentage. Similarly, when the range of body weight increases from 66-70 to 71-

Results and Discussion

75 kgs, the highest deformation in femur bone was raised by 7 percentage. During the deep squat posture the lateral component of the resultant load becomes insignificant unlike the previous postures due to the geometric position of the femur head and thereby the components of forces are affected. This eventually led to sudden decrease of deviatoric stresses. The maximum stress in case of deep squat posture is observed at posterior portion of the distal femur. This may be due to the resting style of femur on tibia. During deep squat the femur rests on tibia through posterior portion instead of mid portion of the condyle.

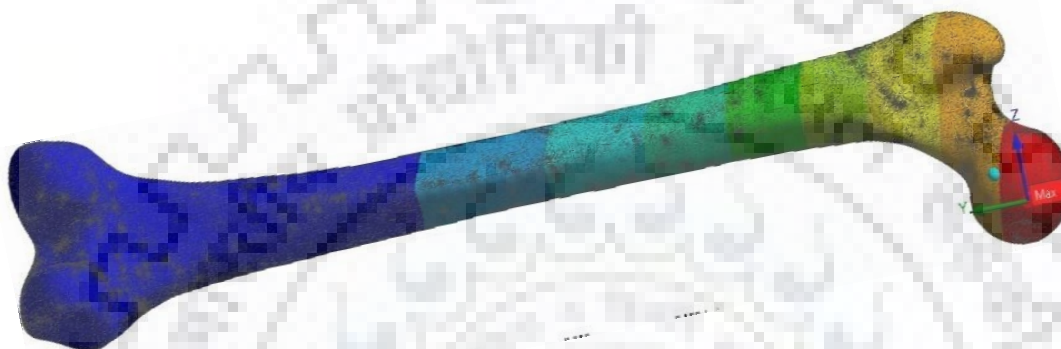


Figure 6.12 Total deformation in a femur bone with knee flexion under different body postures (M = 60 kgs)

On the other hand, the maximum stress in the femur bone was noticed to vary its location based on the body posture. The maximum stress is observed at the “intercondylar fossa - just above the lateral condyle”, which could be seen in the posterior view of the femur bone as shown in Figure 6.13.

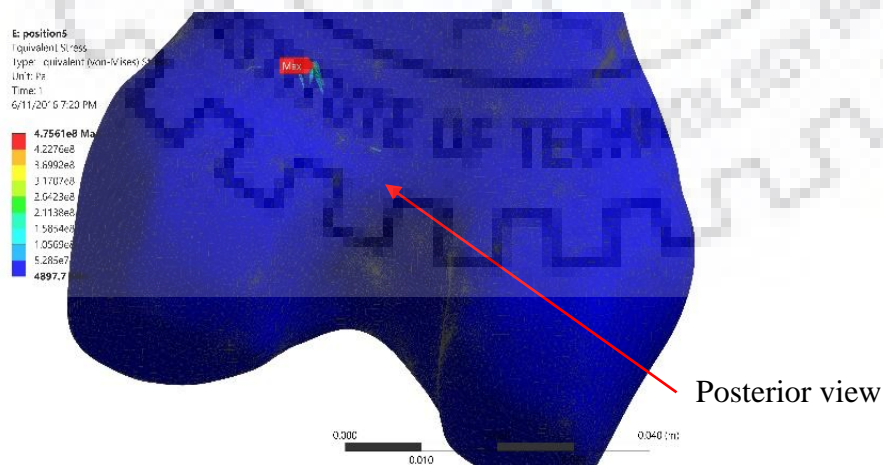


Figure 6.13 Location of maximum stress for different posture

Results and Discussion

It can be inferred from the Figure 6.5, Figure 6.7, Figure 6.9, Figure 6.11 and Figure 6.13 that, in case of all the posture styles the maximum stress is obtained at distal femur. The results show a very close agreement to the results of Sowmianarayanan, (2003). The distal femur experiences the maximum stress and its location changes circumferentially with respect to the posture style.



6.2. Experimental investigation

The experimental set-up has been built for evaluating the strain against the load variation under different postures of the successful deep squat. The experimental set-up was built to perform the tests on a dry bone under static equilibrium conditions. The familiar body postures viz., standing, knee bend, chair, pre-squat and deep squat postures of successful deep squat were examined to evaluate the stress distribution under different body weights. The above familiar body postures were attained through knee flexion of 0° , 45° , 90° , 135° and 155° . The five familiar postures of deep squat were examined with varying body weight from 55 to 75 kgs. The strength of the femur bone and pelvis bone were estimated through strain values obtained from the experiments. All the experimental readings were noted while decreasing the load. The medial condyle and lateral condyle of femur bone together firmly fixed such that, a knee joint was resembled. The femur head left for constrained oscillation in vertical direction (clockwise rotation) and loaded through pelvis bone.

6.2.1 Strain distribution

The strain gauges were fixed at critical locations of the femur bone as well as the pelvis bone viz. Just above the convexity of 'Pelvis bone' – Opposite wall of Acetabulum cup, Metaphysis femur shaft – Near Trochanters, Diaphysis femur shaft – Minimum cross section area, and Anterior metaphysis femur – near to condyles. The strain gauge values were recorded for each posture with different weights. These strain values were evaluated on the basis of load transferred through the contact area at hip joint for the posture. The details of location of strain gauges, verity and specifications has been shown in the Table 6.1. Four strain gauges were provided on the femur-pelvis bone system to read the strain values at different locations. Since, the young's moduli for cortical and cancellous bones are known Rho et al., (1998), the internal stresses were estimated at the required locations. The nature of the stress viz., compression or tension, described by the femur bone configuration.

The femur bone was set to the specified posture viz., standing, knee bend, chair, pre-squat and deep squat and loaded with weights through pelvis bone. The body postures were attained through knee flexion to 0° , 45° , 90° , 135° & 155° . All the body postures were tested for the range of body weights varies from 55-75 kgs in the steps of 5 kgs. Four strain values were noted for each femur-pelvis configuration. The variation of strain values are plotted in Figure 6.14. A significant effect of strain gauge location is also confirmed from the Figure 6.14.

Table 6.1 Details of location of strain gauges

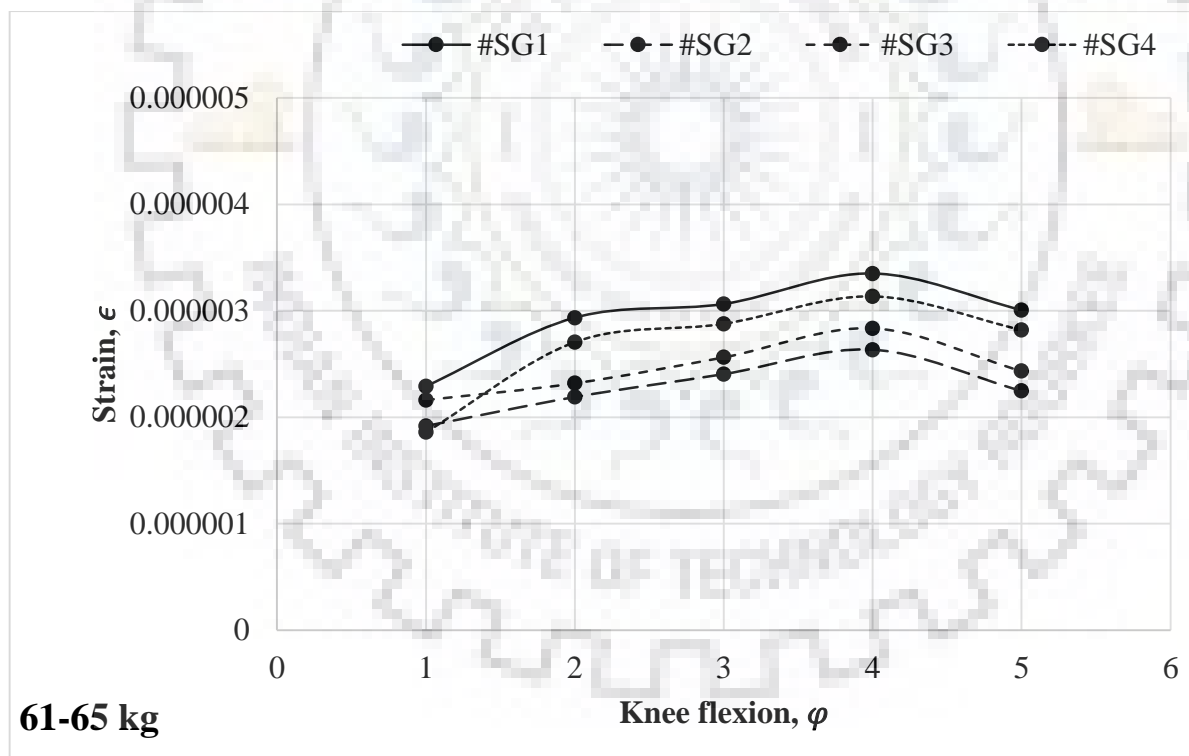
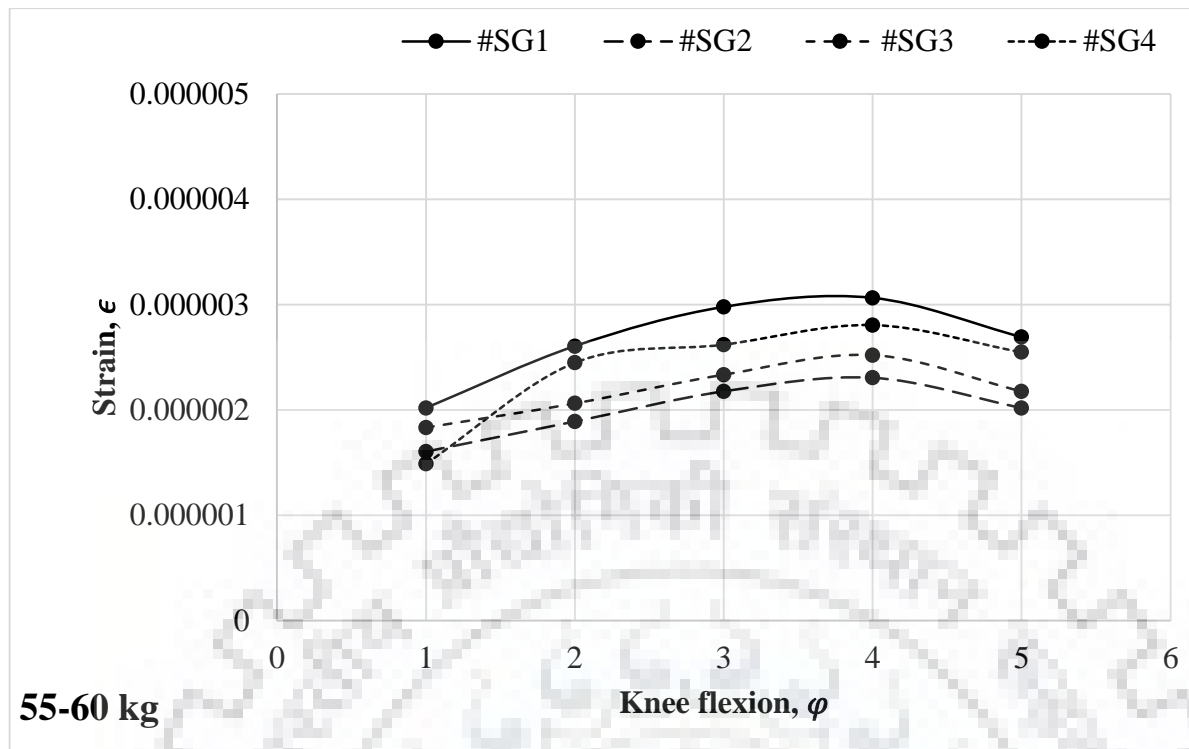
Tag	Location of strain gauge	Specification	Wheatstone bridge type
#SG1	Just above the convexity of 'Pelvis bone' – Opposite wall of Acetabulum cup		Full
#SG2	Metaphysis femur shaft – Near Trochanters	BKNIC-20 GF 1.98 ±	Full
#SG3	Diaphysis femur shaft – Minimum cross section area	2% and GL 5mm	Half
#SG4	Distal femur – Just above the Condyles		Full

*GF - Gauge factor & *GL - Gauge length

The effective load on the hip joint causes the deformation of bone and which induces strain in the joint. Since, the load is being transferred through the bone, all the portions of the femur bone and pelvis bone are to be strained. The effective load on the bone causes the strain. However, the material and geometrical properties of the test section significantly affects the strain to vary. Strain gauges mounted on specified critical locations returns the value of strain. The higher magnitude of strain could be seen in the pelvis bone for all the postures. However, the remaining wheat-stone bridges produces the strain values based on the kinematic constraints.

A lowest magnitude of strain could be seen in the metaphysis region of the distal femur – above condyles for standing posture. It is to be noted that, there is 8.8-23 % higher strain at diaphysis femur shaft – minimum cross section area, as compared to the distal femur - above condyles. This could be due to the least cross sectional area of the femur bone. A significant increase in strain observed in the distal femur – above condyles as the knee was flexed to $\varphi = 45^\circ$. A linear increase strain was also observed at Metaphysis femur shaft – Near Trochanters and Diaphysis femur shaft. It may be due to the couple generated by the body weight after leaving the standing posture. Further, a substantial increase of strain at all Wheatstone bridges was observed with knee flexion of ' $\varphi = 90^\circ$ ' i.e., chair posture. There is a 6.5-15% higher strain in the distal femur - above condyles, as compared to diaphysis femur shaft – minimum cross section area. The higher magnitudes of couple could be the reason for the above. The strain was further increased while progression of knee flexion to $\varphi = 135^\circ$ i.e., pre-squat posture. The increment of 3-13% was observed in comparison to chair posture. Although there was a slight decrease in moment, the strain was scattered up. A reduced arc of contact between the femur head and acetabulum cup resulting the less resisting area to work against the tensile stress could be the reason for the above.

Results and Discussion



Results and Discussion

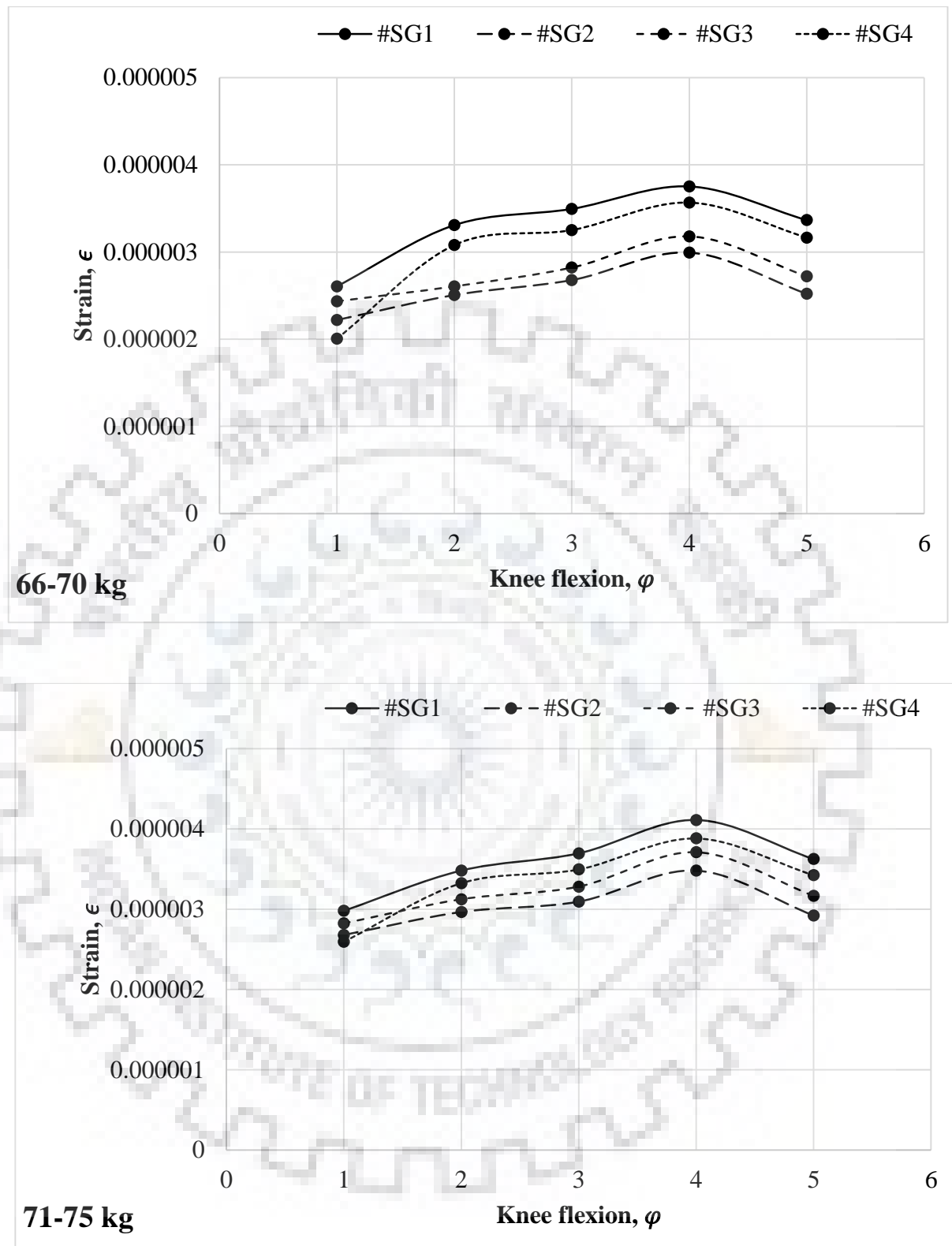


Figure 6.14 Variation of magnitude of strain with respect to knee flexion and location of strain gauge for different body weights

Subsequently, the higher stresses were developed in the test section. A less deformation due to the reduced moment was observed. However, the reduced area become predominant factor for the stress to rise throughout the test section. A substantial decrease of strain was

Results and Discussion

noticed with knee flexion of ' $\varphi = 155^\circ$ ' i.e., deep-squat posture. It is also evident that, the deep squat posture shows an independent effect to reduce the strain by 9-16%. A significant decrease of distance between the axis of applied load and the strain gauge location could be the reason for the above.

On the other hand, from the Figure 6.14, it is also evident that, the pre-squat-posture produces more strain as compared to other locations. The pre-squat posture produced a 9-16 %, 3-13%, 13-22% and 31-77% higher strain as compared to deep-squat, chair, knee-bend and standing postures respectively.

6.2.2 Estimation of bone strength

In the process of estimating the strength of the femur and pelvis bones, the normal stress has been evaluated by using the strain values obtained from the experiments. In order to evaluate the stresses under different configurations of the hip-joint, the physical properties viz., modulus of elasticity of the femur bone were used. When the knee is flexing from 0° to 90° , the nature of stress in the femur bone is to be compressive, while the knee is flexing from 90° to 155° , the nature of the stress is to be tensile. In the present study, the magnitude of stress acting in the femur bone and pelvis bone was considered to estimate the bone strength regardless of the nature of the stress. The tensile or compressive nature of the stress would be useful in evaluating the type of failure of the joint/bone.

The acetabular labrum (glenoidal labrum of the hip joint) works against both compressive and tensile load during successful deep squat. On the other hand, the acetabular notch works against the tensile load only. The acetabular labrum is a ring of cartilage that surrounds the acetabulum of the hip joint. Which provides an articulating surface for the acetabulum, allowing the femur head to articulate with the pelvis. While the acetabular notch is a deep notch in the acetabulum of the hip bone. From the chair posture to deep squat, partial tensile load is taken by the acetabular labrum and remaining taken by the acetabular notch. The deep squat posture exhibits appropriate fit between the femur head and acetabular notch. While the pre-squat posture exhibits partial contact with both acetabular labrum and acetabular notch. All the strain values obtained during the experiments were used to estimate the stress by using the following relation.

$$\frac{\sigma}{\epsilon} = E \quad 6.3$$

σ – Stress, KPa

ϵ – strain

E – Modulus of elasticity, MPa

Results and Discussion

6.2.2.1 Effect of location of strain gauge on stress

The modulus of elasticity has distinct values for different portions (cortical and cancellous) of the femur and pelvis bone. The use of modulus of elasticity, E, depends on the location of strain gauge i.e., whether cortical or cancellous bone. The stress along the femur and pelvis bone were evaluated by using the modulus elasticity and plotted in Figure 6.15, Figure 6.16, Figure 6.17, and Figure 6.18 for four different strain gauges #SG1, #SG2, #SG3 and #SG4 respectively.

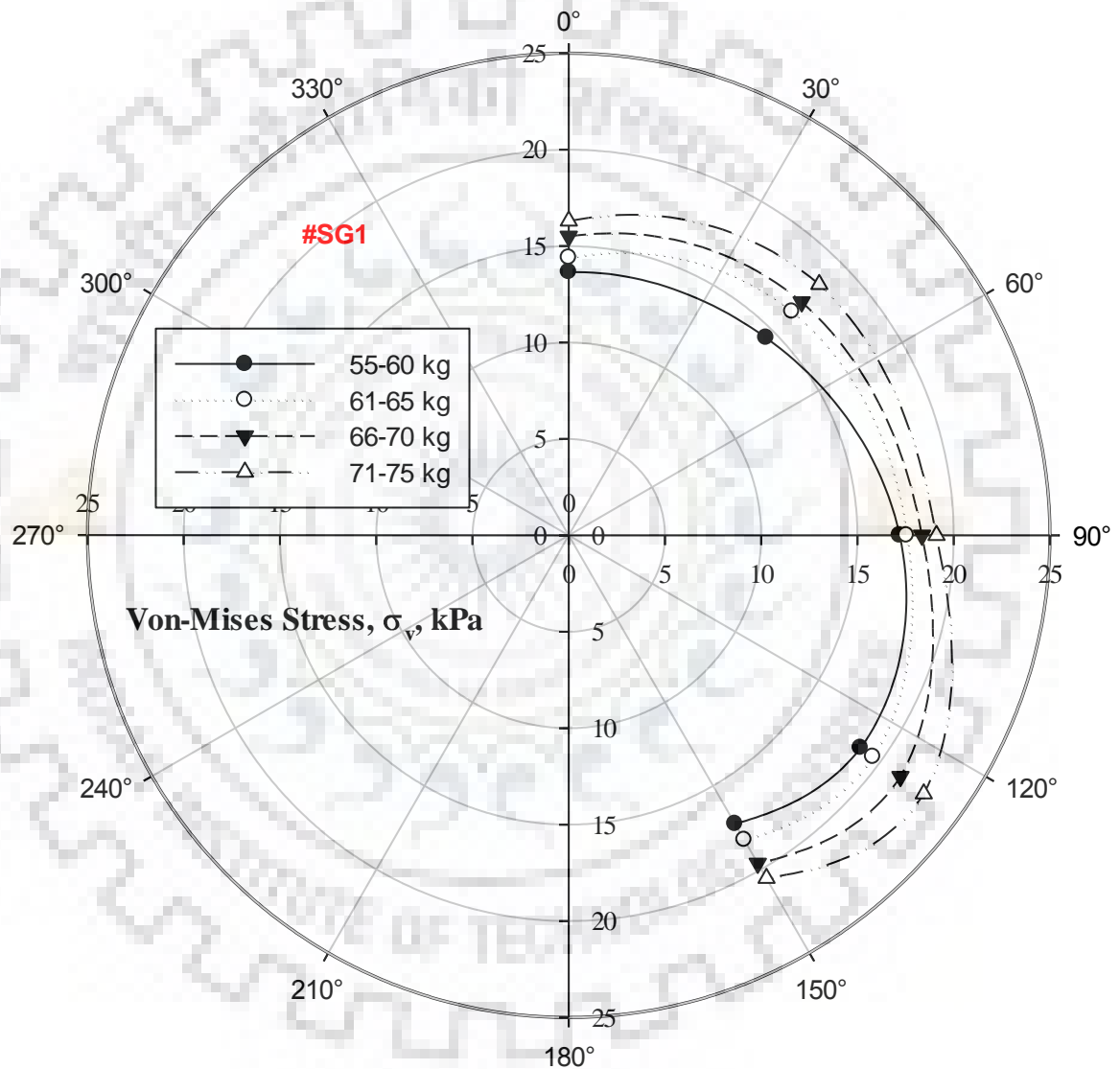


Figure 6.15 Stress distribution above the convexity of 'Pelvis bone' – Opposite wall of Acetabulum cup, under different body configurations

The stress values in an ascending order in context to the location of the strain gauge for standing posture is: Distal femur – Just above the Condyles, Diaphysis femur shaft – Minimum cross section area, Metaphysis femur shaft – Near Trochanters and Just above the convexity of 'Pelvis bone' – Opposite wall of Acetabulum cup.

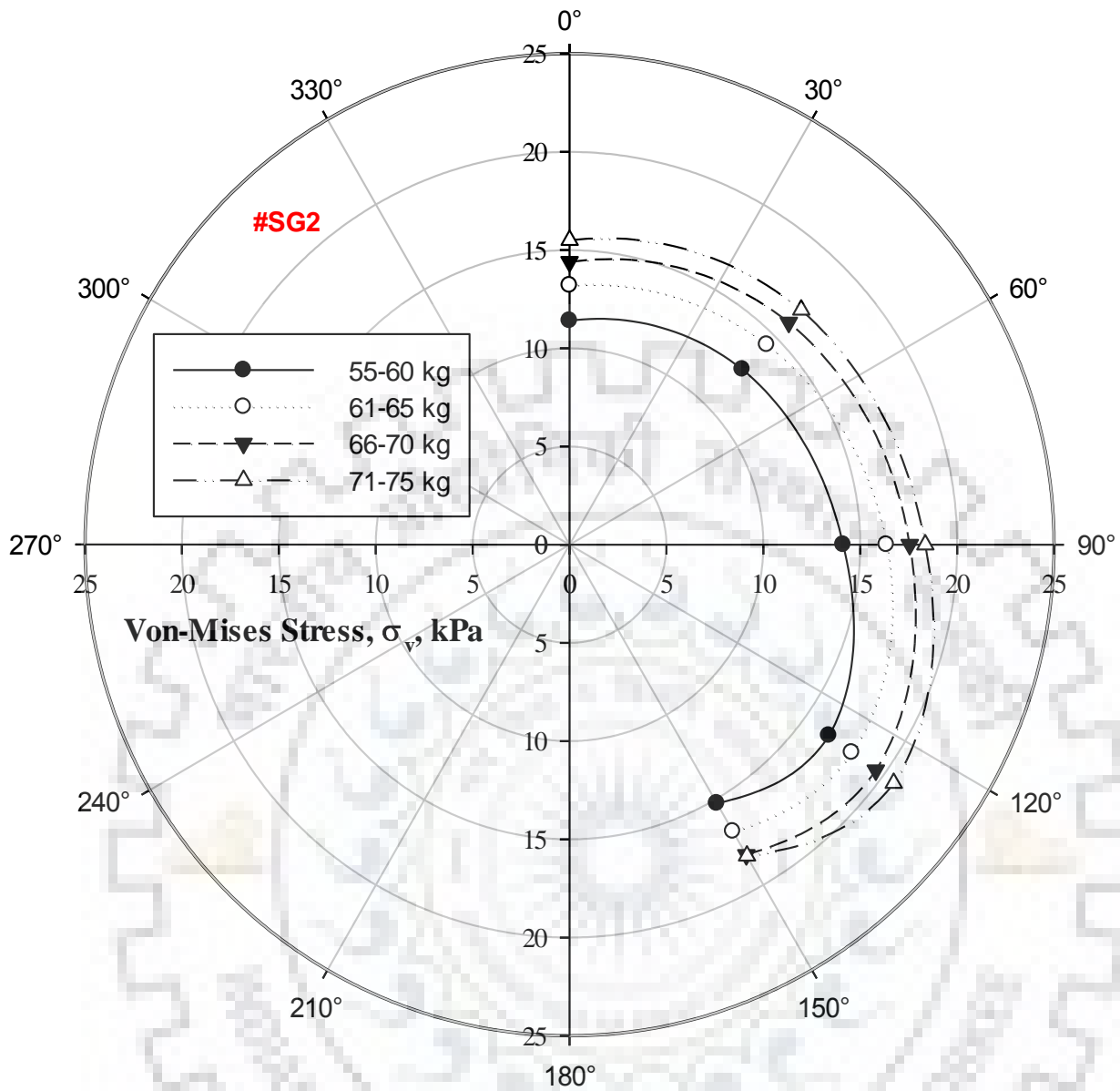


Figure 6.16 Stress distribution at Metaphysis femur shaft – Near Trochanters, under different body configurations

The stress values in an ascending order in context to the location of the strain gauge for knee bend posture is: Metaphysis femur shaft – Near Trochanters, Diaphysis femur shaft – Minimum cross section area, Distal femur – Just above the Condyles and Just above the convexity of ‘Pelvis bone’ – Opposite wall of Acetabulum cup. The stress values in an ascending order in context to the location of the strain gauge for chair posture is: Metaphysis femur shaft – Near Trochanters, Diaphysis femur shaft – Minimum cross section area, Distal femur – Just above the Condyles and Just above the convexity of ‘Pelvis bone’ – Opposite wall of Acetabulum cup. The stress values in an ascending order in context to the location of the strain gauge for pre-squat posture is: Metaphysis femur shaft – Near Trochanters, Diaphysis

Results and Discussion

femur shaft – Minimum cross section area, Distal femur – Just above the Condyles and Just above the convexity of ‘Pelvis bone’ – Opposite wall of Acetabulum cup.

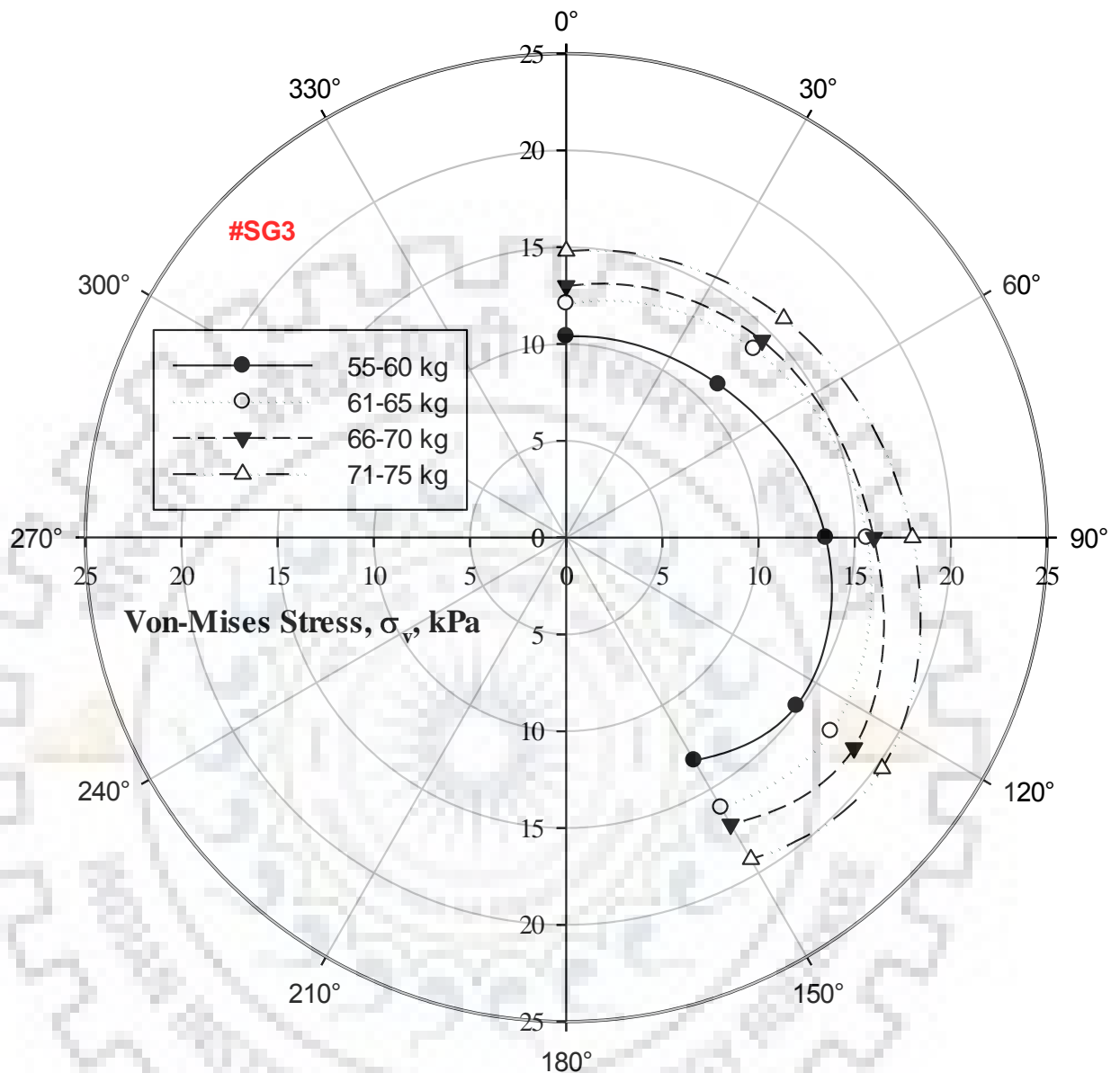


Figure 6.17 Stress distribution at Diaphysis femur shaft – Minimum cross section area, under different body configurations

The stress values in an ascending order in context to the location of the strain gauge for deep-squat posture is: Metaphysis femur shaft – Near Trochanters, Diaphysis femur shaft – Minimum cross section area, Distal femur – Just above the Condyles and Just above the convexity of ‘Pelvis bone’ – Opposite wall of Acetabulum cup.

Henceforth, the stress behavior with respect to the strain gauge location for critical body postures would be as follows.

$$\sigma_{SG4} < \sigma_{SG2} < \sigma_{SG3} < \sigma_{SG1}; \text{ #standing posture};$$

Results and Discussion

- $\sigma_{SG3} < \sigma_{SG2} < \sigma_{SG4} < \sigma_{SG1}$; #knee bend posture;
- $\sigma_{SG3} < \sigma_{SG2} < \sigma_{SG4} < \sigma_{SG1}$; #chair posture;
- $\sigma_{SG3} < \sigma_{SG2} < \sigma_{SG4} < \sigma_{SG1}$; #pre – squat posture;
- $\sigma_{SG3} < \sigma_{SG2} < \sigma_{SG4} < \sigma_{SG1}$; #deep – squat posture;

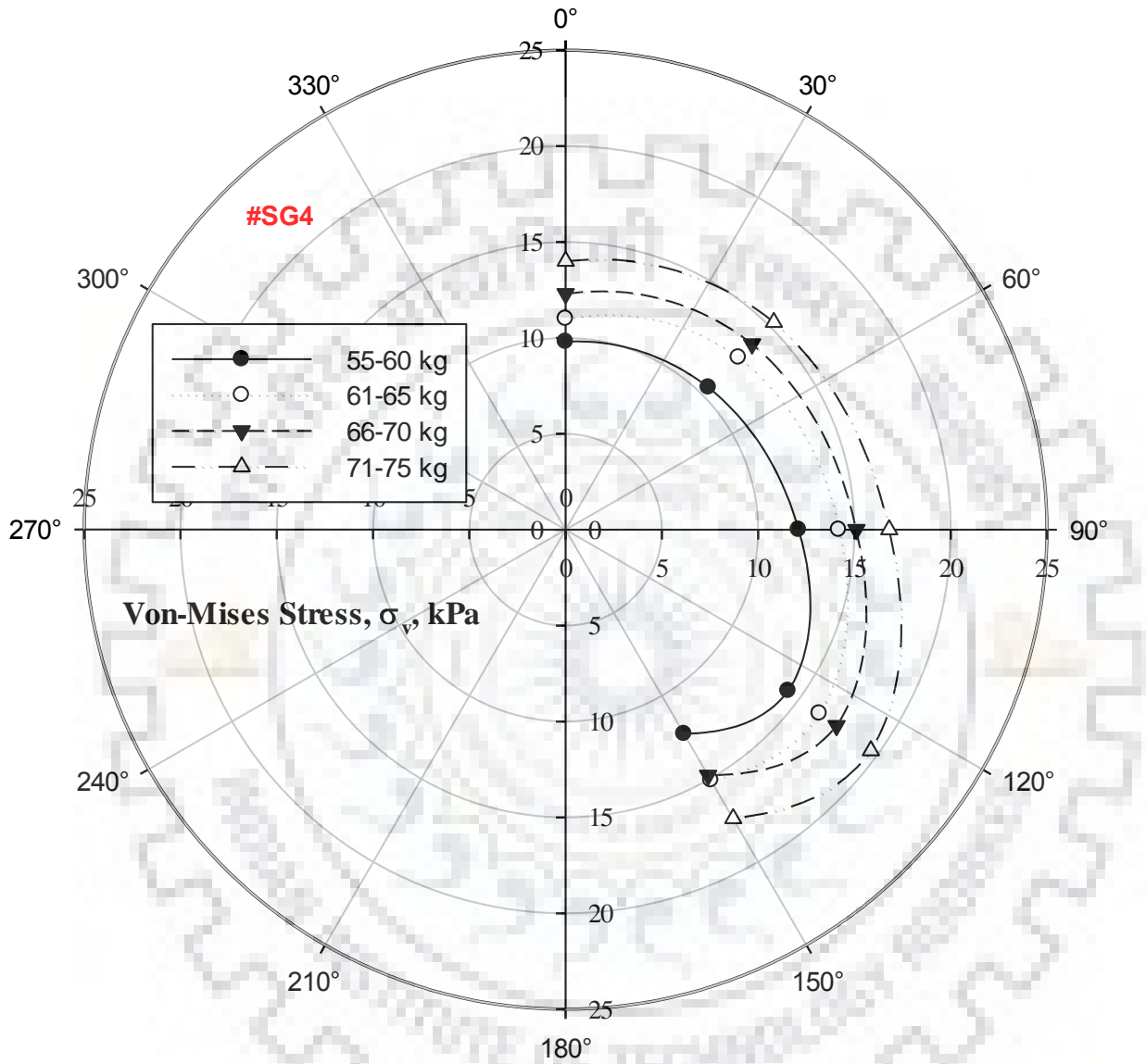


Figure 6.18 Stress distribution at distal femur – Just above the Condyles, under different body configurations

The percentage variation in stress based on the location of the strain gauge is shown in Table 6.2. This variation is mainly due to the change in elastic properties of the cortical and cancellous bones, resisting area of contact at hip joint and distance of strain gauges from the load application point. Lower strain is expected in the bone with high modulus of elasticity and vice versa.

Table 6.2 Increase of magnitude of stress according to the location of the strain gauge

Location of the strain gauge	With reference to	Percentage	remark
Distal femur	Diaphysis femur shaft	3-17	Increase
Diaphysis femur shaft	Metaphysis femur shaft	4-12	Increase
Metaphysis femur shaft	Just above the convexity of 'Pelvis bone'	3-10	Increase

6.2.2.2 Effect of body mass on stress

The variation of stress with respect to body mass is noted to be independent. The higher body mass results high stress. From the Figure 6.21 to Figure 6.23, it is to be noted that, when the body mass range shifted from 55-60 kg to 61-65 kg band, the stress induced at the convexity of the pelvis bone – opposite wall of the acetabulum cup increased by 4-13 percentage. Similarly, when the body mass range shifted from 61-65 kg to 66-70 kg band, the stress induced at the convexity of the pelvis bone – opposite wall of the acetabulum cup increased by 4-9 percentage. Also, when the body mass range shifted from 66-70 kg to 71-75 kg band, the stress induced at the convexity of the pelvis bone – opposite wall of the acetabulum cup increased by 4-7 percentage. However, the compressive and tensile nature of the stress distribution is same.

6.3. Mathematical model

The proposed mathematical model was simulated to evaluate the magnitude of force along the femur bone while performing a successful deep squat. In the present study the knee flexion, knee extension, mass of the upper body, time period for each duty cycle, tibia angle, length of the femur and length of the tibia are considered to be most influencing parameters on the mechanical force along the femur bone. The 'time period for one duty cycle' was collected from 180 human subjects with different body weights covering wide range of age group. In the present study a person standing ($\varphi = 0^\circ$ to sagittal plane) performs a successful deep squat ($\varphi = 155^\circ$ to sagittal plane) through knee flexion and come back to standing posture ($\varphi = 0^\circ$) by extension of knee is define to be a one Duty cycle. Several factors like gender, age, stamina or fitness, are highlighted to influence the time period of one duty cycle and thereby the forces in femur bone would also be affected. Sufficient care has taken to consider the discrepancy of the above factors while displaying the results.

In the present study the Femur bone is divided into three portions to avoid the complexity. The plots have been made to show the variation of stress along three major portions of the femur bone viz., Femur head, Neck and Shank. From the geometric structure of the hip joint arrangement, the femur head experiences the crushing or direct compressive stress. While the shank and neck portions subjected to simple tension and compressive stress. The direct compression stress has been estimated by using Hertzian contact theory of contact mechanics subjected to a pull Bhandari, (2010); WANG et al., (2005b). The stresses in shank and neck portions of femur bone have been evaluated by using the reaction force and the cross section area. The cross section area was estimated through following assumptions.

1. The femur head is approximately resembling the sphere
2. The cross section of the shank portion is assumed to be circle and uniform
3. The stress is concentrating at mid portion of the femur neck, and whose cross section is circle

In order to simulate the mathematical model, the following specifications or operating parameters were evaluated and used as inputs.

6.3.1 The geometry of femur bone

The shape and size of the human body and its parts entirely depends on several factors viz. genetics, routine activities, living and working lifestyle, geographical locations etc. Therefore, no fixed rule is applied for the dimension of any human organ. Although, femur is the longest

Results and Discussion

and strongest bone in human body Masood et al., (2013); Norkin & White, (2009) followed by the tibia, fibula and humerus bones in descending order. The size of the femur and tibia, bones under observation in the study, were measured by the X-Ray images of the human subjects who volunteered to participate in the study. The length of the femur bone was measured from the femur head to the distal most point at the medial condyle of the femur bone while the length of the tibia bone was measured form the lateral intercondylar tubercle to medial malleolus of the tibia bone.

6.3.2 Time period of one duty cycle

The samples were collected from healthy human subjects. Time period of one duty cycle depends on several factors related to subjects' physicality, daily routine, geographical origin, etc. To consider all these factors such as gender, stamina, fitness which effects the time period, the subjects were instructed to perform a repeated number of 40 deep squats in four sets each of 10 deep squats and the corresponding time was noted. A total of 180 samples collected from different human subjects used for the simulation of proposed mathematical model. Few such samples have been presented in appendix C. The average of the samples was assumed to be the average time period of the one duty cycle under the selected category viz., subject's type i.e. Male or female, subject's routine i.e. athletic or normal, etc. The factorial design of simulation of mathematical model comprising the details of geometric specifications, age, gender, etc., are shown in the Table 6.3. The time period used to evaluate the angular velocity of the tibia.

Table 6.3 The factorial design of simulation of mathematical model

Gender	Age group	Body mass	Routine/ Activity	Geometry	
				Femur (l)	Tibia (r)
Male	21-25	55-60	Deep Squat	Subject length	Subject length
		61-65	Deep Squat	Subject length	Subject length
		66-70	Deep Squat	Subject length	Subject length
		71-75	Deep Squat	Subject length	Subject length
	26-30	55-60	Deep Squat	Subject length	Subject length

Gender	Age group	Body mass	Routine/ Activity	Geometry	
				Femur (l)	Tibia (r)
		61-65	Deep Squat	Subject length	Subject length
		66-70	Deep Squat	Subject length	Subject length
		71-75	Deep Squat	Subject length	Subject length
		55-60	Deep Squat	Subject length	Subject length
	31-35	61-65	Deep Squat	Subject length	Subject length
	31-35	66-70	Deep Squat	Subject length	Subject length
	31-35	71-75	Deep Squat	Subject length	Subject length
		55-60	Deep Squat	Subject length	Subject length
	36-40	61-65	Deep Squat	Subject length	Subject length
	36-40	66-70	Deep Squat	Subject length	Subject length
	36-40	71-75	Deep Squat	Subject length	Subject length

6.3.3 Effective weight on the pelvis

The weight distribution of different body parts varies and depends on several factors such as routine activity, lifestyle, work culture, dietary habits, etc. However, on an average, it is estimated that the trunk portion has two-third share of the total body weight thus the remaining half below the transverse plain to be one-third of the total body weight. Each individual lower extremity share one-sixth of the body weight. Therefore, the effective weight on each pelvis bone will be five-sixth of the total body weight.

Results and Discussion

6.3.4 Tibial flexion

It is to be assumed that, the tibia's movement resembles the "simple harmonic motion (SHM)". The successful deep squat is achieved through knee flexion in sagittal plane and the standing posture is attained through the knee extension in the same plane. Certainly, the approximate maximum knee flexion is 20° . Figure 6.19 shows the angular velocity of tibia with respect to time step for one cycle of tibia flexion and extension. It is clear that, the angular velocities near standing and deep squat postures to be low in magnitude. This is due to the deceleration towards the standing and deep squat postures.

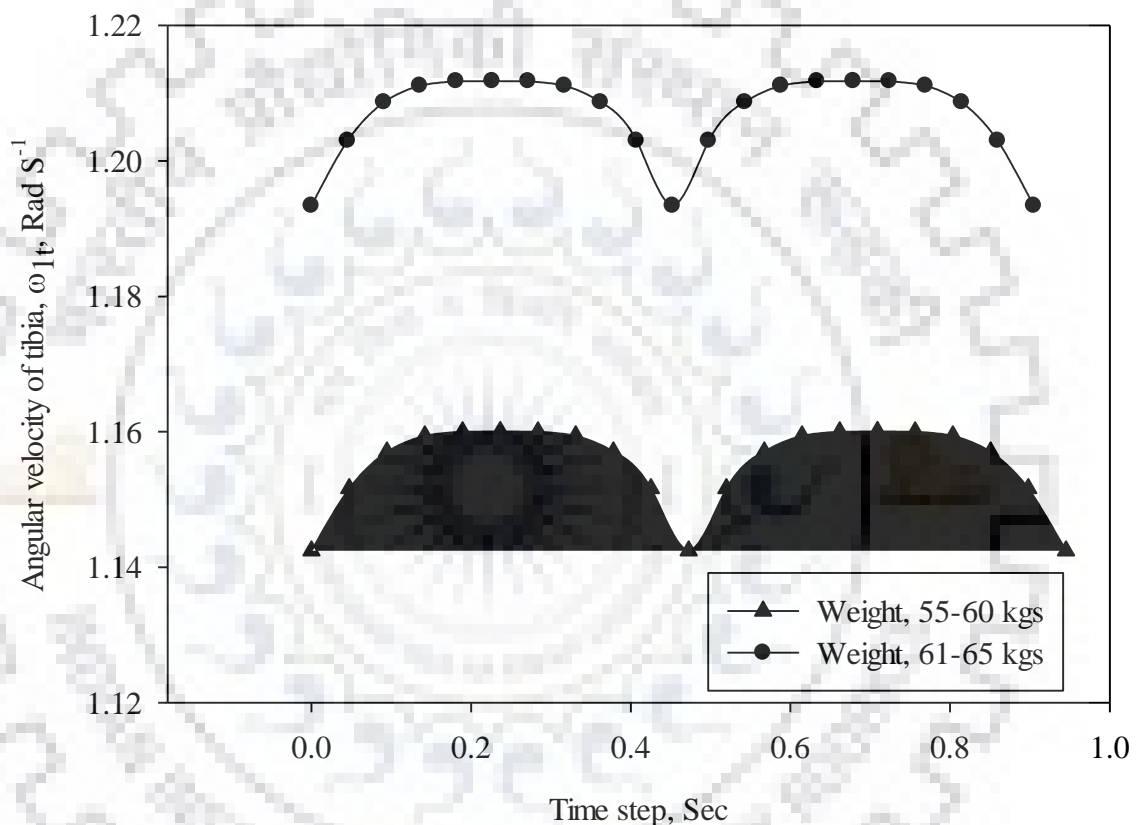


Figure 6.19 Change of angular velocity of 'tibia' with time step for one complete duty cycle of successful deep squat

6.3.5 Knee flexion

The successful deep squat is achieved through flexion of the knee and the standing posture is attained through the extension of the knee. Certainly, the approximate maximum knee flexion is 155° . Figure 6.20 shows the angular velocity of femur with respect to time step for one cycle of knee flexion and extension. It is clear that, the angular velocities near standing and deep squat postures to be low in magnitude. This is due to the deceleration towards the standing and deep squat postures.

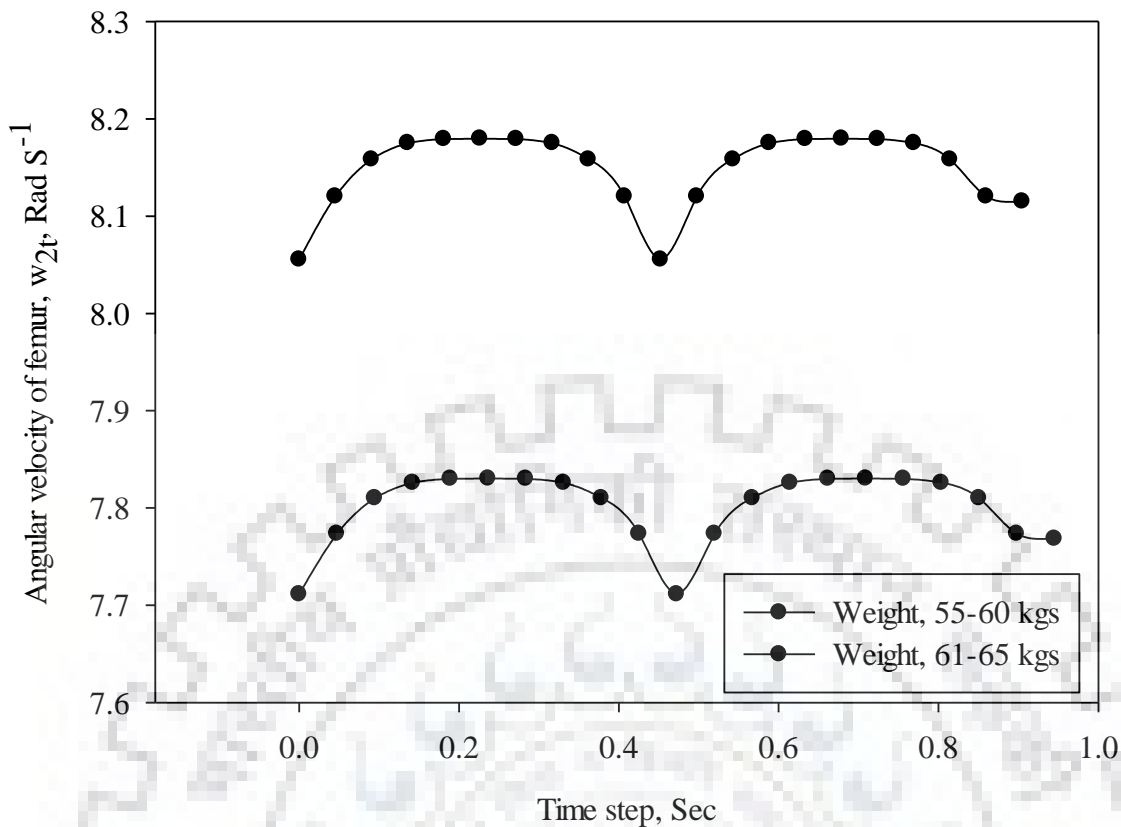


Figure 6.20 Change of angular velocity of ‘femur’ with time step for one complete duty cycle of successful deep squat

The proposed mathematical model was solved with the above inputs based on the factorial design. Two familiar activities sitting-down and standing-up have been considered in the present study. The outcomes of analytical model for the femur bone are separately plotted in the Figure 6.21. A common observation is that; the magnitude of stress is relatively high in pre-squat posture while performing successful squat as well as standing activity. It is evident that, the stresses in femur head are insignificant as compared to the shank and neck portions of the femur bone. However, the nature of the stress distribution along three portions of the femur bone are noticed to be same. The nature is that, the pre-squat posture exhibits more stresses under both flexion and extension of knee under deep squat activity.

Results and Discussion

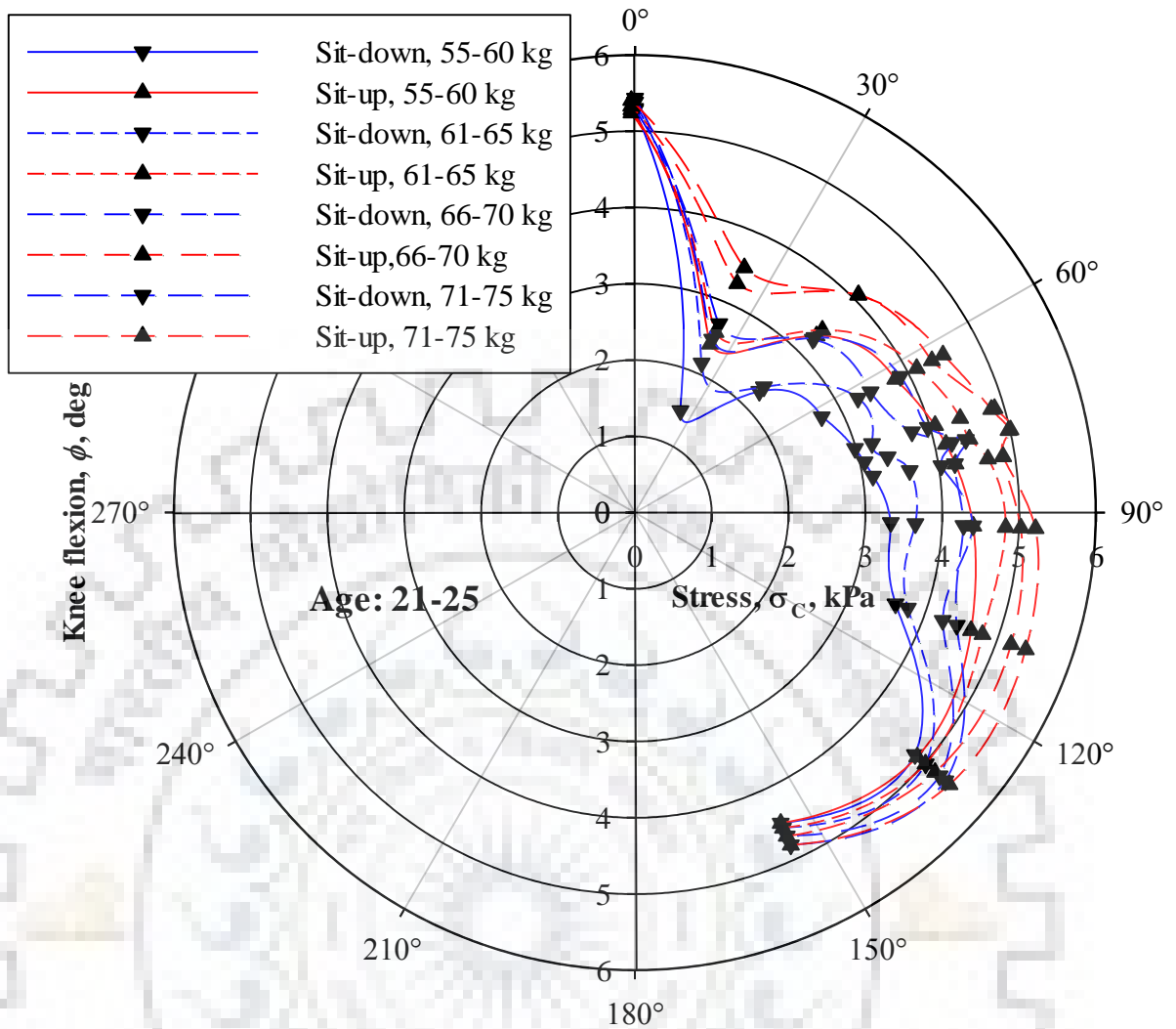


Figure 6.21 Stress distribution along the “Femur head” with respect to knee flexion during one working cycle of successful deep-squat

The neck portion experiences high stress as compared to femur shaft and femur head portions. This is due to the less area to resist the internal stress developed by the applied force. This fact is true for the all the postures of the successful deep squat. In all three zones of the femur bone the compressive or tensile stress is noticed to be increased with the knee flexion till pre-squat posture. However, while the extension of the knee i.e., the standing-up activity exhibits more compressive or tensile stress than the sitting-down activity. This is due to the weight of the body acts against during the standing-up activity, while it assists in sitting-down activity. The magnitude of the stresses is affected by the body weight significantly. The Figure 6.22 shows stress along the femur bone is scattered right with the increase of weight of the body.

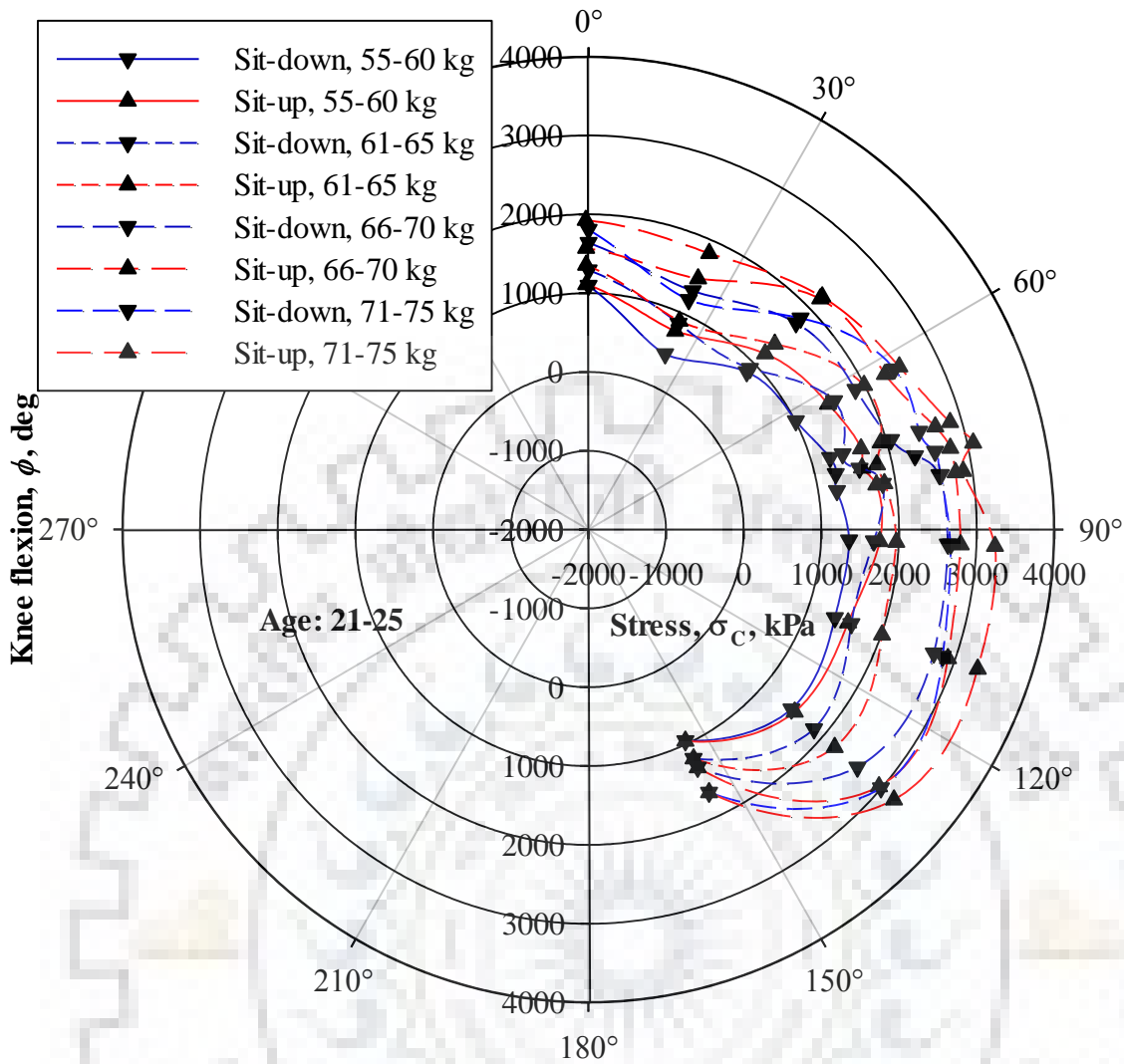


Figure 6.22 Stress distribution along the “Neck” with respect to knee flexion during one working cycle of successful deep-squat

The deep squat posture exhibits less stress as compared to pre-squat posture as shown in Figure 6.23. This is due to the fact that the upper extremity body decelerate towards the deep squat posture after pre-squat and reaches acceleration becomes zero at maximum knee flexion. On the other hand, the nature of the stress was also evaluated for complete duty cycle. When the knee flexion varies from 0 to 90°, the femur bone experiences compression stress i.e., while performing deep squat, till knee bend the femur bone bears the compression load. While the remaining portion from 90° to 155°, the femur bone experiences tensile stress i.e., after knee bend the femur bone and portion of acetabulum bears tensile load.

Results and Discussion

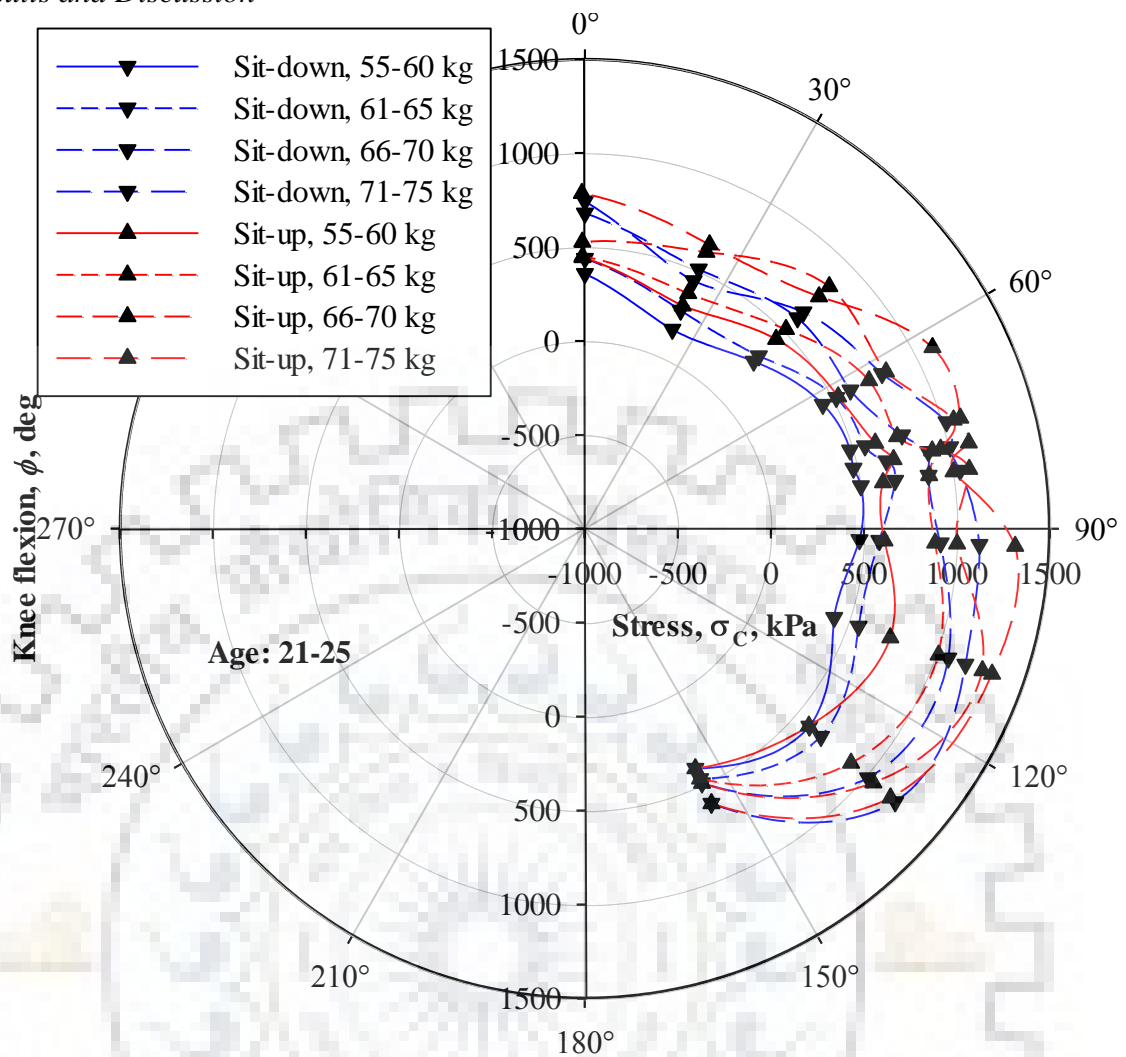


Figure 6.23 Stress distribution along the “Diaphysis femur shaft – Minimum cross section area” with respect to knee flexion during one working cycle of successful deep-squat

The plots for individual activity viz., standing up and sitting down have been presented in the appendix B.

6.4. Summary

As a result of the above discussion, all the investigations predicted the stress distribution along the femur and pelvis bone. All the investigations predict that; the maximum stress occurs under pre-squat posture as compared to other postures. The mathematical model over predicts the stress values over the specific region of study. However, the nature of the stress distribution remains unchanged. The over prediction could be due the several assumptions considered in development of mathematical model.

6.4.1 Implant design

The common materials of implants are steel, titanium, etc. Certainly, the elastic properties of implant materials are far ahead of the bone. These materials bring some compatibility issues related to design and mobility, even after successful hip-arthritis. Macker et al., (2011) claimed patients avoid surgery as it limits their routine activities. Also, orthopedicians suggests not to go for deep flexion activities which affects lifestyle. Subsequently, the large strength variation in the bone and implant material also leads to mechanical failures of joint. Bourne et al., (2010) examined 1703 patients with western lifestyle and finds that the satisfaction level of the patients after surgery is 70-86%. Since, south Asian population frequently adopt complex postures like kneeling, squatting, cross leg sitting etc., the satisfaction level might be worse for south Asian population.

In the above discussion, the maximum stress involved in the femur bone and pelvis bone were estimated. Therefore, the above results would assist to choose the suitable material for the implant. Shireesha et al., (2013) tested titanium alloys for normal activities. Same alloys may be tested for complex activities. Singh et al., (2015) and Kumar et al., (2018) coated nano hydroxyapatite on available implants to test the artificial implants for better results. The selection of material must be incorporated with some factor of safety to consider the different factors viz., jumping, climbing, etc. This factor of safety however must also account the assumptions made during the present study. Thereafter, a further testing should be carried out for the compatibility issues if any with the new proposed design and material.

A prototype model of human hip joint would be fabricated with the help of suitable material like calcium hydroxyapatite etc. The femur and pelvis bone system would be tested under the different varieties of loading for the mechanical failures. It is to propose that, a suitable analysis technique such as gait analysis would be done for flexion and extension of muscle for stance and swing body behavior for complex postures. The failure strengths of the femur and pelvis bones to be compared with the present measured bone strengths.

The selection of suitable material and dimensions for Asian life style population are being challenge to the implant designer. From the present investigation, as discussed above the selection of material would be based on the design stress incorporated with factor of safety. Secondly, the dimensions of femur head and neck can be evaluated through trial and error method applied to the following equations.

Results and Discussion

Femur neck and shaft:

$\sigma_{c, Neck, shaft}$

$$\sigma_{c, Neck, shaft} = \frac{m \cdot \sqrt{(-\omega_{2t}^2 l \sin \theta_{2t} - \omega_{1t}^2 r \sin(\theta_0 \sin(\omega t)))^2 + (-\omega_{2t}^2 l \cos \theta_{2t} - \omega_{1t}^2 r \cos(\theta_0 \sin(\omega t)))^2} \pm m \cdot g \cdot \cos\left(\frac{\pi}{2} - \theta_{2t}\right)}{\frac{\pi}{4} d^2}; \quad 6.4$$

Femur head:

$$\sigma_{c, Femur head} = \frac{F}{4\pi} \left[\sqrt[3]{\frac{3d_1 d_2 F (E_2 (v_1^2 - 1) + E_1 (v_2^2 - 1))}{(d_1 - d_2) E_1 E_2}} \right]^2 \quad 6.5$$

Where, F is reaction force by femur, ν is Poisson's ratio, E is young's modulus, d is diameter; 1 represent femur head and 2 represent acetabulum cup.



7. SUMMARY, CONCLUSIONS AND FUTURE SCOPE

7.1. Summary

The need of estimation of strength of the bone to understand the limitation of the capacity/capability of bone and its joints under different configurations of human body viz., different activities, dissimilar weights, altered postures, etc. The human bones possess different strengths like mechanical elements and linkages, under different configurations i.e., the shoulder joint, hip joint, femur bone, knee joint, tibia, etc., would have different load carrying capacities. The load carrying capacities are described by the bone strength. In the present study authors highlighted the stresses in the bone under different configuration of successful deep squat through numerical, experimental and mathematical investigations. The summary of the present work is briefed below.

Chapter 1 introduces the motivation of the current work. In addition, the Anatomy and geometry-terminology of the human bones, ligaments and joints were briefed. The importance of biomechanics and kinetics along with past research trends have also been presented.

Chapter 2 describes the current state of the art through an exhaustive literature survey related to the human hip-joint, bone material, muscle forces in hip-joint, etc. The literature study comprises the numerical, mathematical and experimental investigations. The research gaps have been highlighted at the end of the review and the possible opportunities have also been identified. Based on the literature review and research gaps, a suitable problem has been formulated with certain objectives.

Chapter 3 briefs the methodology of numerical simulation followed by the discretization and meshing of 3D CAD model. The mesh and number of nodes also presented. The boundary conditions with free body diagram is discussed to understand the loading conditions of different body configurations viz., standing, knee bend, chair, pre-squat and deep squat. The definition of material used in the numerical simulation has been included.

Chapter 4 presents the experimental set-up with line diagram along with the key components viz. proximal femur holder, distal femur holder. The type and location of the strain gauges have been discussed. The detailed specifications of test section i.e., dry bone is presented.

Chapter 5 comprises the agreement of mathematical model prediction to the experimental and numerical results. In addition, the equations to predict the stress in femur neck, femur shaft

and femur head have also been developed. The kinematic analogy to obtain the above equation is discussed.

In the Chapter 6, the results of numerical, experimental and mathematical investigations have been discussed. The maximum stress involved in the femur bone and pelvis bone were estimated. Therefore, the above results would assist to choose the suitable material for the implant. The selection of material must be incorporated with some factor of safety to consider the different factors viz., jumping, climbing, etc. This factor of safety however must also account the assumptions made during the present study. Thereafter, a further testing should be carried out for the compatibility issues if any with the new proposed design and material.

7.2. Conclusions

The mechanical failure characteristics and strength of the femur and pelvis bones were revealed through experimental and numerical investigations. A mathematical model to predict the stress distribution along the axis of femur bone has been developed. The highlights of experimental and numerical investigations are presented in the following sections. Subsequently, the mathematical model predictions have also been presented.

7.2.1 Numerical simulation

- For all the postures, the maximum stress is obtained at distal femur.
- The location of the maximum stress in distal femur changes circumferentially with respect to the knee flexion and extension.
- The non-uniform distribution of the stress along the femur bone is due to irregular geometry, the change of bone properties, physical configuration of the femur bone and loading conditions.
- Standing posture: The maximum stress is observed at the “medial epicondyle”, which could be seen in the anterior view of the femur bone.
- Knee bend posture: The maximum stress is observed at the “patellar surface - close to lateral epicondyle”, which could be seen in the anterior view of the femur bone.
- Chair posture: The maximum stress is observed at the “patellar surface – close to medial epicondyle”, which could be seen in the anterior view of the femur.
- Pre-squat posture: The maximum stress is observed at the “patellar surface - close to lateral epicondyle”, which could be seen in the anterior view of the femur bone.
- Deep squat posture: The maximum stress is observed at the “intercondylar fossa - just above the lateral condyle”, which could be seen in the anterior view of the femur bone.

7.2.2 Experimental highlights

The dry bone has been investigated experimentally to reveal the stress distribution along the femur bone as well as to estimate the stresses in critical locations of pelvis bone.

- The variation of stress with respect to body mass is noted to be independent. The higher body mass results high stress.
- The stress behavior with respect to the strain gauge location for critical body postures would be as follows.

$$\sigma_{SG4} < \sigma_{SG2} < \sigma_{SG3} < \sigma_{SG1}; \text{ \#standing posture;}$$

$$\sigma_{SG3} < \sigma_{SG2} < \sigma_{SG4} < \sigma_{SG1}; \text{ \#knee bend posture;}$$

$$\sigma_{SG3} < \sigma_{SG2} < \sigma_{SG4} < \sigma_{SG1}; \text{ \#chair posture;}$$

$$\sigma_{SG3} < \sigma_{SG2} < \sigma_{SG4} < \sigma_{SG1}; \text{ \#pre – squat posture;}$$

$$\sigma_{SG3} < \sigma_{SG2} < \sigma_{SG4} < \sigma_{SG1}; \text{ \#deep – squat posture;}$$

- The magnitude of stress is relatively high in pre-squat posture while performing successful squat as well as standing activity.
- The neck portion experiences high stress as compared to femur shaft and femur head portions.

7.2.3 Mathematical prediction

In all three zones of the femur bone the compressive or tensile stress is noticed to be increased with the knee flexion till pre-squat posture. Further, the extension of the knee i.e., the standing-up activity exhibits more compressive or tensile stress than the sitting-down activity. The deep squat posture exhibits less stress as compared to pre-squat posture. On the other hand, the nature of the stress was also evaluated for complete duty cycle. When the knee flexion varies from 0 to 90°, the femur bone experiences compression stress. While the remaining portion from 90° to 155°, the femur bone experiences tensile stress.

7.3. Future Scope

- Use of state of the art facilities like GAIT lab could improve the quality of investigation.
- More realistic experimentation is possible with wet bones instead of dry bones.
- There is a scope to observe Effect of ligaments, tendons, and muscular forces separately.
- The mathematical model to be developed by considering the transverse plane movement. Three dimensional study is recommended.



REFERENCES

- Acker, S. M., Cockburn, R. A., Krevolin, J., Li, R. M., Tarabichi, S., & Wyss, U. P., Knee Kinematics of High-Flexion Activities of Daily Living Performed by Male Muslims in the Middle East, *The Journal of Arthroplasty*, 26(2), 319–327, 2011.
- Amornsamankul, S., Kaorapapong, K., & Wiwatanapataphee, B., Three-dimensional simulation of femur bone and implant in femoral canal using finite element method, *International Journal of Mathematics and Computers in Simulation*, 4(4), 171–178, 2010.
- Anderson, A. E., Ellis, B. J., Maas, S. A., & Weiss, J. A., Effects of idealized joint geometry on finite element predictions of cartilage contact stresses in the hip, *Journal of Biomechanics*, 43(7), 1351–1357, 2010.
- Arnold, E. M., Ward, S. R., Lieber, R. L., & Delp, S. L., A model of the lower limb for analysis of human movement, *Annals of Biomedical Engineering*, 38(2), 269–279, 2010.
- Baca, V., Horak, Z., Mikulenka, P., & Dzupa, V., Comparison of an inhomogeneous orthotropic and isotropic material models used for FE analyses, *Medical Engineering and Physics*, 30(7), 924–930, 2008.
- Báča, V., Klimeš, J., Tolar, V., Zimola, P., Balliu, I., Vitvarová, I., ... Čelko, A. M., A 1-year prospective monocentric study of limb, spinal and pelvic fractures: Can monitoring fracture epidemiology impact injury prevention programmes?, *Central European Journal of Public Health*, 26(4), 298–304, 2018.
- Bergmann, G., Bergmann, G., Deuretzbacher, G., Deuretzbacher, G., Heller, M., Heller, M., ... Duda, G. N., Hip forces and gait patterns from routine activities, *Journal of Biomechanics*, 34, 859–871, 2001.
- Bhandari, V. B., *Design of Machine Elements*, (3rd ed.),. New Delhi: Tata McGraw-Hill Education, 2010.
- Birnbaum, K., & Pandorf, T., Finite element model of the proximal femur under consideration of the hip centralizing forces of the iliotibial tract, *Clinical Biomechanics*, 26(1), 58–64, 2011.
- Bourne, R. B., Chesworth, B. M., Davis, A. M., Mahomed, N. N., & Charron, K. D. J., Patient Satisfaction after Total Knee Arthroplasty: Who is Satisfied and Who is Not?, *Clinical Orthopaedics and Related Research*®, 468(1), 57–63, 2010.
- Buchanan, T. S., Lloyd, D. G., Manal, K., & Besier, T. F., Neuromusculoskeletal modeling: estimation of muscle forces and joint moments and movements from measurements of neural command., *Journal of Applied Biomechanics*, 20(4), 367–95, 2004.

- Chowdhury, S., & Kumar, N., Estimation of Forces and Moments of Lower Limb Joints from Kinematics Data and Inertial Properties of the Body by Using Inverse Dynamics Technique, *Journal of Rehabilitation Robotics*, 1, 93–98, 2013.
- Collins, J. J., & O’connor, J. J., Muscle-Ligament Interactions at the Knee during Walking, *Proceedings of the Institution of Mechanical Engineers, Part H: Journal of Engineering in Medicine*, 1991.
- Cristofolini, L., Cappello, A., McNamara, B. P., & Viceconti, M., A minimal parametric model of the femur to describe axial elastic strain in response to loads, *Medical Engineering and Physics*, 1996.
- D’Lima, D. D., Patil, S., Steklov, N., Colwell, C. W., & Jr, The 2011 ABJS Nicolas Andry Award: ‘Lab’-in-a-knee: in vivo knee forces, kinematics, and contact analysis., *Clinical Orthopaedics and Related Research*, 469(10), 2953–70, 2011.
- Dash, P. P., Kishor, K., & Panda, S. K., Biomechanical Stress Analysis of Human Femur Bone, *International Conference on Computer Aided Engineering (CAE-2013)*, (February), 1–6, 2013.
- De Vos, W., Casselman, J., & Swennen, G. R. J., Cone-beam computerized tomography (CBCT) imaging of the oral and maxillofacial region: A systematic review of the literature, *International Journal of Oral and Maxillofacial Surgery*, 38(6), 609–625, 2009.
- Delp, S. L., Loan, J. P., Hoy, M. G., Zajac, F. E., Topp, E. L., & Rosen, J. M., An interactive graphics-based model of the lower extremity to study orthopaedic surgical procedures, *IEEE Transactions on Biomedical Engineering*, 37(8), 757–767, 1990.
- Delp, S. L., Loan, J. P., Hoy, M. G., Zajac, F. E., Topp, E. L., Rosen, J. M., ... Alto, P., An interactive graphics-based model of the lower extremity to study orthopaedic surgical procedures, *IEEE Transactions on Biomedical Engineering*, 37(8), 757–67, 1990.
- Duda, G. N., Heller, M., Albinger, J., Schulz, O., Schneider, E., & Claes, L., Influence of muscle forces on femoral strain distribution., *Journal of Biomechanics*, 31(9), 841–6, 1998.
- Francis, A., Student, M. E., Engineering, G., & College, E., Computational Modeling of Human Femur using CT Data for Finite Element Analysis, *International Journal of Engineering Research & Technology*, 1(6), 1–7, 2012.
- Giri, A., Pandey, C., Mahapatra, M. M., Sharma, K., & Singh, P. K., On the estimation of error in measuring the residual stress by strain gauge rosette, *Measurement: Journal of the International Measurement Confederation*, 2015.
- Gullett, J. C., Cillnan, M. D., Gutierrez, G. M., & Chow, J. W., A biomechanical comparison

- of back and front squat in healthy trained individual, *Journal of Strength and Conditioning Research*, 23(1), 284–292, 2008.
- Hamai, S., Moro-oka, T. A., Miura, H., Shimoto, T., Higaki, H., Fregly, B. J., ... Banks, S. A., Knee kinematics in medial osteoarthritis during in vivo weight-bearing activities, *Journal of Orthopaedic Research*, 27(12), 1555–1561, 2009.
- Hamilton, N., *Kinesiology: Scientific Basis of Human Motion*, Faculty Book Gallery, 2011.
- Hara, D., Nakashima, Y., Hamai, S., Higaki, H., Ikebe, S., Shimoto, T., ... Iwamoto, Y., Kinematic analysis of healthy hips during weight-bearing activities by 3D-to-2D model-to-image registration technique, *BioMed Research International*, 2014(1), 1–9, 2014.
- Hara, D., Nakashima, Y., Hamai, S., Higaki, H., Ikebe, S., Shimoto, T., ... Iwamoto, Y., Clinical Biomechanics Dynamic hip kinematics in patients with hip osteoarthritis during weight-bearing activities, *JCLB*, 32, 150–156, 2016.
- Heckman, J. D., *Campbell's Operative Orthopaedics*. 11th ed., *J Bone Joint Surg Am*, 90(4), 943–944, 2008.
- Hefzy, M. S., Kelly, B. P., & Cooke, T. D. V., Kinematics of the knee joint in deep flexion: A radiographic assessment, *Medical Engineering and Physics*, 20(4), 302–307, 1998.
- Hodge, W. A., Fijan, R. S., Carlson, K. L., Burgess, R. G., Harris, W. H., & Mann, R. W., Contact pressures in the human hip joint measured in vivo., *Proceedings of the National Academy of Sciences*, 83(9), 2879–2883, 1986.
- Holzappel Gerhard, A., & Ogden ray, W., *Biomechanical modelling at the Molecular, Cellular and Tissue levels*., Springer Science and Business Media, 2009.
- Hospital, B. I., Pinilla - Impact Direction from a Fall Influences the Failure Load of the Proximal Femur as Much as Age-Related Bone Loss.pdf, 231–235, 1996.
- Iglic, A., Iglic, V. K., Antolic, V., Srakar, F., & Stanic, U., Effect of the periacetabular osteotomy on the stress on the human hip joint articular surface, *IEEE Transactions on Rehabilitation Engineering*, 1(4), 207–212, 1993.
- Ipavec, M., Brand, R. A., Pedersen, D. R., Mavčič, B., Kralj-Iglič, V., & Iglič, A., Mathematical modelling of stress in the hip during gait, In *Journal of Biomechanics*, 1999.
- JOST, H. P., & SCHOFIELD, J., Energy Saving Through Tribology: a Techno-Economic Study., *Pet Rev*, V 36(N 428), 34–37, 1982.
- Judet, J., & Judet, R., The use of an artificial femoral head for arthroplasty of the hip joint, *The Journal of Bone and Joint Surgery. British Volume*, 71(1), 1950.
- Keyak, J. H., & Rossi, S. A., Prediction of femoral fracture load using finite element models: An examination of stress- and strain-based failure theories, *Journal of Biomechanics*,

33(2), 209–214, 2000.

Khas, K. S., Pandey, P. M., & Ray, A. R., Rapid manufacturing of a clubfoot model imitating soft tissue and bones: This paper reports an exploration of fabricating a composite clubfoot model consisting of both soft and hard tissues for biomechanical assessment of infant clubfoot, *Virtual and Physical Prototyping*, 8(3), 187–192, 2013.

Khas, K. S., Pandey, P. M., & Ray, A. R., Design and development of a device to measure the deformities of clubfoot, *Proceedings of the Institution of Mechanical Engineers, Part H: Journal of Engineering in Medicine*, 229(3), 194–204, 2015.

Khas, K. S., Pandey, P. M., & Ray, A. R., Development of an orthosis for simultaneous three-dimensional correction of clubfoot deformity, *Clinical Biomechanics*, 51, 67–75, 2018.

Kirkwood, R., Gomes, H., Sampaio, R., Culham, E., & Costigan, P., Biomechanical analysis of hip and knee joints during gait in elderly subjects, *Acta Ortopédica Brasileira*, 15(5), 267–271, 2007.

Kourtis, L. C., Carter, D. R., Kesari, H., & Beaupre, G. S., A new software tool (VA-BATTS) to calculate bending, axial, torsional and transverse shear stresses within bone cross sections having inhomogeneous material properties., *Computer Methods in Biomechanics and Biomedical Engineering*, 11(5), 463–76, 2008.

Krebs, D. E., Elbaum, L., Riley, P. O., Hodge, W. A., & Mann, R. W., Exercise and Gait Effects on In Vivo Hip Contact Pressures, *Physical Therapy*, 71(4), 301–309, 1991.

Kumar, S. R., Patnaik, A., Bhat, I. K., & Singh, T., Optimum selection of nano- and micro-sized filler for the best combination of physical, mechanical, and wear properties of dental composites, *Proceedings of the Institution of Mechanical Engineers, Part L: Journal of Materials: Design and Applications*, 232(5), 416–428, 2018.

Lamontagne, M., Beaulieu, M. L., Varin, D., & Beaulieu, P. E., Lower-limb joint mechanics after total hip arthroplasty during sitting and standing tasks, *Journal of Orthopaedic Research*, 30(10), 1611–1617, 2012.

Lutz, F., Mastel, R., Runge, M., Stief, F., Schmidt, A., Meurer, A., & Witte, H., Calculation of muscle forces during normal gait under consideration of femoral bending moments, *Medical Engineering and Physics*, 38(9), 1008–1015, 2016.

Mahmoodian, R., Leasure, J., Gadikota, H., Capaldi, F., & Siegler, S., Mechanical properties of human fetal talus, In *Clinical Orthopaedics and Related Research*, (Vol. 467, pp. 1186–1194),. Springer New York, 2009.

Margo, K., Drezner, J., & Motzkin, D., Evaluation and management of hip pain: an algorithmic approach., *The Journal of Family Practice*, 52(8), 607–617, 2003.

- Masood, M. S., Ahmad, A., & Mufti, R. A., Unconventional Modeling and Stress Analysis of Femur Bone under Different Boundary Condition, *International Journal of Scientific and Engineering Research*, 4(12), 293–296, 2013.
- Mouzakis, D., Zaoutsos, S. P., Bouropoulos, N., Rokidi, S., & Papanicolaou, G., Influence of artificially-induced porosity on the compressive strength of calcium phosphate bone cements, *Journal of Biomaterials Applications*, 31(1), 112–120, 2016.
- Nagura, T., Dyrby, C. O., Alexander, E. J., & Andriacchi, T. P., Mechanical loads at the knee joint during deep flexion, *Journal of Orthopaedic Research*, 20(4), 881–886, 2002a.
- Nagura, T., Dyrby, C. O., Alexander, E. J., & Andriacchi, T. P., Mechanical loads at the knee joint during deep flexion, *Journal of Orthopaedic Research*, 20(4), 881–886, 2002b.
- Nareliya, R., Biomechanical Analysis of Human Femur Bone, *International Journal of Engineering Science and Technology*, 3(4), 3090–3094, 2011.
- Nayak, A., Jain, P. K., & Kankar, P. K., Progress and issues related to designing and 3D printing of endodontic guide, In *Lecture Notes in Mechanical Engineering*, (pp. 331–337),. Pleiades Publishing, 2019.
- Nayak, A., Jain, P. K., Kankar, P. K., & Jain, N., Image-based method for analysis of root canal geometry, In *Lecture Notes in Computational Vision and Biomechanics*, (Vol. 30, pp. 1491–1497),. Springer Netherlands, 2019.
- Nayak, A., Kankar, P., Jain, P. K., & Jain, N., Force and vibration generated in apical direction by three endodontic files of different kinematics during simulated canal preparation: An in vitro analytical study, *Proceedings of the Institution of Mechanical Engineers, Part H: Journal of Engineering in Medicine*, 095441191985457, 2019.
- Nayak, A., Kankar, P. K., Jain, N., & Jain, P. K., Force and vibration correlation analysis in the self-adjusting file during root canal shaping: An in-vitro study, *Journal of Dental Sciences*, 13(3), 184–189, 2018.
- Nigg, B. M., MacIntosh, B. R., & Mester, J. (Joachim), *Biomechanics and biology of movement*,. Human Kinetics, 2000.
- Norkin, C. C., & White, D. J., *Measurement of joint motion : a guide to goniometry*,. F.A. Davis, 2009.
- Pandey, C., Mahapatra, M. M., & Kumar, P., A comparative study of transverse shrinkage stresses and residual stresses in P91 welded pipe including plasticity error, *Archives of Civil and Mechanical Engineering*, 18(3), 1000–1011, 2018.
- Pandey, C., Mahapatra, M. M., Kumar, P., & Saini, N., Effect of strain rate and notch geometry on tensile properties and fracture mechanism of creep strength enhanced ferritic P91 steel,

- Journal of Nuclear Materials*, 498, 176–186, 2018a.
- Pandey, C., Mahapatra, M. M., Kumar, P., & Saini, N., Effect of Weld Consumable Conditioning on the Diffusible Hydrogen and Subsequent Residual Stress and Flexural Strength of Multipass Welded P91 Steels, *Metallurgical and Materials Transactions B*, 49(5), 2881–2895, 2018b.
- Papagiannis, G. I., Roumpelakis, I. M., Triantafyllou, A. I., Makris, I. N., & Babis, G. C., No Differences Identified in Transverse Plane Biomechanics Between Medial Pivot and Rotating Platform Total Knee Implant Designs., *The Journal of Arthroplasty*, 1–7, 2016.
- Politis, A. N., Siogkas, G. K., Gelalis, I. D., & Xenakis, T. A., Patterns of stress distribution at the proximal femur after implantation of a modular neck prosthesis. A biomechanical study, *Clinical Biomechanics*, 28(4), 415–422, 2013.
- Rho, J. Y., Kuhn-Spearing, L., & Zioupos, P., Mechanical properties and the hierarchical structure of bone, *Medical Engineering and Physics*, 20(2), 92–102, 1998.
- Schileo, E., Balistreri, L., Grassi, L., Cristofolini, L., Taddei, F., Medica, T., & Rizzoli, I. O., To what extent can linear finite element models of human femora predict failure under stance and fall loading configurations?, *Journal of Biomechanics*, 47(14), 3531–3538, 2014.
- Schoenfeld, B. J., Squatting kinematics and kinetics and their application to exercise performance, *Journal of Strength and Conditioning Research*, 24(12), 3497–3506, 2010.
- Sharma, A., Alam, S., Sharma, C., Patnaik, A., & Kumar, S. R., Static and dynamic mechanical behavior of microcapsule-reinforced dental composite, *Proceedings of the Institution of Mechanical Engineers, Part L: Journal of Materials: Design and Applications*, 233(6), 1184–1190, 2019.
- Shireesha, Y., Ramana, S. V., & Rao, P. G., Modelling and static analysis of femur bone by using different implant materials, 7(4), 82–91, 2013.
- Singh, S., Meena, V. K., Sharma, M., & Singh, H., Preparation and coating of nano-ceramic on orthopaedic implant material using electrostatic spray deposition, *Materials & Design*, 88, 278–286, 2015.
- Smith, S. M., Cockburn, R. A., Hemmerich, A., Li, R. M., & Wyss, U. P., Tibiofemoral joint contact forces and knee kinematics during squatting, *Gait & Posture*, 27(3), 376–386, 2008.
- Sowmianarayanan, S., Finite Element Analysis of Proximal Femur Nail for Subtrochanteric Fractured Femur, *Interfaces*, 2003.
- Susan Standring (Ed.), *Gray's Anatomy: The Anatomical Basis of Clinical Practice*, (41st ed.),.

Elsevier, 2016.

- Vishvesha, A., Pandey, C., Mahapatra, M. M., & Mulik, R. S., On the estimation and control of welding distortion of guide blade carrier for a 660 MW turbine by using inherent strain method, *International Journal of Steel Structures*, 17(1), 53–63, 2017.
- Wagner, D. W., Divringi, K., Ozcan, C., Grujicic, M., Pandurangan, B., & Grujicic, A., Combined musculoskeletal dynamics/structural finite element analysis of femur physiological loads during walking, *Multidiscipline Modeling in Materials and Structures*, 6(4), 417–437, 2010.
- WANG, X., WANG, T., JIANG, F., & DUAN, Y., THE HIP STRESS LEVEL ANALYSIS FOR HUMAN ROUTINE ACTIVITIES, *Biomedical Engineering: Applications, Basis and Communications*, 17(03), 153–158, 2005a.
- WANG, X., WANG, T., JIANG, F., & DUAN, Y., THE HIP STRESS LEVEL ANALYSIS FOR HUMAN ROUTINE ACTIVITIES, *Biomedical Engineering: Applications, Basis and Communications*, 17(03), 153–158, 2005b.
- Yousif, A. E., & Aziz, M. Y., Biomechanical Analysis of the human femur bone during normal walking and standing up, *IOSR Journal of Engineering*, 2(8), 9–12, 2012.
- Zaoutsos, S. P., & Iakovakis, V., an Experimental and 3-D Numerical Investigation of the Wallis Interspinus Implant, (June), 1–10, 2010.



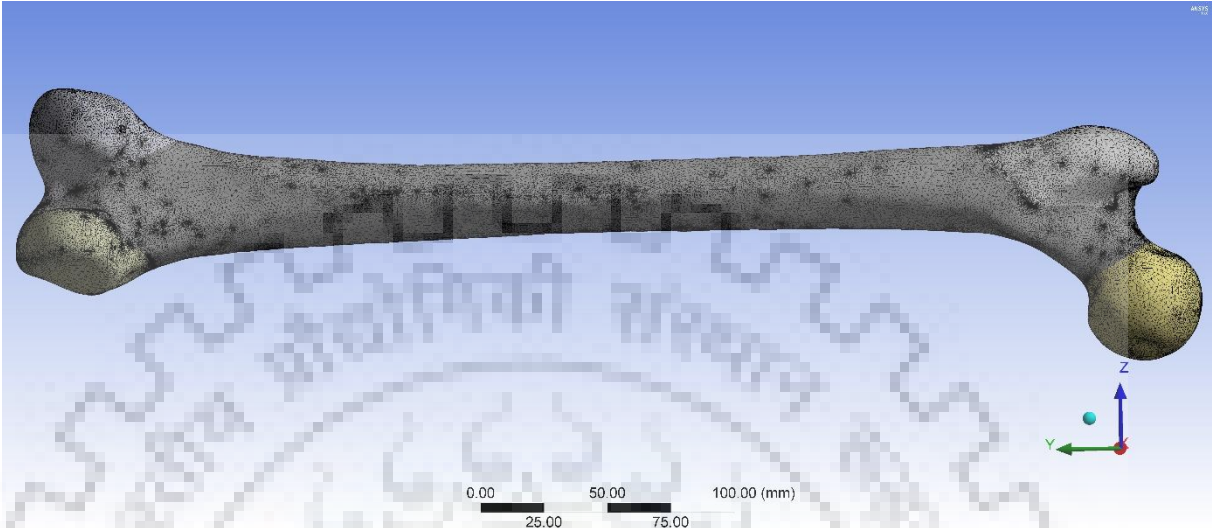


Figure A.1 Meshing and Discretization



Figure A.2 Load configuration in standing posture

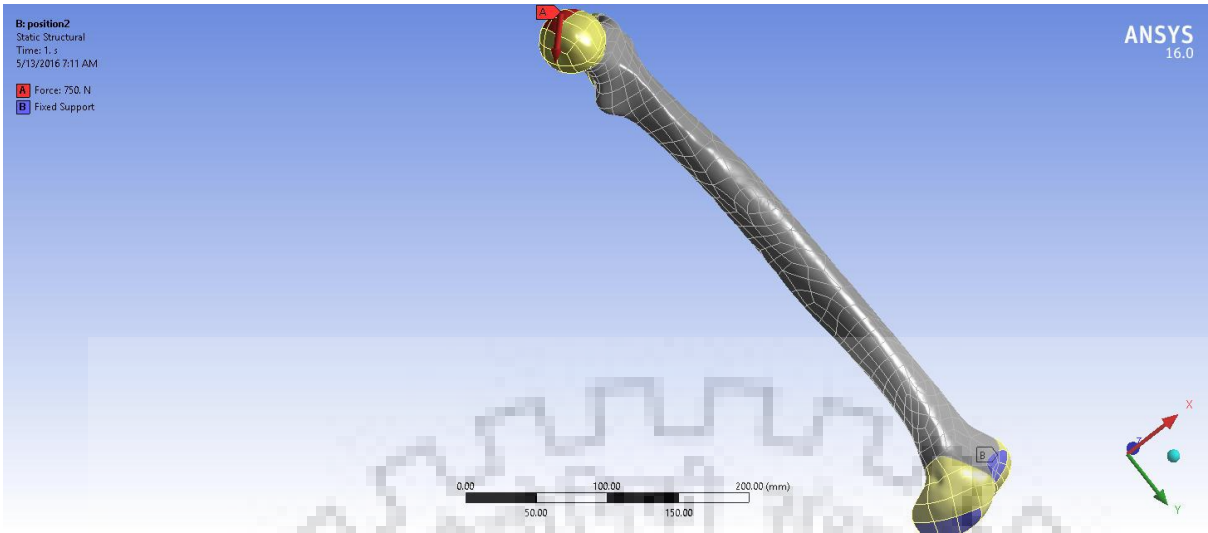


Figure A.3 Load configuration in knee bend posture

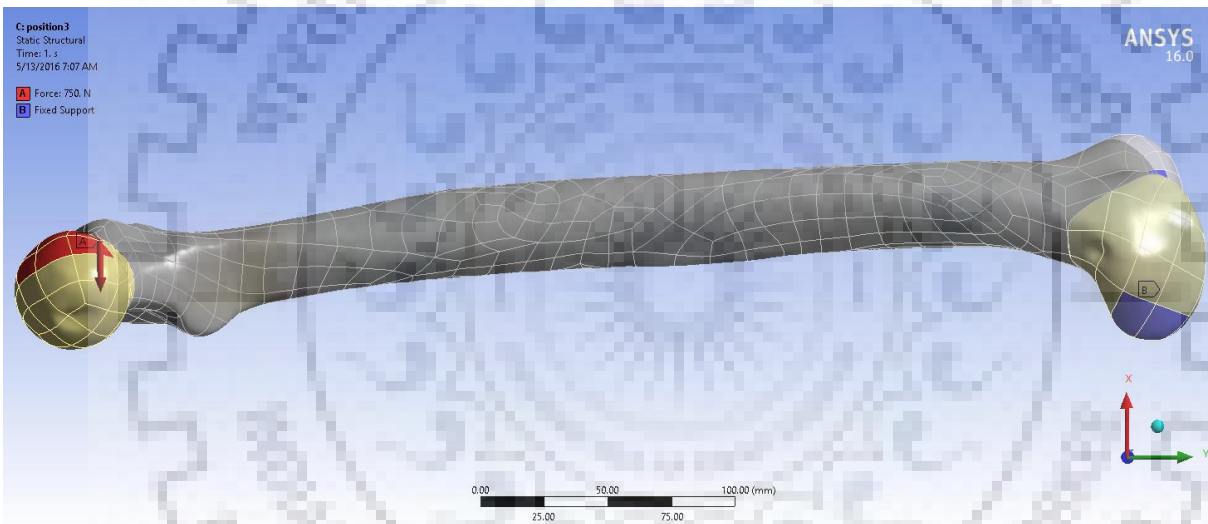


Figure A.4 Load configuration in chair posture

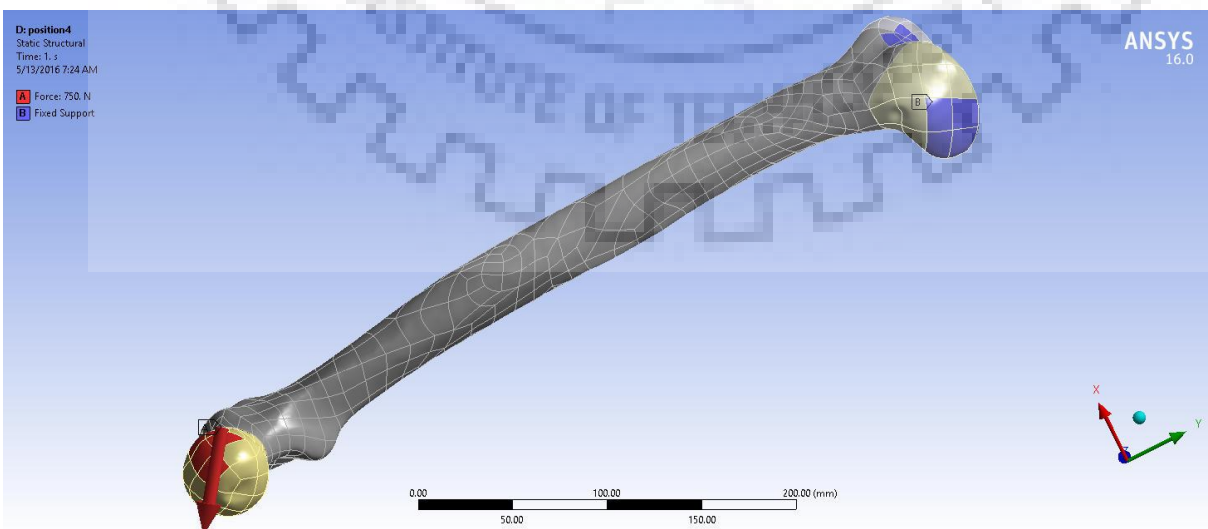


Figure A.5 Load configuration in pre-squat posture

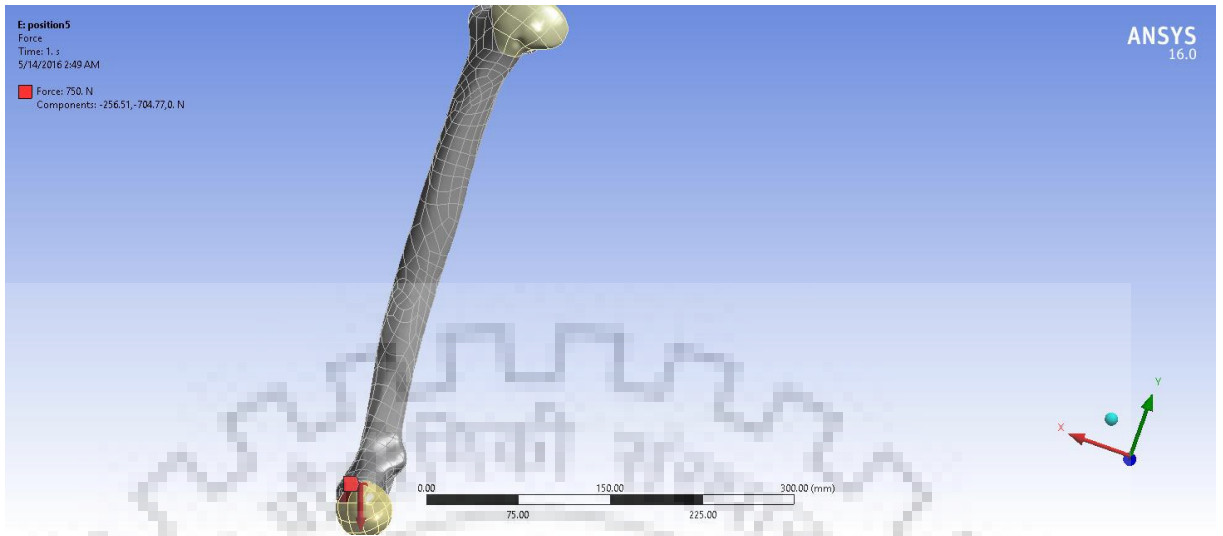
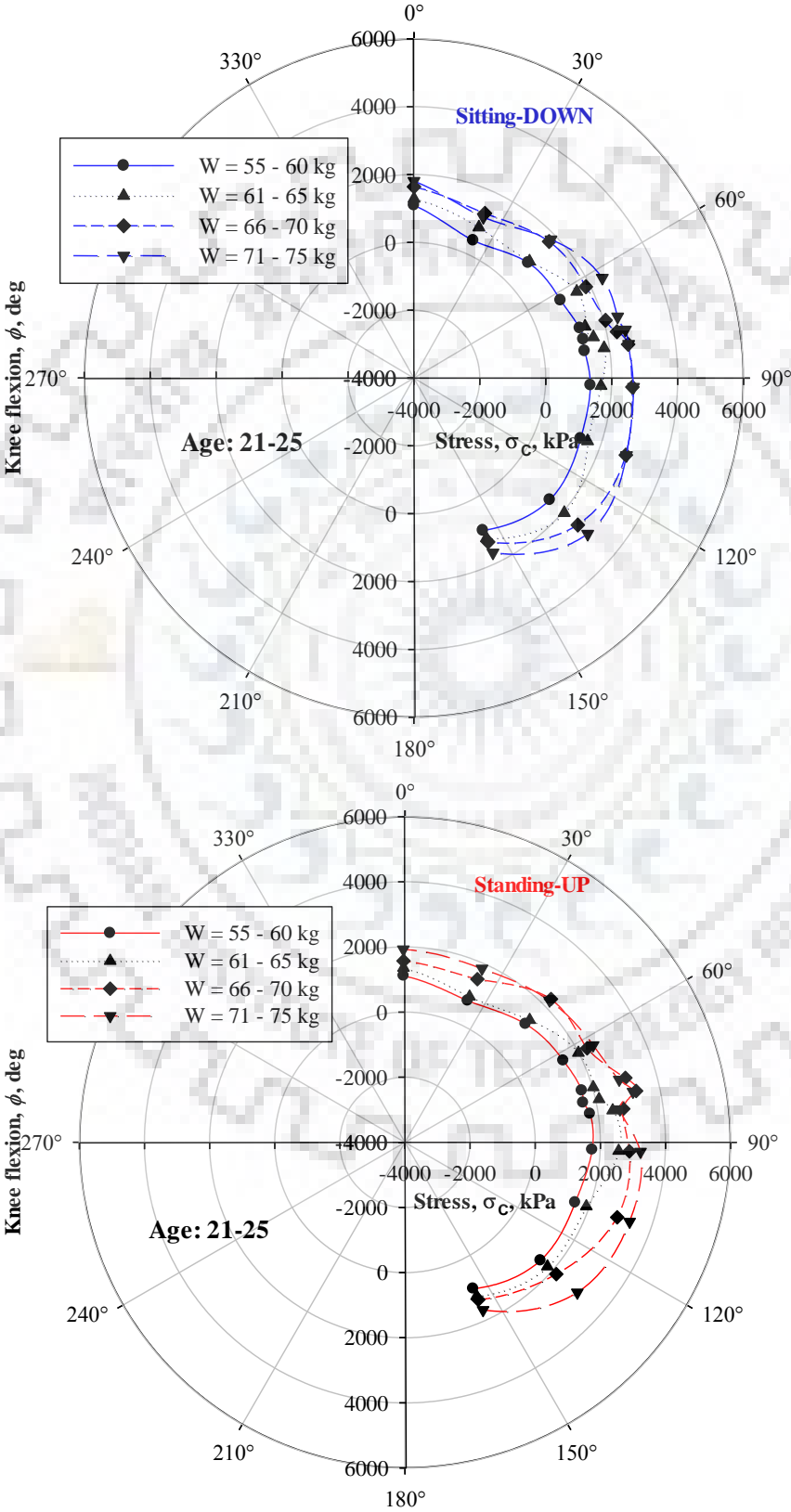
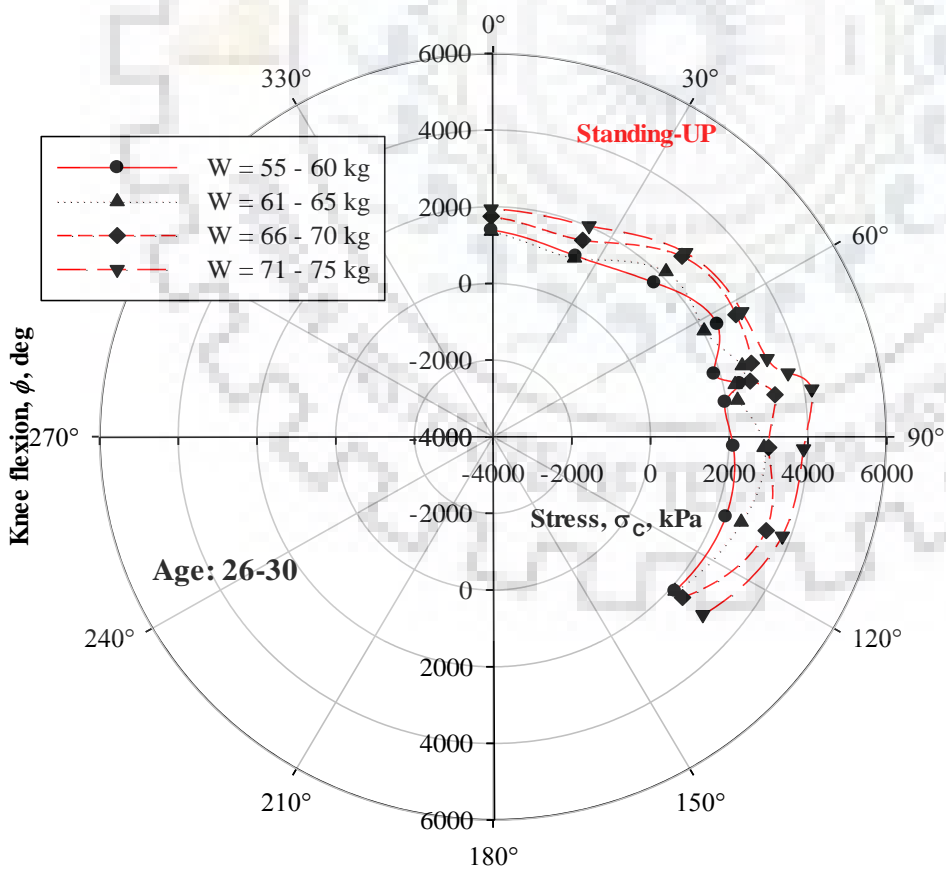
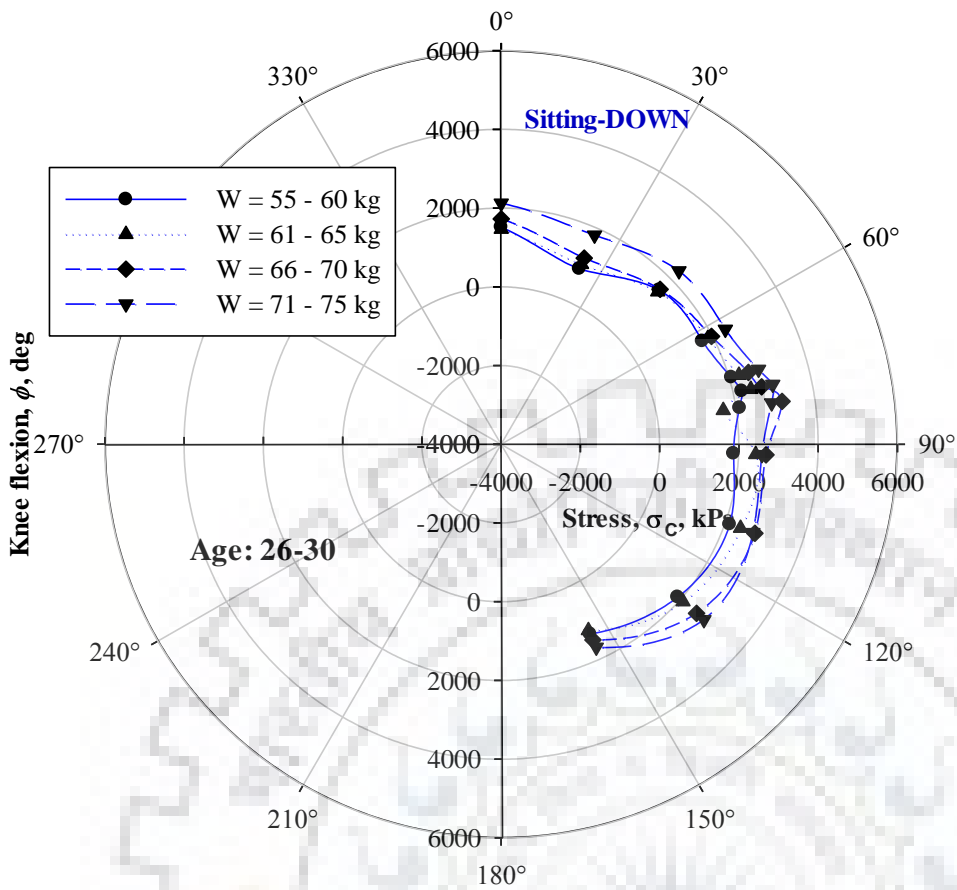


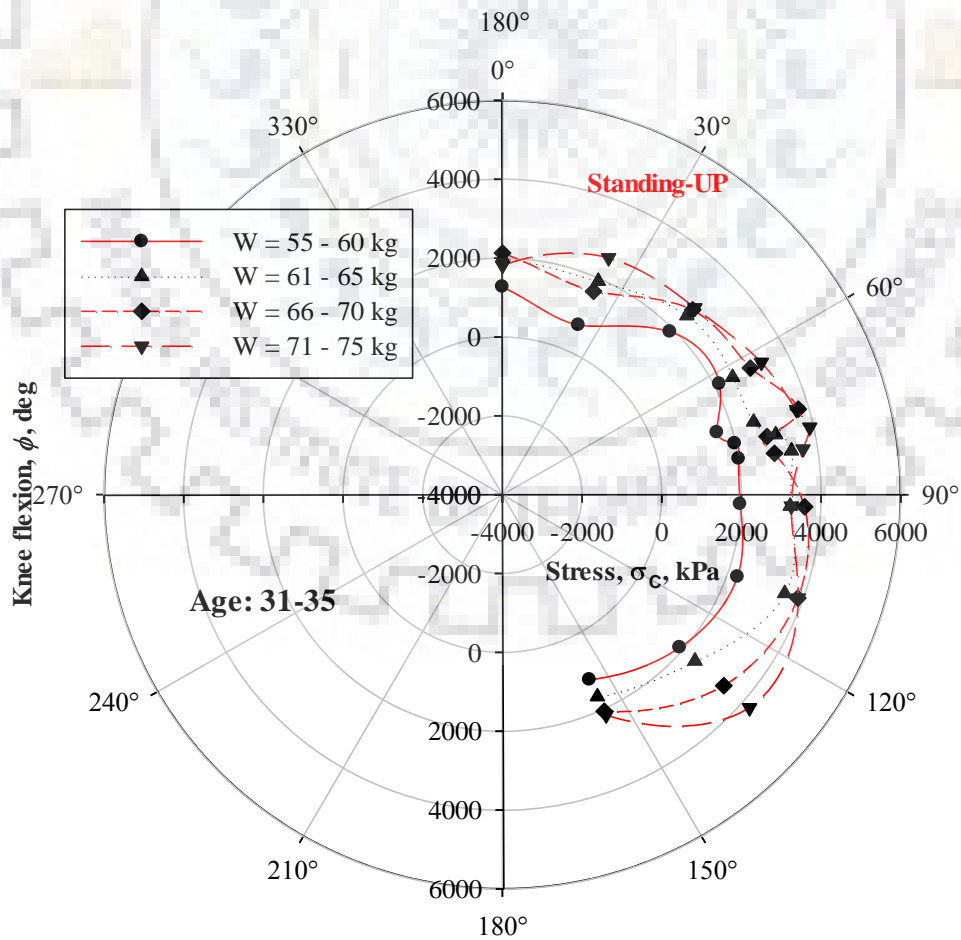
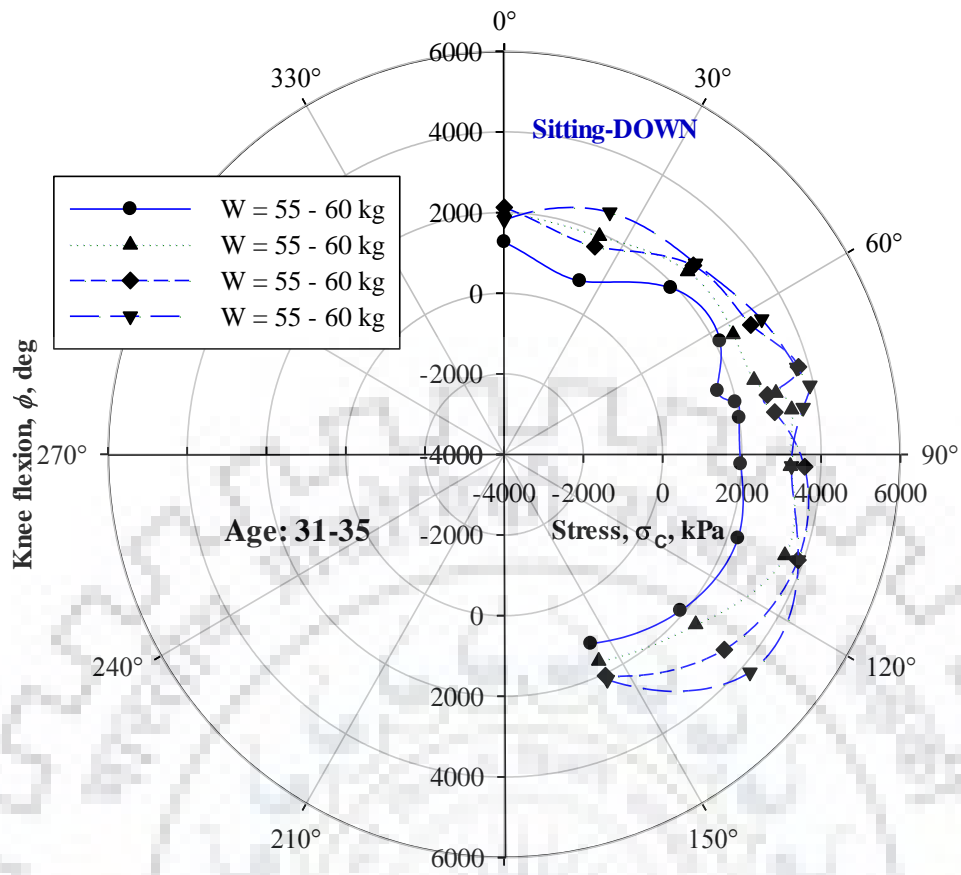
Figure A.6 Load configuration in deep-squat posture

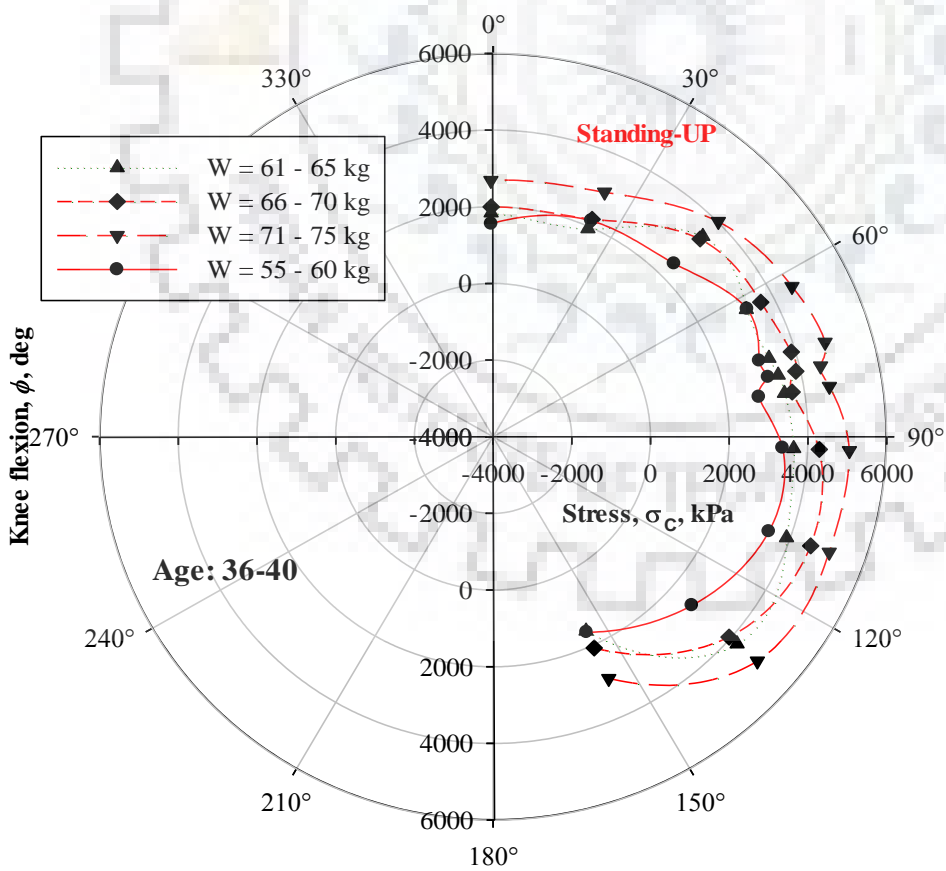
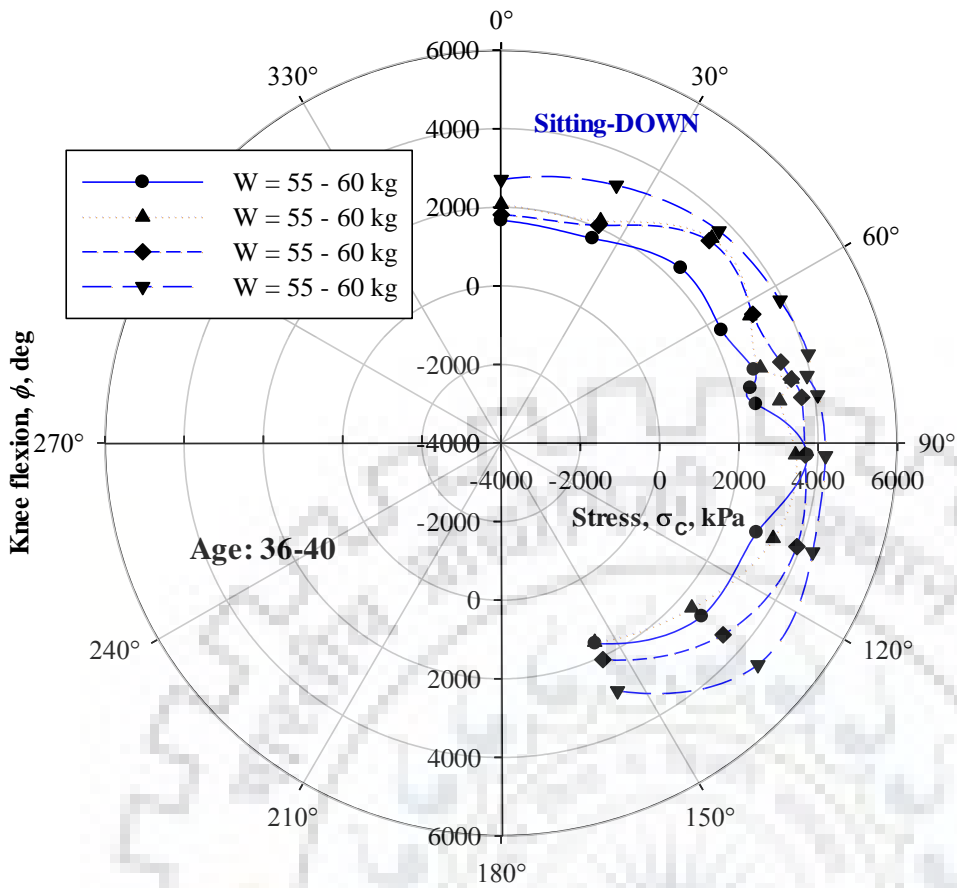


B.1. Compressive or tensile stress distribution along the “neck” of the femur bone with respect to knee flexion under sitting-down and standing-up activities

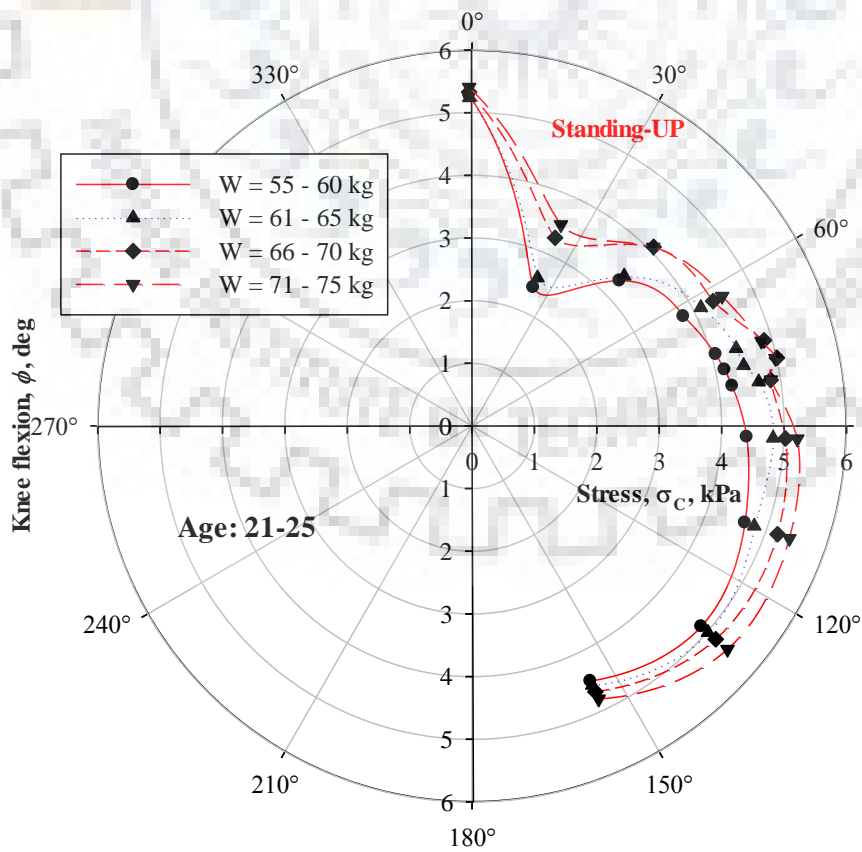
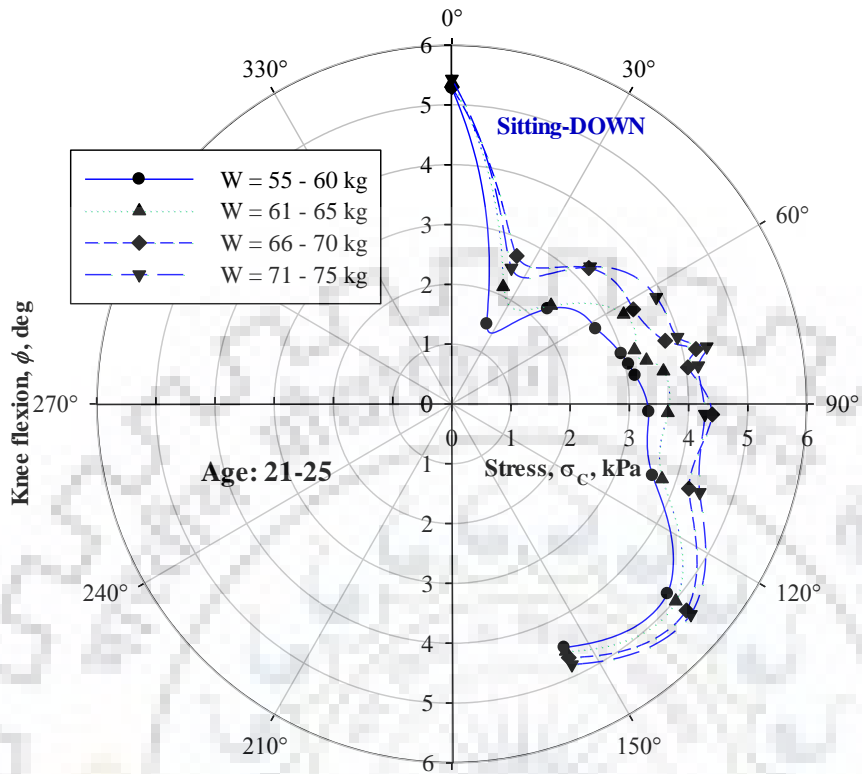


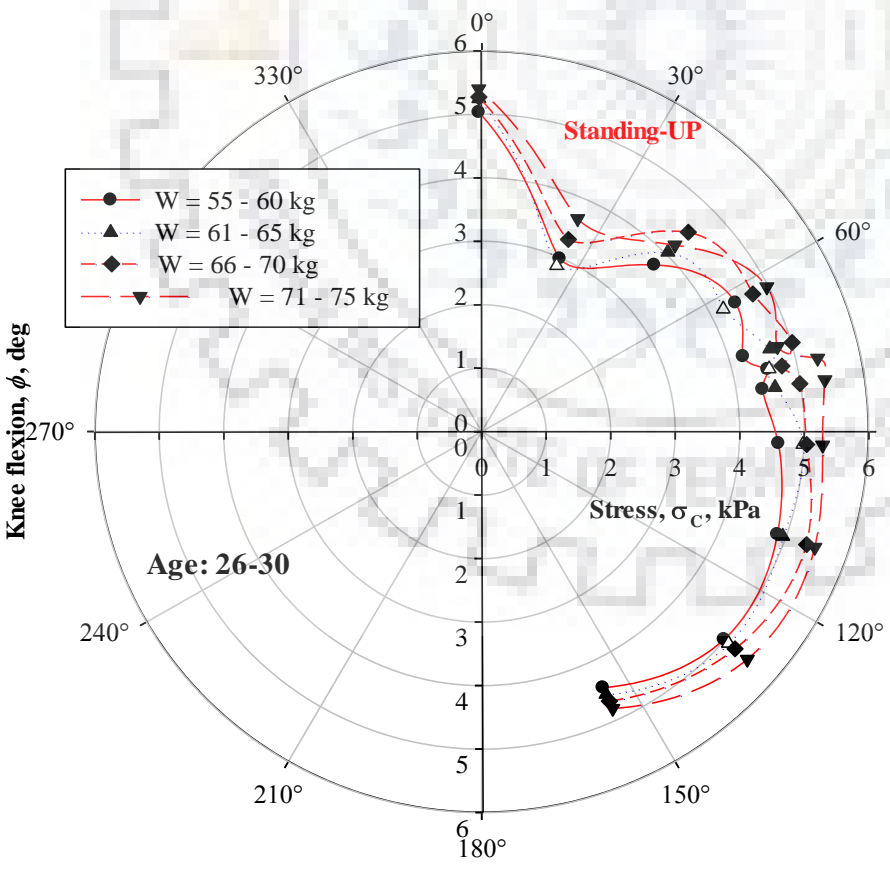
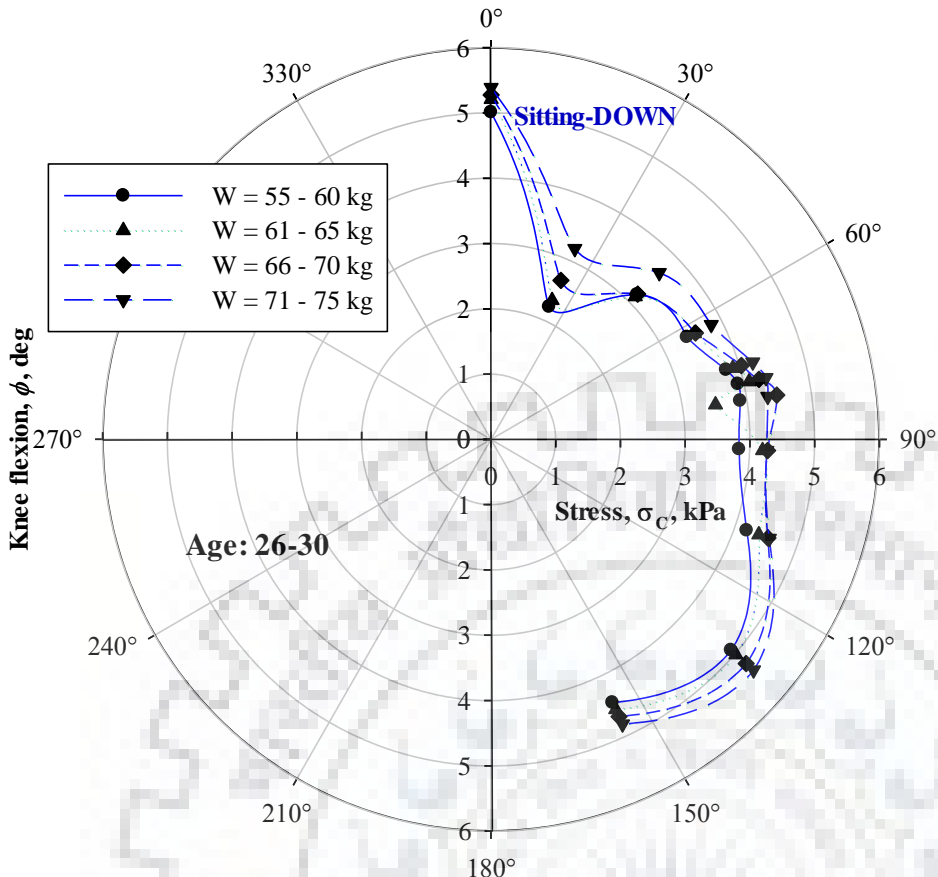


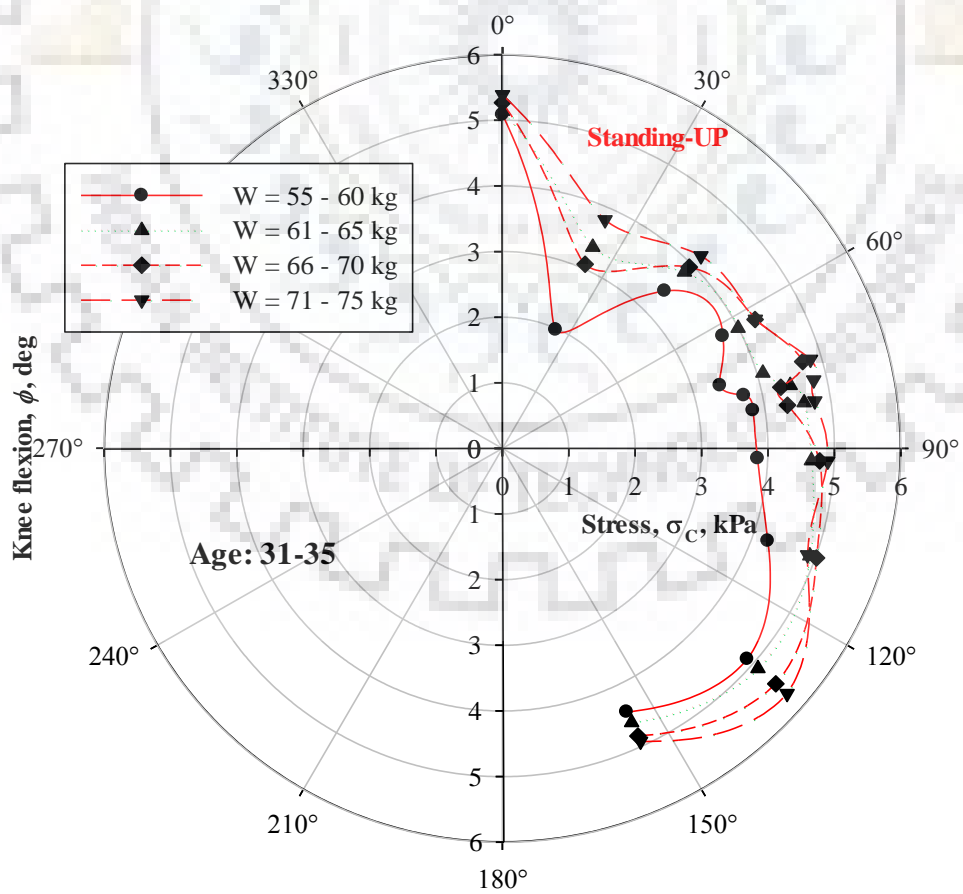
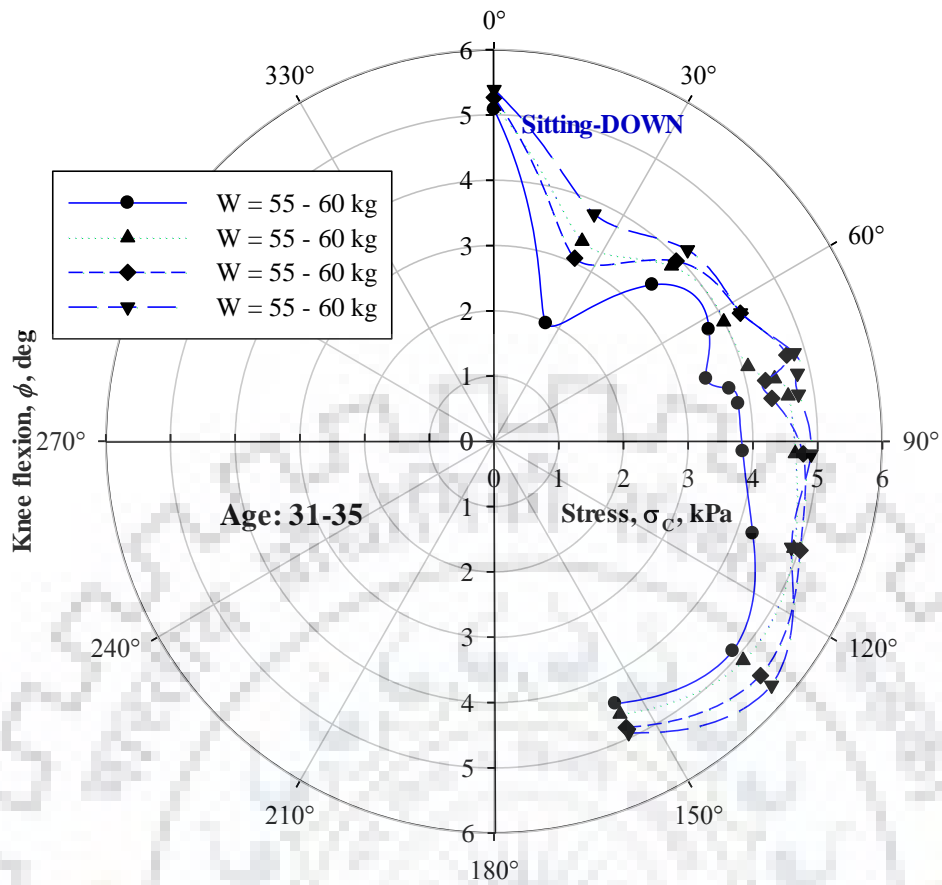


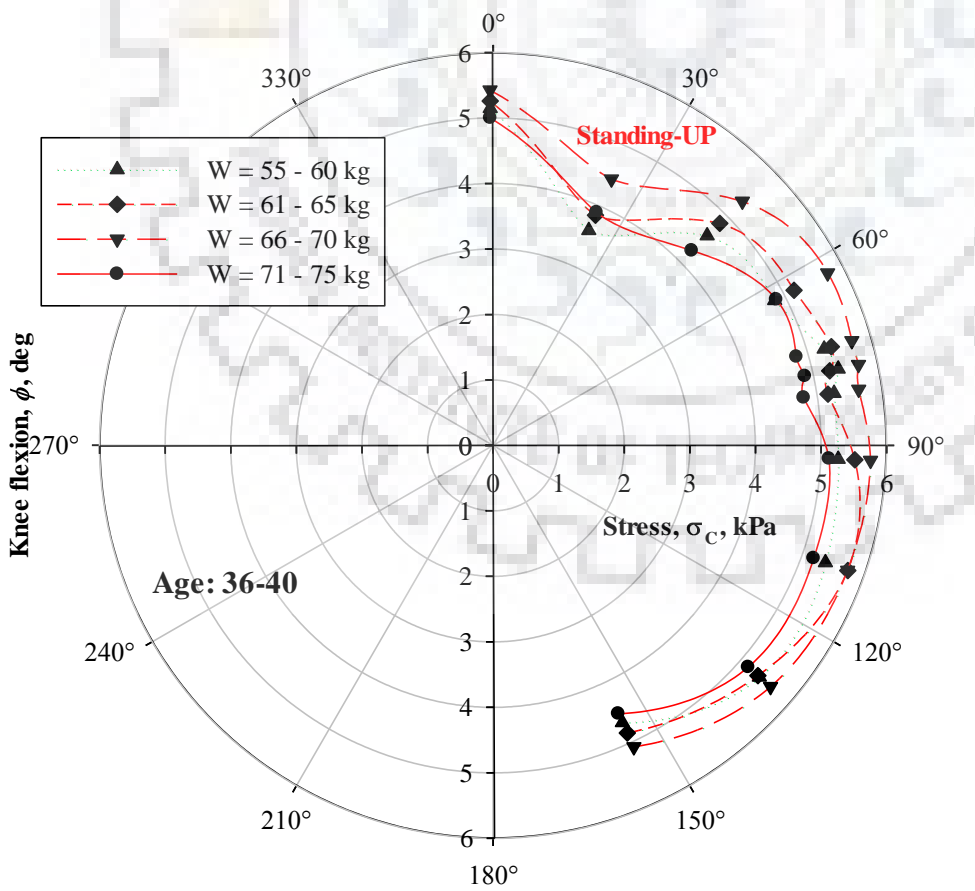
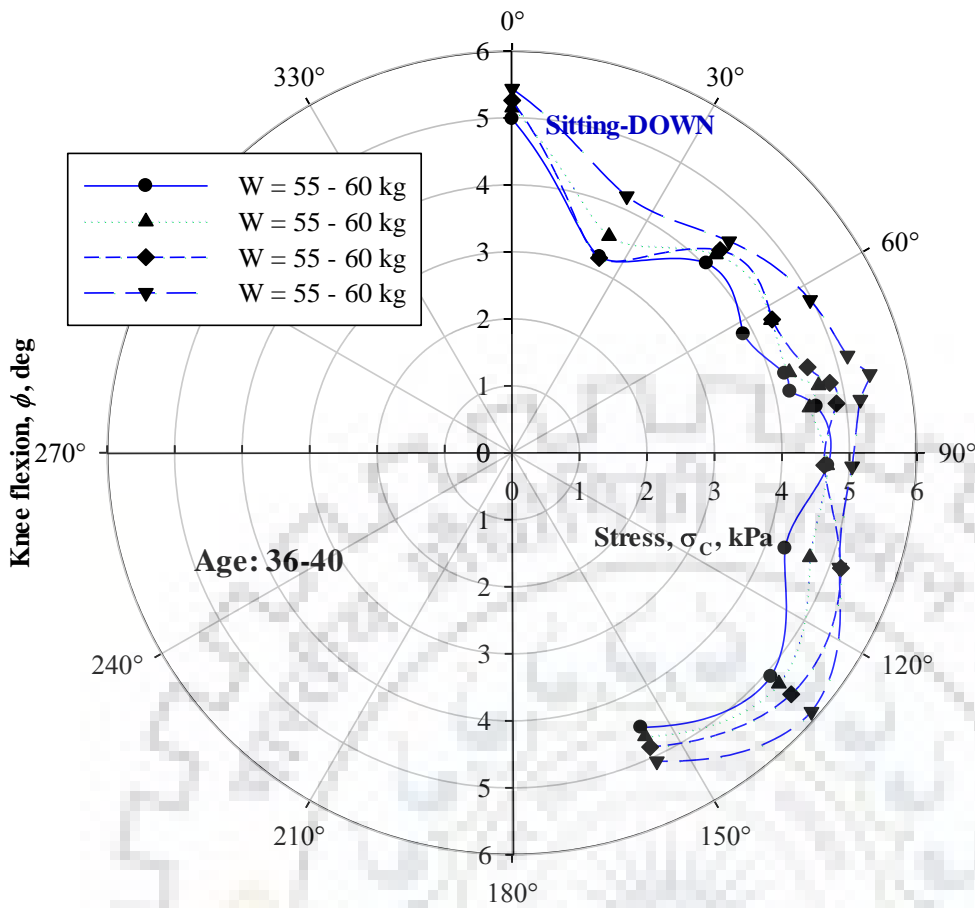


B.2. Compressive or tensile stress distribution along the “Femur-Head” of the femur bone with respect to knee flexion under sitting-down and standing-up activities

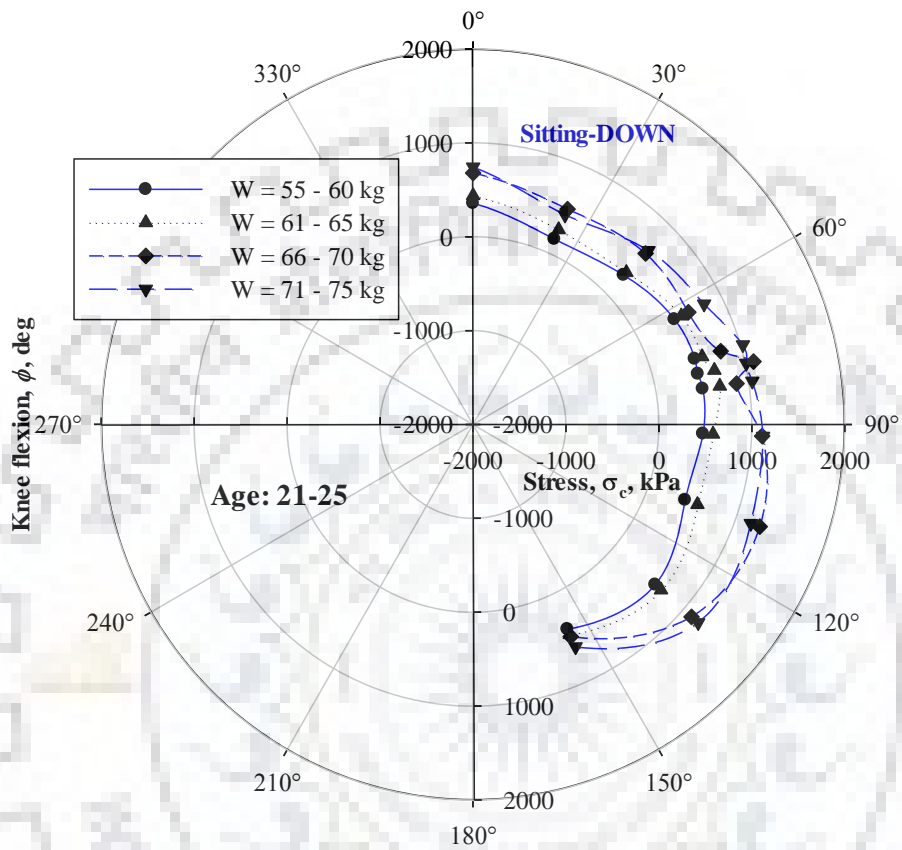


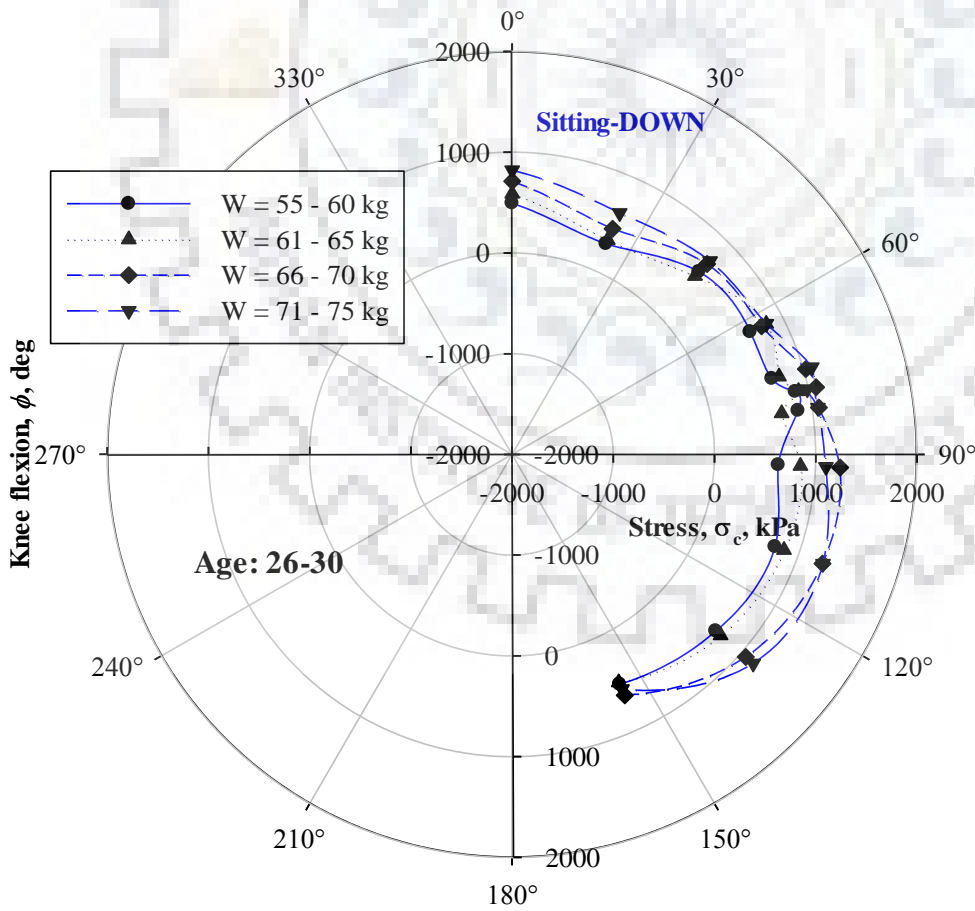
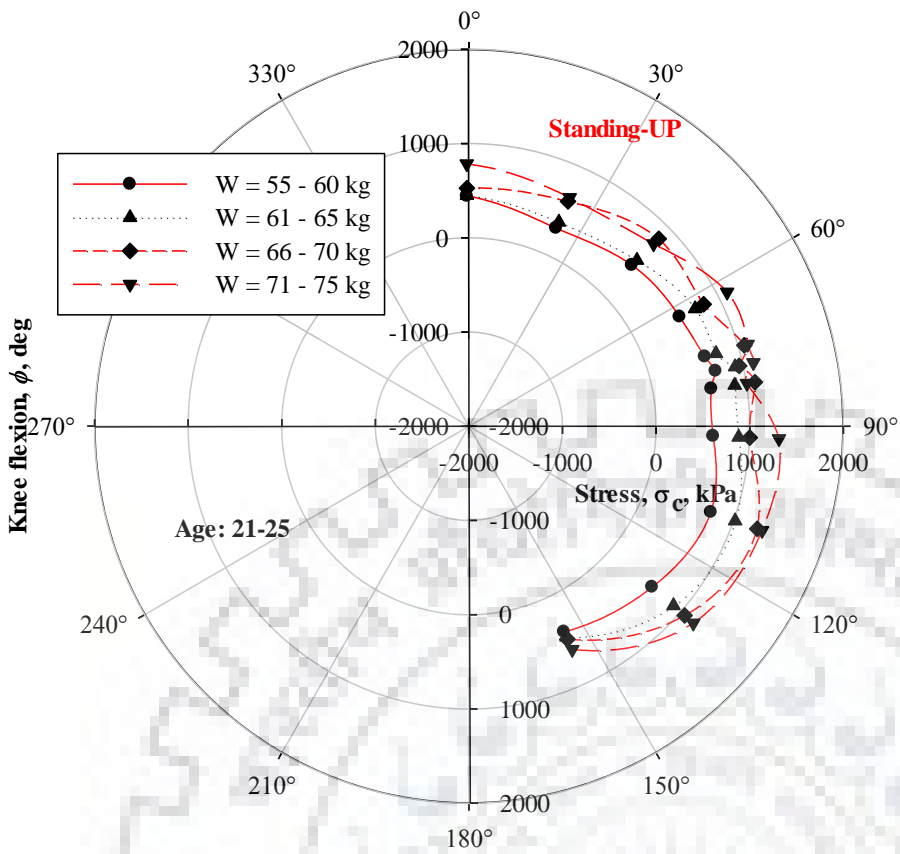


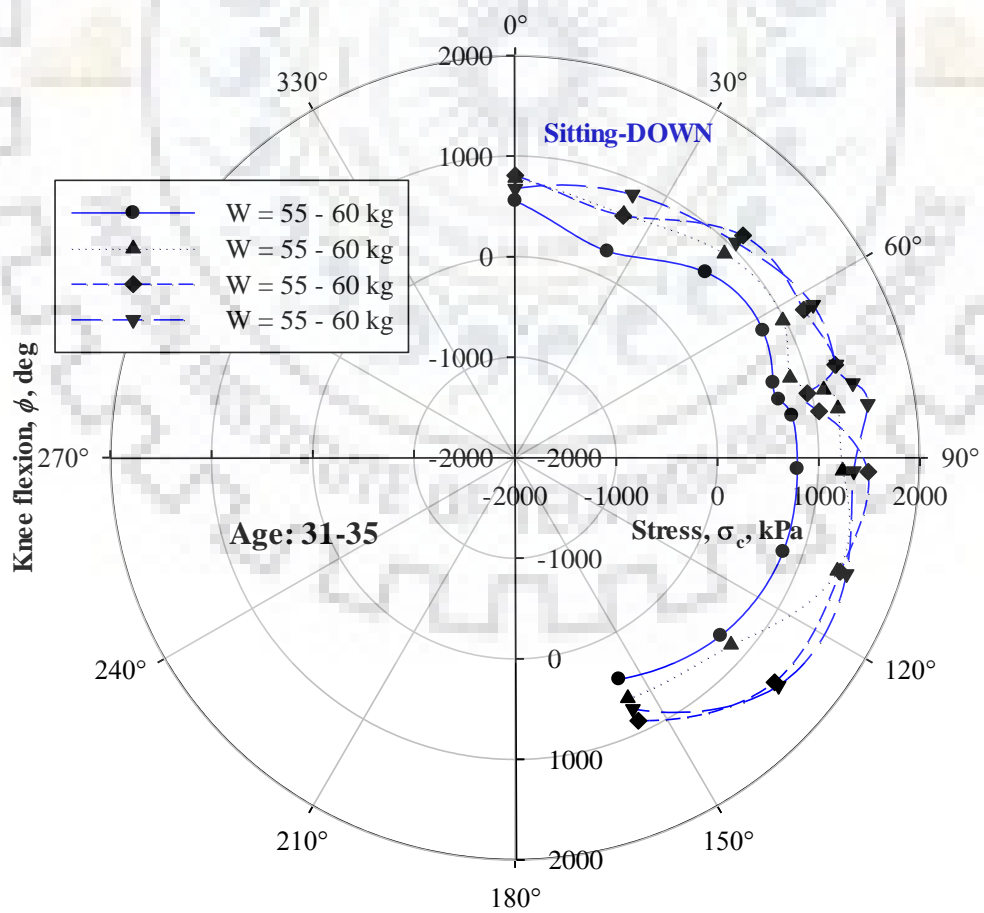
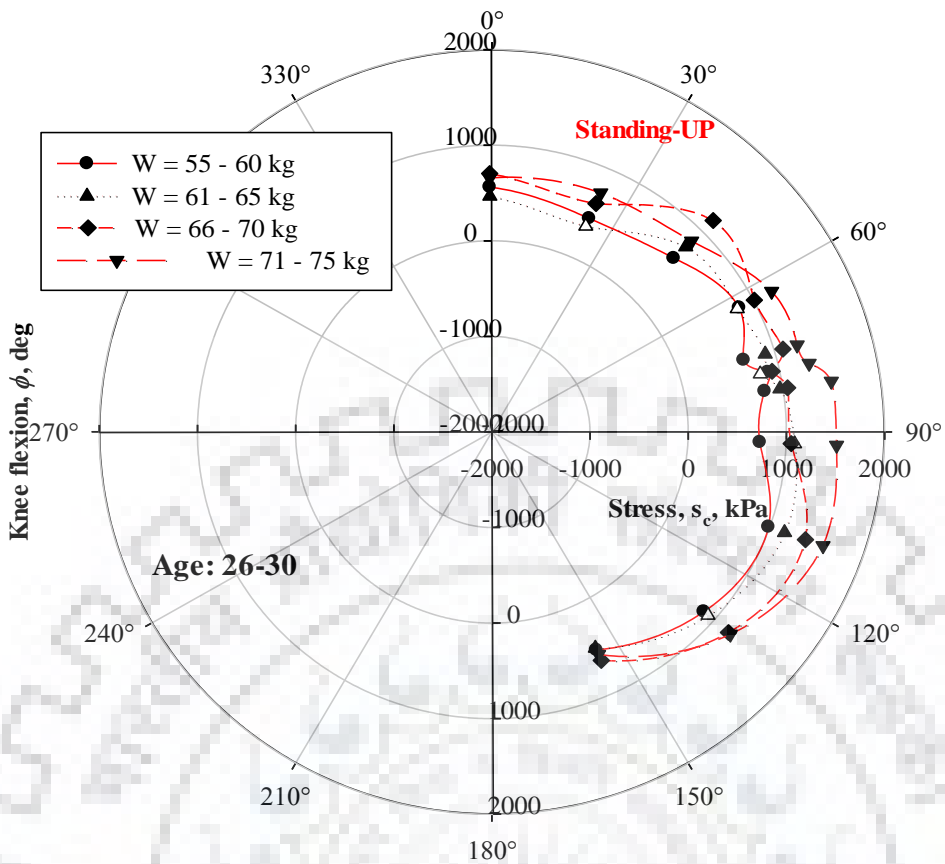


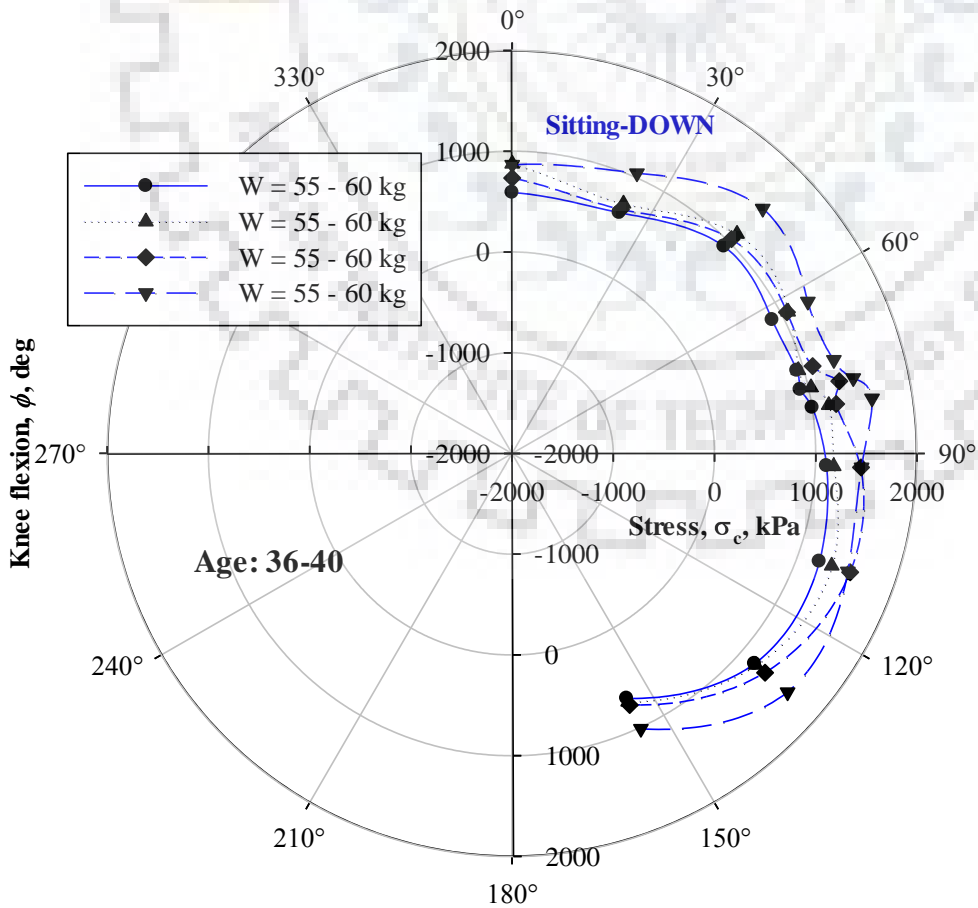
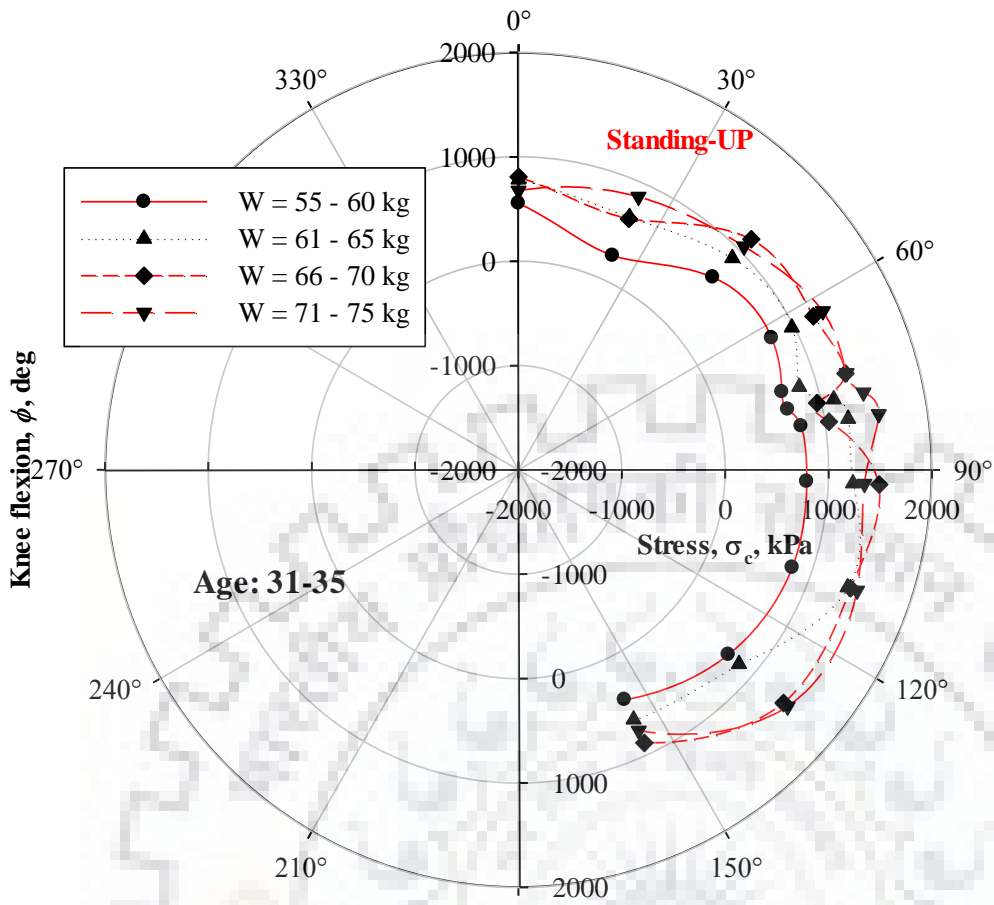


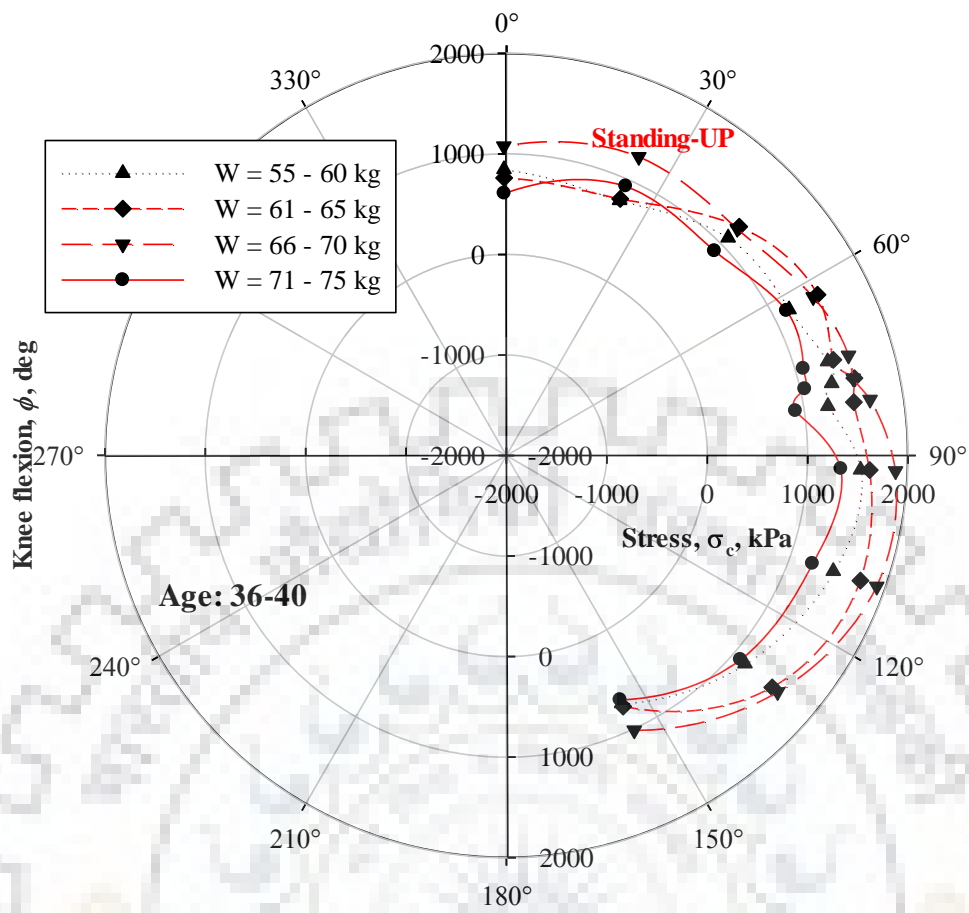
B.3. Compressive or tensile stress distribution along the “Shank” of the femur bone with respect to knee flexion under sitting-down and standing-up activities













APPENDIX C. DUTY CYCLE OF HUMAN SUBJECTS

Table C.1 Details of human subjects and time period (1-DC) to perform deep squat

Age	Category	Individual name	Height		Body mass	Sit-ups				Sit-ups avg
			Femur	Tibia		1st	2nd	3rd	4th	
15-20	Athletes	Sejal Wasnik	51	42	45	8	8	7	7	7.5
		Mukul	49	42	55	10	10	8	7	8.75
		Mohd. Musa	48	40	50	9	9	9	9	9
		Roodra	47	38	61	8	8	7	7	7.5
		Hritik	58	48	70	9	9	8	8	8.5
	Normal	Alpna	39	33	41	8	9	8	8	8.25
		Ankur	47	43	55	9	8	8	7	8
		Priyam	49	44	54	10	9	8	8	8.75
		Shuchita	45	39.5	45	8	8	7	4	6.75
		Pranay	50	44	57	9	9	9	8	8.75
Athletes	Jagdish Godara	54	45	74	10	8	9	8	8.75	
	Saurav	58	52	66	10	10	9	10	9.75	
	Priya Das	48	43	73	9	8	7	8	8	
	Pankaj	54	49	79	10	10	9	10	9.75	
	Charu Meena	52	45	73	9	9	9	8	8.75	
21-25	Athletes	Mansi	46	41	45	8	8	7	7	7.5
		Aniket	51	45	52	7	6	6	7	6.5
	Normal	Anuj	49	44	53	7	6	6	5	6
		Himanshu	48	40	61	8	8	6	7	7.25
		Pooja	49	44	73	6	7	6	2	5.25

Age	Category	Individual name	Height		Body mass	Sit-ups				
			Femur	Tibia		1st	2nd	3rd	4th	avg
26-30	Athletes	Priyanka Gunjan	46	39	67	8	8	8	7	7.75
		Toshi Sharma	50	42	53	8	8	7	7	7.5
		Santhosh	49	42	59	10	9	9	8	9
		Jasbir	48	41.5	62	10	8	9	8	8.75
		Harshit	51	45	61	10	9	8	8	8.75
	Normal	Anubha	45	40	48	9	8	7	7	7.75
		Deepmala	48	43	51	8	8	8	6	7.5
		Abhishek	50	44.5	65	9	8	8	7	8
		Ankit	49	44	74	10	9	7	8	8.5
		Bhaskar	48	42.5	69	8	8	7	7	7.5
31-35	Athletes	Prince	53	46	64	6	5	6	5	5.5
		Vineet Sharma	51	45	66	7	6	6	6	6.25
		Sandeep Shukla	48	40	70	9	9	8	7	8.25
		Navrattan	50	43	65	10	9	9	8	9
		Avinash	50	46	69	9	8	9	8	8.5
	Normal	Ritika	42	37	56	8	7	5	1	5.25
		Deepak Bhatt	53	44	92	8	7	6	7	7
		Ali	45	40	77	10	9	9	9	9.25
		Anand Solanki	49	44	75	5	4	3	3	3.75
		Nitesh Datt	39	37	69	8	7	6	7	7

Age	Category	Individual name	Height		Body mass	Sit-ups				
			Femur	Tibia		1st	2nd	3rd	4th	avg
36-40	Athletes	Arun	52	46	81	11	11	10	10	10.5
		Juwal	50	41	68	8	8	7	7	7.5
		Shamsher Singh	44	41	75	9	7	8	9	8.25
		Mukesh Raghav	49	45	83	8	8	7	7	7.5
		Hema	52	46	77	9	8	7	2	6.5
	Normal	Puneet Gaur	45	41	75	7	7	6	6	6.5
		Sibli Tyagi	41	40	74	6	5	5	5	5.25
		Mukesh Kumar	43.2	40.6	56	7	8	7	8	7.5
		Ajay Chaudhary	51	45	82	9	8	8	9	8.5
		Awadh Kishore	46	40	73	9	8	7	9	8.25

Note:

- 1. All the human subjects were thoroughly familiarized with the study design and written informed consent to participant in the study was taken.*
- 2. All the human subject data were measured under the supervision and guidance of Mr. Rohit Powel Joseph (Physiotherapist, IIT Roorkee Hospital, Roorkee) and Mrs. Taru Saxena (Physiotherapist, Bareilly).*